

Enhanced Anti-Cancer Photodynamic Activity with Photobiomodulation Therapy at Different Wavelengths

Submitted to the Graduate School of Natural and Applied Sciences
in partial fulfillment of the requirements for the degree of

Master of Science

in Biomedical Engineering

by

Büşra Sirek

ORCID 0000-0002-2788-1149

January, 2023

This is to certify that we have read the thesis **Enhanced Anti-Cancer Photodynamic Activity with Photobiomodulation Therapy at Different Wavelengths** submitted by **Büşra Sirek**, and it has been judged to be successful, in scope and in quality, at the defense exam and accepted by our jury as a MASTER'S THESIS.

APPROVED BY:

Advisor:

Dr. Nermin Topalođlu Avşar
İzmir Kâtip Çelebi University

Committee Members:

Assoc. Prof. Dr. Didem Şen Karaman
İzmir Kâtip Çelebi University

Assoc. Prof. Dr. Haşim Özgür Tabakođlu
İzmir Bakırçay University

Date of Defense: November 11, 2023

Declaration of Authorship

I, **Büşra Sirek**, declare that this thesis titled **Enhanced Anti-Cancer Photodynamic Activity with Photobiomodulation Therapy at Different Wavelengths** and the work presented in it are my own. I confirm that:

- This work was done wholly or mainly while in candidature for the Master's degree at this university.
- Where any part of this thesis has previously been submitted for a degree or any other qualification at this university or any other institution, this has been clearly stated.
- Where I have consulted the published work of others, this is always clearly attributed.
- Where I have quoted from the work of others, the source is always given. This thesis is entirely my own work, with the exception of such quotations.
- I have acknowledged all major sources of assistance.
- Where the thesis is based on work done by myself jointly with others, I have made clear exactly what was done by others and what I have contributed myself.

Date: 11.01.2023

Enhanced Anti-Cancer Photodynamic Action with Photobiomodulation Therapy at Different Wavelengths

Abstract

Photodynamic therapy (PDT) is a non-invasive therapy that induces photochemical reactions for treating many diseases including cancer using the advantages of light. It is based on the interaction of light at a specific wavelength and light-sensitive chemical which does not have dark toxicity. Thus, PDT is an anticancer therapeutic modality yielding cancer cell death. As with other anticancer therapies, some drawbacks reduce or limit the efficacy of PDT. To eliminate the disadvantages resulting in increased efficacy of PDT, it is combined with other anticancer treatment methods. Together use of PDT with another light therapy that is not used for anticancer purposes normally called photobiomodulation (PBM) or low-level laser/light therapy (LLLT) is becoming popular. The application of PBM to cancer cells has been controversial due to its unwanted and negative effects on them such as increased cell proliferation and metastasis capacities. Nowadays, it has been shown that the application strategy of PBM to the cancer cells before the anticancer treatment has a positive impact on cancer cell death. But this result is highly influenced by cell type, energy densities, and wavelengths of light. In this study, the efficacy of PDT was tried to be increased on PC3 human prostate cancer by pre-treating cells with PBM therapy with 655 and 808-nm wavelengths at 1, 3, and 5 J/cm² energy densities. PDT was conducted on the cells after incubation of indocyanine green (ICG) at 25, 50, and 100 μM and Chlorin (Ce6) at 2.5, 5, 10, and 25 μM concentrations. As a result, increased cell deaths were

observed especially with the PBM application at 808-nm wavelength followed by Ce6-mediated PDT at 50 J/cm² energy density with maximum additional 63.44% cell death compared to only PDT while increased cell deaths were not observed with PBM application at 655-nm wavelength followed by ICG-mediated PDT at 100 J/cm² energy density. In addition to the cell viability, the cellular uptake of ICG and Ce6 and amount of ATP produced after PBM with both wavelengths; live and death analysis via staining after Ce6-mediated PDT; the amount of nitric oxide released, reactive oxygen species produced, change in mitochondrial membrane potential after the PBM with both wavelengths and Ce6-mediated PDT were examined. Thus, it can be accomplished by PBM application at specific wavelength and energy density is a promising way to enhance cell death obtained from photodynamic action.

Keywords: Prostate cancer, Photodynamic therapy, Photobiomodulation, Chlorin e6, Indocyanine green, 808-nm diode laser, 655-nm diode laser

Farklı Dalga Boylarında Fotobiyomodülasyon Uygulaması ile Anti-Kanser Fotodinamik Aktivitenin Arttırılması

ÖZ

Fotodinamik terapi (FDT), ışığın avantajlarını kullanarak kanser dahil birçok hastalığı tedavi etmek için fotokimyasal reaksiyonları indükleyen invazif olmayan bir terapidir. Belirli bir dalga boyundaki ışığın ve karanlık toksisitesi olmayan ışığa duyarlı kimyasalın etkileşimine dayanır. Bu nedenle FDT, kanser hücre ölümü sağlayan bir antikanser terapötik modalitedir. Diğer antikanser tedavilerinde olduğu gibi, FDT'nin etkinliğini azaltan veya sınırlayan bazı dezavantajlar vardır. FDT'nin dezavantajları ortadan kaldırarak etkinliğinin artması için diğer antikanser tedavi yöntemleri ile birleştirilir. FDT'nin fotobiyomodülasyon (FBM) veya düşük seviyeli lazer/ışık tedavisi (LLLT) olarak adlandırılan normalde antikanser amaçlar için kullanılmayan başka bir ışık tedavisi ile birlikte kullanımı popüler hale gelmektedir. FBM'nin kanser hücrelerine uygulanması, artan hücre proliferasyonu ve metastaz kapasiteleri gibi istenmeyen ve olumsuz etkiler oluşturma potansiyellerinden dolayı tartışmalı olmuştur. Günümüzde antikanser tedavi öncesi kanser hücrelerine FBM uygulama stratejisinin kanser hücresi ölümü üzerinde olumlu bir etkiye sahip olduğu gösterilmiştir. Ancak bu sonuç, hücre tipi, enerji yoğunlukları ve ışığın dalga boylarından oldukça etkilenir. Bu çalışmada, PC3 insan prostat kanseri hücreleri 1, 3 ve 5 J/cm² enerji yoğunluklarında 655 ve 808-nm dalga boylarındaki FBM tedavisi ile

ön işleme tabi tutularak FDT'nin etkinliği artırılmaya çalışılmıştır. FDT, indosiyanin yeşili (İSY)'nin 25, 50 ve 100 μM 'de ve Klorin (Ke6)'nin 2.5, 5, 10 ve 25 μM konsantrasyonlarda inkübasyonundan sonra hücreler üzerinde gerçekleştirmiştir. Sonuç olarak, özellikle 808-nm dalga boyunda FBM uygulaması ve ardından 50 J/cm^2 enerji yoğunluğunda Ke6 aracılı FDT uygulaması ile sadece FDT'ye kıyasla maksimum ek %63,44 hücre ölümleri gözlenirken 655-nm dalga boyunda FBM uygulaması ve ardından 100 J/cm^2 enerji yoğunluğunda İSY aracılı FDT uygulaması ile artan hücre ölümleri gözlemlenmemiştir. Hücre canlılığına ek olarak, her iki dalga boylarındaki FBM sonrası İSY ve Ke6'nın hücre alımı ve üretilen ATP miktarı; Ke6 aracılı FDT'den sonra boyama yoluyla canlı ve ölüm analizi; salınan nitrik oksit miktarı, üretilen reaktif oksijen türleri, mitokondriyal membran potansiyelindeki değişim her iki dalga boylarındaki FBM ve Ke6 aracılı FDT uygulamaları sonrası incelenmiştir. Bu nedenle, belirli bir dalga boyu ve enerji yoğunluğundaki FBM uygulaması fotodinamik eylemden elde edilen hücre ölümünü arttırmanın umut verici bir yoldur.

Anahtar Kelimeler: Prostat kanseri, Fotodinamik terapi, Fotobiyomodülasyon, Klorin e6, İndosiyanin yeşili, 808-nm diyot lazer, 655-nm diyot lazer

To my lovely and supportive family...

Acknowledgment

First, I would like to thank my advisor, Dr. Nermin Topalođlu Avşar, for her endless support, trust, patience, guidance, and encouragement. I learned a lot from her during my master's degree and she taught me a lot academically. She is always kind, loving, friendly, and sincere with me. I feel fortunate to have had a chance to work with her. I hope I will have the opportunity to work together for a longer time.

I would like to acknowledge and thank Prof. Dr. Ayşę Nalbantsoy from the Department of Bioengineering, Ege University for kindly providing the PC3 human prostate cell line that I used in my master's degree experiments. Also, I would like to thank Ziyaşan Buse Yaralı Çevik for her contributions and for helping me with the experimental protocol. Also, thank you Assoc. Prof. Dr. Didem Şen Karaman for their support. I would like to express my thanks to my labmate Biomedical Optics and Laser Applications Laboratory member Emel Bakay for her support and help with experimental protocols and especially to Dilara Portakal Koç and all colleagues from other laboratories for their friendship.

Also, I would like to acknowledge The Scientific and Technological Research Council of Turkey (TUBITAK) for supporting me financially under the 2210-National MSc/MA Scholarship Programs '2210/A National General MSc/MA Scholarship Program' subprogram code during my master's degree study.

I would like to sincerely thank my lovely family for their endless support in every subject, their respect for every decision I made, and for helping me overcome every challenge in my life. Dad, mom, and my sister Berra, this thesis could not have been formed without your support.

I also thank my friends, especially Samet, Yunus, Dilara, Nevin, and Erdi, for their support, friendship, motivation, patience, and encouragement. Finally, thank you Deniz for your understanding, patience, encouragement, and friendship and for always being by my side. You are the joy of my life.

Table of Contents

Declaration of Authorship	ii
Abstract	iii
Öz	v
Acknowledgment	viii
List of Figures	xi
List of Tables	xv
List of Abbreviations	xvi
List of Symbols	xix
1 Introduction	1
1.1 Prostate Cancer	5
1.2 Anticancer Conventional Treatments	7
1.3 Anticancer Photodynamic Therapy	9
1.3.1 Action Mechanism of Photodynamic Therapy	14
1.3.2 Photosensitizers	16
1.3.3 Light and Light Sources	17
1.4 Strategies for Increasing the Efficacy of Anticancer Photodynamic Therapy	19
1.4.1 Photobiomodulation	21
2 Materials and Methods	26
2.1 Cell Culture	27
2.2 Photosensitizers	27
2.3 Light Sources and Optical Setup	28

2.4	PBM-induced Anticancer PDT Applications	30
2.4.1	655-nm PBM-induced ICG-mediated PDT Applications	32
2.4.2	808-nm PBM-induced Ce6-mediated PDT Applications	32
2.5	Cellular Uptake Analysis of Photosensitizers	32
2.6	Cell Viability Analysis	33
2.7	Nitric Oxide Release Analysis	34
2.8	ATP Production Analysis	35
2.9	Intracellular Reactive Oxygen Species Production Analysis	36
2.10	Mitochondrial Membrane Potential Change Analysis	37
2.11	Cell Viability Analysis by Acridine Orange/Propidium Iodide Staining	38
2.12	Statistical Analysis	39
3	Results	40
3.1	Effects of Laser Light on PC3 Cells	40
3.2	Cytotoxicity of Photosensitizers on PC3 Cells	41
3.3	Cellular Uptake of Photosensitizers by PC3 Cells	43
3.4	Phototoxicity of PBM-induced PDT on PC3 Cells	46
3.5	Nitric Oxide Release in PC3 Cells after PBM and PDT Applications	51
3.6	ATP Production in PC3 Cells after PBM Applications	54
3.7	Intracellular Reactive Oxygen Species Production in PC3 Cells after PBM and PDT Applications	55
3.8	Change of Mitochondrial Membrane Potential in PC3 Cells after PBM and PDT Applications	58
3.9	Acridine Orange/Propidium Iodide Staining after PDT Applications	62
4	Discussion	64
5	Conclusion	73
	References	75
	Curriculum Vitae	88

List of Figures

Figure 1.1	The Cell Cycle	2
Figure 1.2	Cancer Metastasis: Invasion, Intravasation, Circulation, Extravasation, and Colonization	4
Figure 1.3	Localization of Prostate Gland in Male Reproductive System	6
Figure 1.4	Phototherapy Conducted with <i>Ammi majus</i> plant via Sunlight in Ancient Egypt	10
Figure 1.5	Anticancer Photodynamic Therapy (Drawn in BioRender)	10
Figure 1.6	Application of Photodynamic Therapy: Steps include administration of PS, incubation of PS for localization at the tumor site, application of light activates PS, and cancer cell death	11
Figure 1.7	Effects of Photodynamic Therapy. PDT induces apoptosis/necrosis, damages tumor niche vasculature, and regulates the immune system via ROS. (Drawn in BioRender)	13
Figure 1.8	Jablonski Diagram Showing Photochemical Mechanisms of PDT: Type I and Type II Energy Transfer (Drawn in BioRender)	14
Figure 1.9	Light Penetration Depth in Tissue. Red light travels approximately 4 mm while near-infrared light travels 5 mm and above into tissue.	18
Figure 1.10	Effects of Photobiomodulation on Cells: Light can activate mitochondria and light-sensitive ion channels.	21
Figure 1.11	Photobiomodulation or Low-Level Light/Laser Therapy (Drawn in BioRender)	22
Figure 2.1	Chemical Structure of Indocyanine Green	28
Figure 2.2	Chemical Structure of Chlorin e6	28
Figure 2.3	655-nm Diode Laser Device (left) and 808-nm Diode Laser Device (right)	29
Figure 2.4	Illustration for the Experimental Setup (Drawn in BioRender)	31
Figure 2.5	Conversion of MTT to Formazan Crystals	34

Figure 2.6	Conversion of Sulfanilic Acid to Azo Dye	35
Figure 2.7	Conversion of Luciferin to Oxyluciferin	36
Figure 2.8	Conversion of DCFH-DA to DCF	37
Figure 3.1	Cell viability analysis after laser irradiation. Each bar represented the average of the normalized with respect to the control group. Differences that were statistically significant were represented as * and ** (p <0.05, * indicates significant differences compared to the control and ** indicates significant differences compared to the experimental groups)	41
Figure 3.2	Cell viability analysis of 25, 50, and 100 μ M of ICG concentrations after 1 and 24 h incubation time. Each bar represented the average of the normalized with respect to the control group.	42
Figure 3.3	Cell viability analysis of 2.5, 5, 10, and 25 μ M of Ce6 concentrations after 2 and 24 h incubation time. Each bar represented the average of the normalized with respect to the control group.	42
Figure 3.4	Cellular uptake analysis of 25, 50, and 100 μ M of ICG concentrations after PBM applications. a) cellular uptake analysis after 1 and b) 24 h of incubation time. Each bar represented the average of the normalized with respect to the control group. Differences that were statistically significant were represented as * and ** (p <0.05, * indicates significant differences compared to the control and ** indicates significant differences compared to the experimental groups)	44
Figure 3.5	Cellular uptake analysis of 2.5, 5, 10, and 25 μ M of Ce6 concentrations after PBM applications. a) cellular uptake analysis after 2 and b) 24 h of incubation time. Each bar represented the average of the normalized with respect to the control group. Differences that were statistically significant were represented as * and ** (p <0.05, * indicates significant differences compared to the control and ** indicates significant differences compared to the experimental groups)	45
Figure 3.6	Cell Viability analysis after ICG-mediated PDT applications at 100 J/cm ² energy density after a) 1 and b) 24 h incubation. Photosensitizer concentrations: 25, 50, and 100 μ M of ICG. Each bar represented the average of the normalized with respect to the control group. Differences	

that were statistically significant were represented as * and ** ($p < 0.05$, * indicates significant differences compared to the control and ** indicates significant differences compared to the experimental groups) 47

Figure 3.7 Cell Viability analysis after Ce6-mediated PDT applications at 50 J/cm^2 after a) 2 and b) 24 h incubation. Photosensitizer concentrations: 2.5, 5, 10, and $25 \mu\text{M}$ of Ce6. Each bar represented the average of the normalized with respect to the control group. Differences that were statistically significant were represented as * and ** ($p < 0.05$, * indicates significant differences compared to the control and ** indicates significant differences compared to the experimental groups) 49

Figure 3.8 Nitrite amounts after 655-nm PBM at 1, 3, and 5 J/cm^2 energy densities. Measurements were taken a) 0 and b) 24 h after the 655-nm PBM applications. Each bar represented the average of the normalized with respect to the control group. Differences that were statistically significant were represented as * ($p < 0.05$, * indicates significant differences compared to the control group) 52

Figure 3.9 Nitrite amounts after 808-nm PBM at 1, 3, and 5 J/cm^2 energy densities. Measurements were taken a) 0 and b) 24 h after the 808-nm PBM applications. Each bar represented the average of the normalized with respect to the control group. 52

Figure 3.10 Nitrite amounts after Ce6-mediated PDT applications at 50 J/cm^2 energy density after a) 2 and b) 24 h incubation. Photosensitizer concentrations: 2.5, 5, 10, and $25 \mu\text{M}$ of Ce6. Each bar represented the average of the normalized with respect to the control group. Differences that were statistically significant were represented as * and ** ($p < 0.05$, * indicates significant differences compared to the control and ** indicates significant differences compared to the experimental groups) 54

Figure 3.11 ATP amounts after 655 and 808-nm PBM applications at 1, 3, and 5 J/cm^2 energy densities. Each bar represented the average of the normalized with respect to the control group. Differences that were statistically significant were represented as * and ** ($p < 0.05$, * indicates significant differences compared to the control and ** indicates significant differences compared to the experimental groups) 55

- Figure 3.12 Reactive oxygen species formation after a) 655-nm and b) 808-nm PBM at 1, 3, and 5 J/cm² energy densities. Each bar represented the average of the normalized with respect to the control group. Differences that were statistically significant were represented as * (p <0.05, * indicates significant differences compared to the control group) 56
- Figure 3.13 Reactive oxygen species formation after Ce6-mediated PDT applications at 50 J/cm² energy density after a) 2 and b) 24 h incubation. Photosensitizer concentrations: 2.5, 5, 10, and 25 μM of Ce6. Each bar represented the average of the normalized with respect to the control group. Differences that were statistically significant were represented as * (p <0.05, * indicates significant differences compared to the control group) 58
- Figure 3.14 Mitochondrial membrane potential change after 655-nm PBM applications at 1, 3, and 5 J/cm² energy densities. Measurements were taken 0 and 24 h after the PBM applications. Each bar represented the average of the normalized with respect to the control group. 59
- Figure 3.15 Mitochondrial membrane potential change after 808-nm PBM applications at 1, 3, and 5 J/cm² energy densities. Measurements were taken 0 and 24 h after the PBM applications. Each bar represented the average of the normalized with respect to the control group. 60
- Figure 3.16 Mitochondrial membrane potential change after Ce6-mediated PDT applications at 50 J/cm² energy density after a) 2 and b) 24 h incubation. Photosensitizer concentrations: 2.5, 5, 10, and 25 μM of Ce6. Each bar represented the average of the normalized with respect to the control group. Differences that were statistically significant were represented as * and ** (p <0.05, * indicates significant differences compared to the control and ** indicates significant differences compared to the experimental groups) 61
- Figure 3.17 Acridine Orange/Propidium Iodide images of PC3 cells with 20X magnification in control, only PDT, and PBM+PDT groups. Ce6-mediated PDT was applied at 50 J/cm² energy density and 808-nm PBM was applied at 5 J/cm² energy density before the PDT. (scale bar: 50 μm, living cells were stained by acridine orange, in green and dead cells were stained by propidium iodide, in red) 63

List of Tables

Table 3.1	Cell Death (%) in Only PDT and PBM+PDT Groups after 2 h of Ce6 Incubation	50
Table 3.2	Cell Death (%) in Only PDT and PBM+PDT Groups after 24 h of Ce6 Incubation	50

List of Abbreviations

ABC	ATP-binding Casette
ADT	Androgen Deprivation Therapy
AIF	Apoptosis-inducing Factor
ALA	Aminolevulinic Acid
AMP	Adenosine Monophosphate
AO/PI	Acridine Orange/Propidium Iodide
AP-1	Activator Protein 1
ATP	Adenosine Triphosphate
BK	Large-conductance Calcium and Voltage-activated Potassium Channels
Cas3	Caspase 3
Cas9	Caspase 9
Ce6	Chlorin e6
CDK	Cyclin-dependent Kinase
Cox	Cytochrome C Oxidase
DCFH	2',7'-Dichlorofluorescein
DCFH-DA	2',7'-Dichlorofluorescein Diacetate
DMSO	Dimethyl Sulfoxide
DNA	Deoxyribonucleic Acid
ER	Endoplasmic Reticulum
FBS	Fetal Bovine Serum
g	Gram
h	Hour

HIF	Hypoxia-inducible Factor
HpD	Hematoporphyrin
HSP	Heat Shock Protein
IL	Interleukin
ICG	Indocyanine Green
iNOS	Inducible Nitric Oxide Synthase
JC-1	Tetramethylbenzimidazolcarbocyanine Iodide
L	Liter
LED	Light-emitting Diode
LH	Luteinizing Hormone
LHRH	Luteinizing Hormone Releasing Hormone
LLLT	Low-level Laser/Light Therapy
MMP	Mitochondrial Membrane Potential
MTT	3-(4,5- dimethylthiazol-2yl)- 2,5 diphenyl tetrazolium bromide
NIR	Near-infrared
NO	Nitric Oxide
NPe6	Mono-L-aspartly Chlorin e6
PBM	Photobiomodulation
PBS	Phosphate Buffered Saline
PCD	Programmed Cell Death
PDT	Photodynamic Therapy
PPIX	Protopohyrin IX
PS	Photosensitizer
PSA	Prostate-specific Antigen
ROS	Reactive Oxygen Species
s	Second
SMAC	Mitochondrial Activator of Caspases

TGF- β	Transforming Growth Factor Beta
TURP	Transurethral Prostatic Resection
UV	Ultra Violet
VEGF	Vascular Endothelial Growth Factor
VIS	Visible
W	Watt

List of Symbols

CO_2	Carbon Dioxide
$^{\circ}\text{C}$	Celsius Degree
G_1	Gap 1
G_2	Gap 2
H_2O_2	Hydrogen Peroxide
$\cdot\text{OH}$	Hydroxyl Radical
$\Delta\Psi_m$	Mitochondrial Membrane Potential
O_2	Oxygen
$^1\text{O}_2$	Singlet Oxygen
$\cdot\text{O}^{2-}$	Superoxide Radical

Chapter 1

Introduction

Cancer is a type of disease that shows two different characteristics: one is unregulated-uncontrolled cell growth and division, and another one is the distribution of the cells to other body parts besides its origin source [1], [2]. There are many different types of cancer and different characteristics due to the tissue where the tumor forms. Many cancers originate from epithelial cells and are therefore called carcinomas. The rest are categorized as sarcomas and adenocarcinomas depending on where cancer cells arise. It is a sarcoma that originates from mesoderm cells such as bone, and an adenocarcinoma that arises from glandular cells in the body [3].

As known, cell growth and division take place when an egg is fertilized; and these processes are regulated and controlled highly to form an embryo in the later human body and during normal development. However, this regulation and control mechanism cannot be maintained in cancer cells. The human body contains trillions of cells that are specialized to maintain itself and their function depends on where they are responsible. Cells grow and divide to replace the injured and dead parts to form and maintain the human body from the tissues to organs [2]. As known, cell proliferation results in two daughter cells from one mother cell. Later at an appropriate time, two formed daughter cells again pass to other cell divisions separately via a process that is named as cell cycle shown in Figure 1.1, and this process is composed of four stages. G₁, S, G₂, and M phases where the first three of them belong to the interphase. As known, the cell grows and prepares itself for division in the interphase, and genetic material DNA is replicated in the S phase. Later, the M phase takes place via two different stages: mitosis and cytokinesis. If mitogens or growth factors are

absent, cells are normally in a state called the G_0 phase where they do not take part in the cell cycle. However, the presence of these parameters induces cells to enter or re-enter the cell cycle and face the G_1 checkpoint first. After that checkpoint, the cell cycle proceeds without any need for the inducing factors or any need. Different checkpoints during the cell cycle enable it to detect and respond to genetic material damage to maintain cell divides without any change in the DNA. If damage in the genetic material occurs, the G_1 checkpoint senses it, and DNA replication cannot occur in the S phase [3].

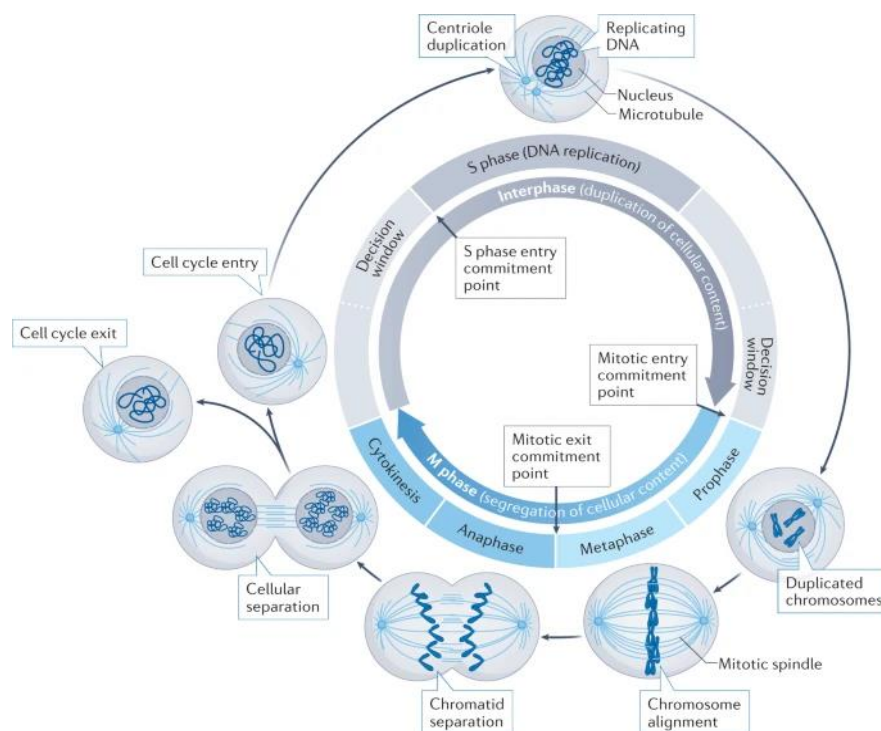


Figure 1.1: The Cell Cycle [4]

On the other hand, the G_2 checkpoint is responsible for proper and full DNA replication that takes place during the S phase and passage to the M phase. Lastly, the M checkpoint ensures the sister chromatids attach correctly to the mitotic spindle during the anaphase stage of the M phase. All of the checkpoints are important for correct cell division and to ensure DNA is replicated correctly and fully as well as daughter cells have the same chromosome number as the mother cell in the end. Failure in any of the checkpoints can give rise to cancer formation. In the case of the tumor cell cycle rather than the normal cell cycle, genes that regulate the cell cycle are mutated. This causes changes in cell cycle regulation, unexpected division-proliferation, and tumorigenesis. For instance, mutations in Cyclin-dependent kinase

(CDK) genes were obtained in cancer patients because they take part in the cell cycle. The other factor is cyclins, which are kinds of proteins that have authority over activating CDKs; their overexpression also causes changes in the cell cycle. Furthermore, deletion of the gene responsible for the p16 protein which is a type of tumor suppressor via slowing the passage of the G1 phase to the S phase [3].

Cells can undergo mutations that induce carcinogenesis due to several factors such as environment, reproductive life, diet, alcohol, smoking, and the body itself. For example, exposure to UV-B lights through the sun can change the DNA structure via forming pyrimidine dimers, the transmittance of viruses that belong to the retrovirus family induce carcinogenesis and products that occurred during the normal metabolism (for example oxygen radicals), and errors in the DNA replication due to any reason can result in carcinogenesis [3].

Cancer cells have specific characteristics rather than normal cells called 'Hallmarks of Cancer' such as showing different energy metabolism (Warburg Effect, it is aerobic glycolysis that cancer cells produce ATP creating lactate from glucose even in the presence of O₂), enhanced angiogenesis, high replication potency via keeping telomeres length is same, activating invasion/metastasis, escaping from cell death and immune system [3], [5], [6]. Also, cancer cells do not need external signals from growth factors for division and do not respond to growth-inhibitory signals [3]. Besides, when cancer cells begin to form, their microenvironment is activated via paracrine communication causing the microenvironment to change and expand the tumor [7]. Thus, in the end, the tumor microenvironment becomes different from the environment of normal healthy tissues [7], [8]. The tumor microenvironment contains many different types of cells such as endothelial cells, pericytes, normal and cancer-associated fibroblasts, mesenchymal stem cells, and immune cells including neutrophils, eosinophils, basophils, mast cells, natural killer cells, T and B lymphocytes [8]. Also, the tumor microenvironment contains many factors such as cytokines, chemokines, different types of proteins, and growth factors that are secreted by cancer cells and other cells of the tumor microenvironment. All components of the tumor microenvironment enable the tumor to express specific characteristics. For example, cancer-associated fibroblasts activate fibroblasts irrevocably and take the role in the tumor microenvironment such as increased proliferation, and metastasis and gaining resistance to anticancer treatment. Of course, immune cells create

inflammation at the tumor site and produce toxic molecules such as reactive oxygen species (ROS) and nitric oxide (NO) [7].

Sometimes, it is possible to treat cancer but if it is not treated eventually cancer cells will grow in the other body parts. As a result of this invasion, organs will not be able to function in a normal way, and in the end death of the cancer patient will take place. Generally, cells reside in specific tissue and organ and the boundaries of the organ are distinct from each other via basement membranes that are built up of extracellular matrix elements such as laminin, collagen, and proteoglycans. As mentioned at the beginning of the chapter, one of the major characteristics of cancer cells is their spread, invasion, and migration to other body parts passing these basement membranes and this process is known as metastasis. Metastasis is the main concern to conclude that cancer cells have benign or malignant characteristics and it is affected by the cancer cells themselves and the tumor microenvironment (Figure 1.2). Along with this, generally, tumors are prone to metastasize to specific places in the body and it creates some problems such as the breakdown of the organ working and rivalry of normal cells with cancer cells for oxygen and nutrients [3].

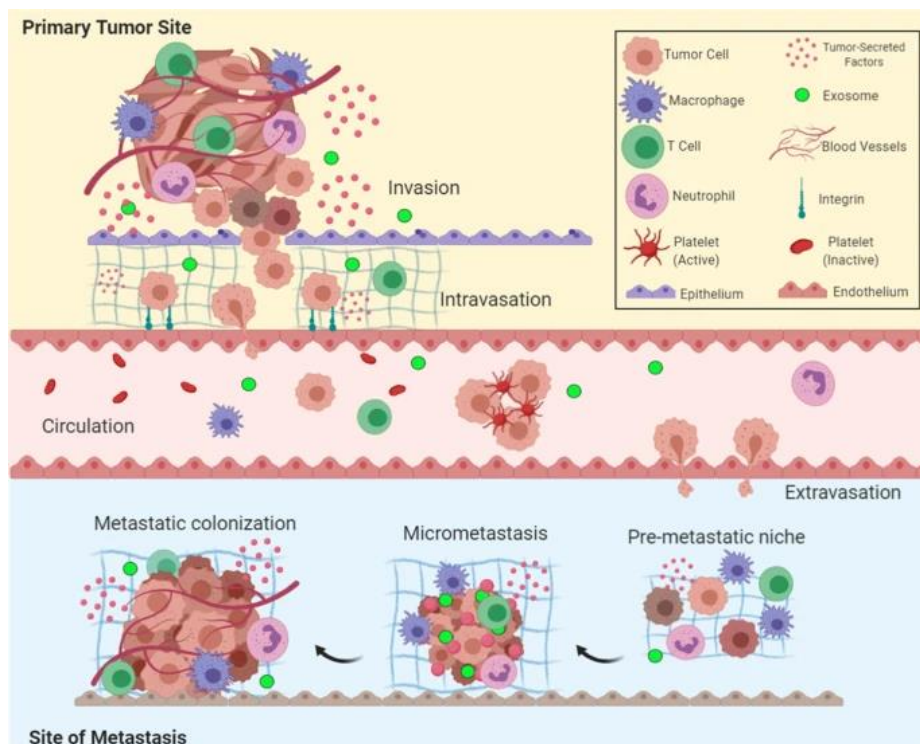


Figure 1.2: Cancer Metastasis: Invasion, Intravasation, Circulation, Extravasation, and Colonization [9].

This process begins with invasion in which cancer cells pass across and migrate the basement membrane, continues with intravasation which cancer cells pass into the vascular structure, circulation which cancer cells are involved in the bloodstream, extravasation which cancer cells pass through the vascular structure to organ site, and ends up with metastatic colonization which cancer cells start to colonize at the specific site [3], [9]. So, it is crucial to diagnose and treat any type of cancer in its stages. The most common cancer type among men with metastatic characteristics is prostate cancer, which causes a nonignorable impact.

1.1 Prostate Cancer

In men, prostate cancer ranks as the second most common cancer type after lung cancer, and it is the most aggressive cancer type regardless of disability, race, education, or income level [10]. This cancer type is characterized by adenocarcinoma, is diagnosed in older men, and is rarely diagnosed in men under the age of 40 [11]–[13]. When risk factors were looked at, it is observed that age, race, genetics, obesity, diet, and smoking increased the chance of developing prostate cancer. Approximately over the age of 45, being from the black race, mutations of genes such as the BRCA2 which are inherited, being obese, smoking, having chronic inflammation, infection, and diet that is high in calcium and dairy increase the prostate cancer risk. The deaths from this type of cancer also come from the beginning of the list being the fifth cause of death from cancer. It is estimated that approximately one man from every 25 men will be diagnosed with this type of cancer during their lifespan worldwide [10]. Moreover, 268,490 new cases of prostate cancer were expected and it is thought that there will be 34,500 deaths from prostate cancer in 2022 [14].

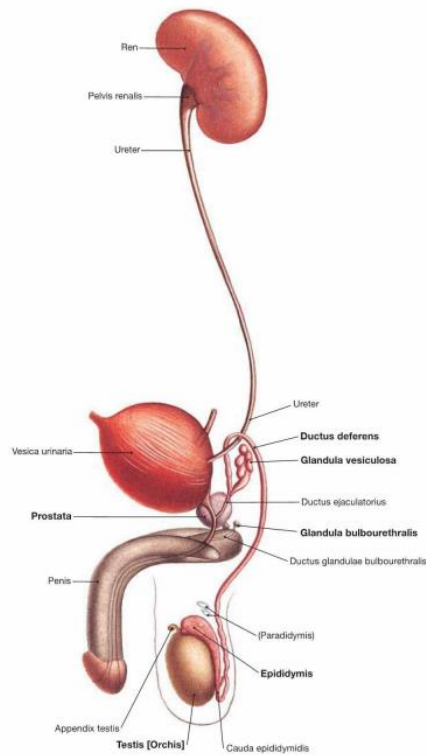


Figure 1.3: Localization of Prostate Gland in Male Reproductive System [15]

The prostate is an important element of the male reproductive system that is located below the bladder and surrounds the urethra shown in Figure 1.3 [16]. It is a small-sized exocrine gland that is responsible for the production of seminal fluid with seminal vesicles that help transportation of sperms (produced in testicles and matured in the epididymis) transport outside the body [10], [16]. Secretion of proteins from the prostate gland preserves sperm and makes semen jelly and fluidic. Also, prostate gland secretion preserves sperm from degradation in the vagina environment which is acidic and helps sperm to reach the egg [16]. Normally, the prostate tends to become larger due to its nature, and this benign prostatic hyperplasia. This condition should not be confused with prostate cancer because cells of this gland become cancerous after any mutation results in cancer [10]. Prostate-specific antigen (PSA) is the main secreted protein of the prostate gland that has importance in indicating prostate health. It is produced by the epithelial cells of the prostate. In healthy men, PSA is secreted into the prostatic ducts and moved away by seminal fluid. So, there is no way to enter these PSA into the bloodstream but it can exude from the ducts to the bloodstream in the condition that the prostate loses its organization due to any chronic inflammation and cancer. PSA production is affected by the androgen

steroid hormone and enables prostate cancer cells to survive and proliferate. Thus, the detection of the PSA in the blood indicates there is prostate cancer in the patient [16]. A biopsy is performed on the prostate, and PSA screening helps the diagnosis of prostate cancer, especially in developed countries. Especially, detection of PSA level enables the detection of prostate cancers that do not express any symptoms and early detection of prostate cancers. As mentioned above, it is normal for the prostate to become larger with age, the PSA level below 4 ng/mL is considered normal, between 4 and 10 ng/mL is considered at risk, and above 10 ng/mL is considered at high risk. With this test, earlier detection of prostate cancer before it metastasizes creates an opportunity to treat it locally and increases the survival from cancer. But, the PSA test may result in overdiagnosis. Because of this kind of scenario, a biopsy is performed after the PSA level is high to conclude that prostate cancer presents itself. After the diagnosis of prostate cancer, there are many different kinds of treatment options for the management of this type of cancer [10].

1.2 Anticancer Conventional Treatments

Of course, there is a global concern and effort in treating cancer at every stage of it. There are conventional anticancer therapy strategies that try to exhibit cytostatic (prevention of cancer cell proliferation) and cytotoxic effects (eradication of cancer cells). The first action for cancer treatment is the surgical removal of the cancerous parts but this treatment can fail in some conditions such as metastasis due to the total removal of all body parts being impossible. Because of this, metastatic cancer cells will be tried to be eradicated via chemotherapy and radiotherapy. But both are lacking in the meaning of selective cancer cell eradication due to broad-acting spectrum drugs of chemotherapy damaging DNA and inducing apoptosis of cells that divide rapidly. Also, side effects such as hair loss (alopecia), ulcer formation, and anemia can be observed because cells related to them also divide rapidly like cancer cells. Besides, conventional therapies are not tumor selective or not enough for tumor elimination due to the development of resistance against conventional therapies [3]. The resistance that cancer cells develop in response to chemicals or radiation. For example hypoxia, a low level of oxygen in the cancer tissue is the result of increased growth, and metabolic changes resulting in resistance against radiotherapy [7]. Mostly, chemotherapy does not work at any stage of cancer when cancer cells develop resistance after the

administration of the chemotherapy drug. Cancer cells create this resistance to specific drugs by inactivating them, inhibiting cell death, altering the metabolism of the drug, changing the target of the drug, and enhancing DNA-repair mechanisms and epigenetic factors [17].

When the issue comes from prostate cancer management, it is not different from the other types of anti-cancer treatments. The local prostate cancers which are not metastasized are tried to be eliminated via transurethral prostatic resection (TURP), radical and laparoscopic prostatectomy in which the total or some part of the prostate gland is surgically removed. Another option is radiotherapy in the form of brachytherapy where radiation is applied from the inside of the body using radioactive chemicals placed into the prostate or external beam radiotherapy where radiation is applied from the outside of the body where the prostate is present. Another treatment option is cryotherapy which uses the low temperature to kill cancer cells together with the prostate gland [10], [18]. With the discovery of a new treatment option for prostate cancer which is androgen deprivation therapy (ADT), surgical removal and radiation therapy used together with this treatment type has gained popularity. Androgen is a steroid man sex hormone and it stimulates the luteinizing hormone releasing hormone (LHRH) production. An Increase of LHRH in the bloodstream stimulates luteinizing hormone (LH) release and LH induces the production of testosterone in the testicles. Prostate cells convert testosterone to dihydrotestosterone and this converted version of the testosterone results in the activation of the transcription of genes related to the cell growth via tightly binding to androgen receptors. In addition to the testicles, the adrenal glands of the kidneys are also responsible for the production of the androgen hormone. So, ADT is a kind of therapy that works depending on hormones that aim to reduce the produced androgen level by surgical removal of testicles or using medicines that lower androgen levels produced by testicles and adrenal glands such as LHRH agonists and antagonists or medicines that stop the action of the androgen such as anti-androgens or hormones that suppress androgen such as female estrogen hormones [18]. Although this therapy is effective in the early stages, its efficacy can reduce due to the creation of androgen-independent prostate cancer over time. If prostate cancer does not respond to hormone therapy, more aggressive chemical drugs are involved in the treatment of prostate cancer. If prostate cancer does not respond to the hormone therapy and it metastasizes to the other parts of the body, chemotherapy is considered

and involved in the treatment. Several cytotoxic agents such as docetaxel, cabazitaxel, mitoxantrone, and estramustine are widely used chemo drugs [10].

Even though the presence of these anti-cancer treatments and their application for the management of prostate cancer in clinics, there are some drawbacks to these treatments. Risk of bleeding due to surgical removal, uneven irradiation distribution (which can increase the temperature) due to radiotherapy, cardiovascular problems due to lowering the testosterone level of the blood by ADT, erectile problem, osteoporosis, anemia and drug resistance due to chemotherapy can be thought as disadvantages [10], [18]. It is clear that resistance created by cancer cells to the specific type of anti-cancer treatments, especially to the used drugs is a problematic condition. Thus, creating and enhancing anti-cancer therapy so that cancer cells cannot develop any resistance is important and necessary to survive cancer [10]. There are many novel anti-cancer therapies and strategies that cancer cells do not express any resistance such as immunotherapy, cold atmospheric plasma application, nanotechnology, and targeted therapies (that aim for specific pathways related to cell growth, apoptosis, and progression of cancer) and laser therapies such as laser interstitial thermal therapy and photodynamic therapy [19]–[24].

1.3 Anticancer Photodynamic Therapy

Light can induce chemical reactions in the cells or tissues as known in the photosynthesis process in plants [25]. The benefits gained by photochemical reactions date back to ancient times. Phototherapy was used for the treatment of many diseases using the advantages of sunlight. Many skin problems and diseases such as vitiligo (lack of melanin pigment in the skin), rickets/osteomalacia (softening of bones), psoriasis (an autoimmune disease in the skin is inflamed), and skin cancer were treated with sunlight, especially in Egypt, China, Greece, and Rome (Figure 1.4). There are examples of phototherapy that were conducted with some plants in ancient Egypt for vitiligo treatment [26].



Figure 1.4: Phototherapy Conducted with *Ammi majus* plant via Sunlight in Ancient Egypt [26]

The rediscovery of it at the beginning of the 20th century enabled us to use this photochemical therapy for many purposes. From the days of the 20th century to these, phototherapy has been used for different purposes. In 1905, Von Tappeiner and Jesionek could treat lupus and genital wart using several chemicals such as eosin and fluorescein. Also, they could inactivate basal cell carcinoma using eosin and sunlight or a lamp. With these results, they laid the foundation of photodynamic therapy (PDT) which is now one of the building blocks of modern cancer treatment [26].

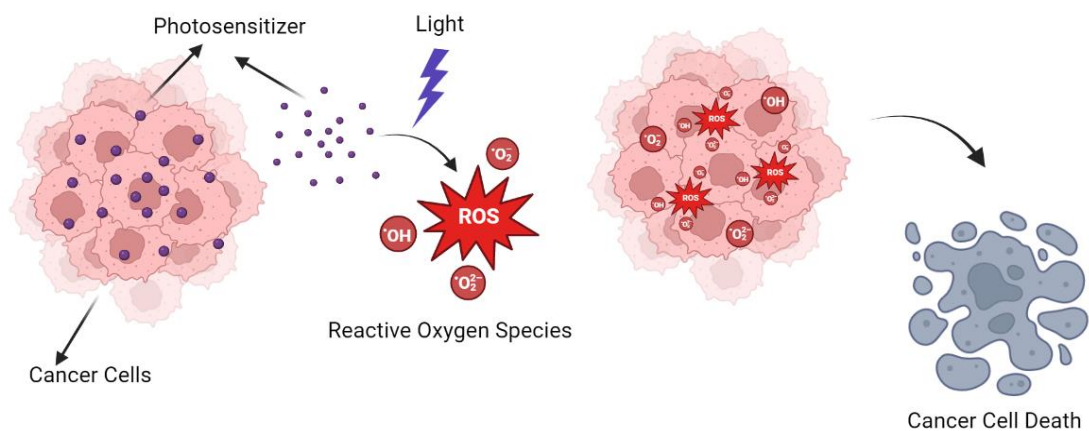


Figure 1.5: Anticancer Photodynamic Therapy (Drawn in BioRender)

PDT is a kind of photochemical interaction requiring the administration of non-toxic chemicals (via systemic, local, and topical administration) and light application that is used for the treatments of infection, diseases, and cancer non-invasively which shown in Figure 1.6 [25], [27]. This mechanism needs 3 main elements: a chromophore that absorbs light at a specific wavelength named photosensitizer (PS), a light, and molecular oxygen. To get photodynamic action, applied light whether from conventional light sources (such as light-emitting diodes (LEDs) or halogen lamps), or lasers should be absorbed by the PS or used light should be matched with the absorption spectrum of PS in other words (Figure 1.5). By that, together use of light and PS can induce cancer cell death while their separate use does not result in any cytotoxicity to them [28]. Energy transfer from light to the PS creates highly reactive cytotoxic chemicals that kill cancer cells. Reactive species especially reactive oxygen species (ROS) induce protein, lipid, and other cellular parts yielding cancer death. In PDT with the aspect of the clinic, first PS should be administered to the where cancer is present in the body to induce cancer cell death via different administration routes such as intravenous or topical. Then, a certain time is allowed for the cancer cells called incubation to uptake the PS into the cells, and light at a specific wavelength is applied to the tumor site superficially or interstitially. With the light application, photodynamic action induces photochemical reactions via the excitation of PS resulting at the end of cancer cell death [29].

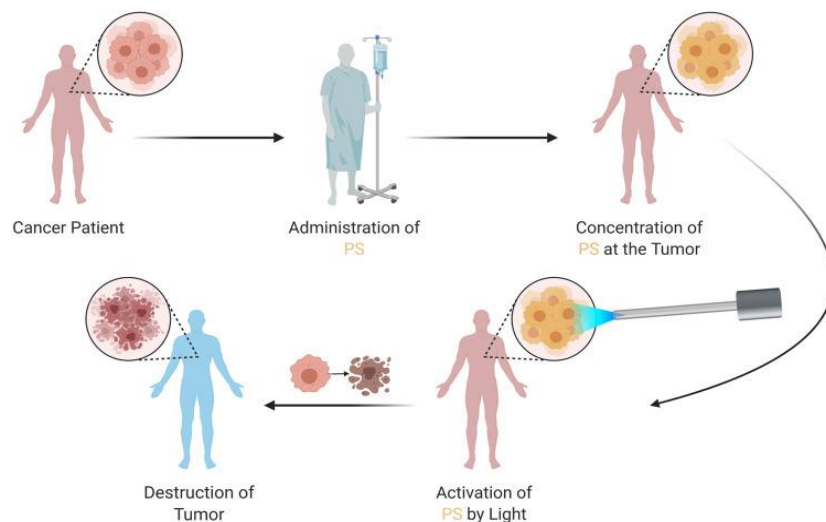


Figure 1.6: Application of Photodynamic Therapy: Steps include administration of PS, incubation of PS for localization at the tumor site, application of light activates PS, and cancer cell death [30].

PDT kills cancer cells via many pathways but mainly these can be categorized as to be direct and indirect cell death by PDT. Direct damage is obtained due to direct interaction with cancer cells via necrosis or apoptosis while indirect damage is due to the creation of hypoxia, and lessened nutrients via vascular damage and the creation of inflammatory response providing cytokines and inflammatory chemicals via the immune system shown in Figure 1.7 [27], [31].

Cancer cells die in two different ways programmed cell death (PCD) and non-programmed cell death processes such as apoptosis, autophagic cell death, and necrosis after PDT is applied. The type of the PCD is changed depending on the transferred energy dose of the light, cell type, oxygen partial pressure, localization, and incubation time of the PS [27], [32]. Induction of apoptosis occurs via localization of the PS. The mitochondria are the main organelle that regulates and controls the apoptotic pathways. Another localization site is the endoplasmic reticulum (ER) that PDT damage the calcium pumps and causes calcium ion release or Bax/Bak which are pro-apoptotic proteins causing a change in the mitochondrial membrane potential (MMP, $\Delta\Psi_m$). Due to the change in the MMP, pores of the mitochondrial membrane are opened and many proteins found in the intermembrane space are released into the cytoplasm [27]. Released proteins such as cytochrome c, the mitochondrial activator of caspases (SMAC), and apoptosis-inducing factor (AIF) are responsible for the induction of apoptosis. In the cytoplasm, cytochrome c combines with inactive forms of caspase 9 (Cas9) and caspase 3 (Cas3) which are responsible for the final stages of apoptosis taking place via inducing chromatin condensation and DNA fragmentation. A combination of them creates apoptosomes (protein structures formed in the apoptosis) that caspases are activated [27], [33]. Also, Bcl-2 apoptotic protein is released from the Bcl-2 gene which is the regulator. PS can also localize in the lysosome. After the PDT, lysosomal membrane disruption is disrupted and cathepsins (a kind of hydrolytic protein) are released into cytosol with the disruption. Cathepsins can activate Bid which is a proapoptotic protein and then apoptosis is induced through mitochondria [27]. Another PCD that is triggered by PDT is autophagy which is a process that enables cells to survive damaged components. If the damage in the cell is pretty much, autophagy induces cell death via autophagosomes (double membrane vacuoles) [27], [34]. PDT application results in autophagy via downregulation of PI3K/AKT-mTOR signaling related to cell cycle regulation (resulting in the reduction

in apoptosis and increase in proliferation) or upregulation of the AMPK pathway related to tumor suppression [34]. In addition, necrosis is a destructive cell death characterized by swelling, and plasma membrane integrity disruption together with inflammation and it can be induced by photodynamic action [32].

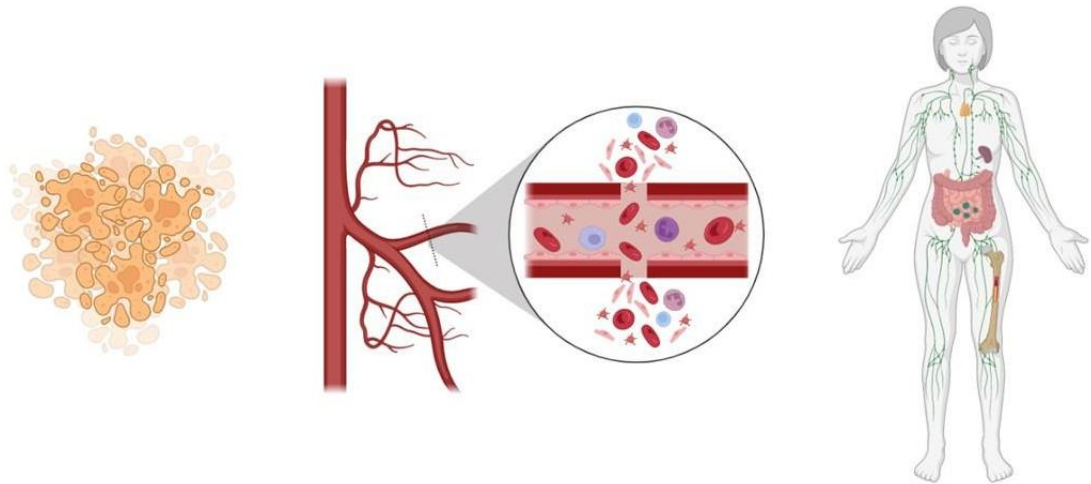


Figure 1.7: Effects of Photodynamic Therapy. PDT induces apoptosis/necrosis, damages tumor niche vasculature, and regulates the immune system via ROS.

(Drawn in BioRender)

Despite the direct cancer-killing whether apoptosis or necrosis, PDT also disrupts the vascular structure of the tumor. PSs that locate endothelial cells of vessels can be activated by the PDT. With the vascular structure disruption, cancer cells starve from oxygen and nutrients, and in the end, they die. Another indirect mechanism is an immune system that suppresses it after local PDT application while it is stimulated after non-local PDT. After the observation of apoptosis and necrosis via PDT, disruption of the tumor and homeostasis induce inflammatory conditions via cytokines, growth factors, and many proteins that we heard about and be familiar with from the COVID-19 pandemic as the cytokine storm [31]. These produced inflammatory products provoke immune cells to clear these apoptotic and necrotic tissues. Thus, PDT has an effect to regulate the immune system to induce cancer cell death via immunostimulation (by exciting cytokines $IL-1\beta$, $IL-6$ and blocking anti-inflammatory cytokines $IL-10$, $TGF-\beta$) or immunosuppression [31], [35].

1.3.1 Action Mechanism of Photodynamic Therapy

The action mechanism of PDT is basically based on the energy transfer from light to the PS and PS to the molecular oxygen in the environment. Absorption of light at a specific wavelength chosen depending on the absorption spectrum of PS by the electrons of PS causes the jump of the PS from the ground energy level to the higher energy state which is an excited singlet state [28], [36]. The lifetime of the electrons at this state is very short, approximately in nanoseconds which makes the interaction of electrons with any compound in this state not impossible. Because of this unstableness, electrons tend to lose their excess energy and lower themselves back to the ground energy level. Electrons lose their energy in the form of light (fluorescence) or heat while going back to ground level. Also, there is another chance that electrons lowered to another state which is above the ground state called a triplet excited state due to their change in electron spins, and this process is called an intersystem. Electrons can locate in this triplet excited state longer than the excited singlet state and shorter than the ground state with approximately milliseconds. The presence of electrons for a longer time at the triplet excited state enables time for them to interact with other compounds [36].

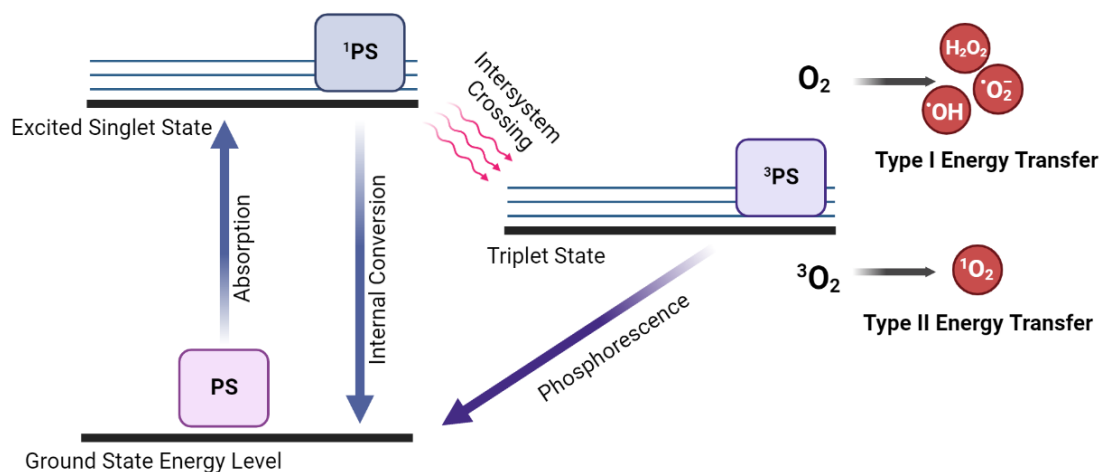


Figure 1.8: Jablonski Diagram Showing Photochemical Mechanisms of PDT: Type I and Type II Energy Transfer (Drawn in BioRender)

There are two possible photochemical mechanisms that could take in this state in the meaning of energy transfer and they are called photochemical mechanisms of PDT can be seen in Figure 1.8 (Type I and Type II photochemical mechanisms). These two

mechanisms may occur alone or together and their accruing percentage depends on the PS type and the environment. In type II photochemical reaction, the excess energy of the PS in the triplet excited state is transferred to molecular oxygen and singlet oxygen ($^1\text{O}_2$) is produced with this energy transfer. Produced $^1\text{O}_2$ interacts with many molecules in the cell and oxidizes proteins and lipids. Like type I photochemical reaction, the excessive energy of triplet excited state PS is transferred but this transferred energy (occurred via electron or hydrogen transfer in direct contact reaction) interacts with biomolecules in the cells producing free radicals. Because of the unstable characteristics of free radicals, they tend to interact with molecular oxygen rapidly and ROS such as superoxide radical ($\cdot\text{O}_2^-$), hydroxyl radical ($\cdot\text{OH}$), and hydrogen peroxide (H_2O_2) are produced. ROS are really oxidizing, cytotoxic, and highly reactive molecules that kill cancer cells via creating oxidative stress resulting in the deformations in proteins, lipids, membranes, DNA, and RNA. Type I energy transfer damages biomolecules violently [28], [36]. Depending on the accumulation location of PS, cytotoxicity can change. It is thought that accumulation inside the cell and membranes including cells and organelles results in a more destructive effect. In particular, the accumulation of PS in the cellular membrane causes the oxidations of lipids and proteins resulting in cell content leakage with the photodynamic action [28].

Denaturation of the protein structure via radicals (produced from type I and type II photochemical mechanisms) results in fragmentation, unfolding, and dimerization causing proteins to not function, and binding of metals or chemical compounds to the proteins causes aggregation. Protein fragmentation that is mediated by ROS involves the removal of hydrogen from the peptide chain and the reaction of this peptide chain with oxygen produces peroxy radicals of protein. Also, further reactions induce the cleavage of proteins resulting in inactive proteins. In addition, PDT causes cross-linking of proteins, especially proteins of membranes and ATPase enzymes [27]. Moreover, interactions of produced reactives (from type I and type II photochemical mechanisms) with phospholipids of the membrane (such as ER, lysosome, mitochondria, and cell membranes) cause lipid peroxidation via different steps including the removal of the hydrogen atom. The first step is the specific reaction, named ene reaction, in which singlet oxygen (produced via type II photochemical mechanism) interacts with lipids giving rise to the formation of hydroperoxide. Another step involves the direct interaction of lipids with type I photochemical

mechanism products. When hydrogen is separated from the unsaturated fatty acid, a lipid radical is formed and this process is unchangeable. Formed lipid radicals are added to their composition the oxygen forming the peroxy radical due to its short lifetime and this chemical starts another reaction that ended up with lipid hydroperoxide. Overall, phospholipid bilayer cell membrane integrity is disrupted in the end [27], [28].

1.3.2 Photosensitizers

Photosensitizing agents are an essential key of the PDT, without them, it cannot be possible to occur photodynamic action. PSs are responsible for light absorption and turn light energy into the formation of ROS via photochemical reactions which are an important element of PDT resulting in cancer cell death without causing any toxicity when irradiation does not occur. Many types of chemicals are used for PDT in the literature. Generally, PSs can be divided into three main categories to be first generation PSs, second-generation PSs, and third-generation PSs [31].

Hematoporphyrin (HpD) and porphyrin which is a kind of HpD belonged to the first-generation PSs that were used first. After the development of the PDT area, the need showed up for enhanced, and effective PS. For that need, second-generation PSs were started to be researched and used. They tried to solve the drawbacks of first-generation PSs by showing higher purity, higher formation of ROS, and deeper tissue penetration (tissue penetration increases by increasing the wavelength of light to 600-800-nm region) with fewer side effects [31], [37]. Chlorins, derivatives of chlorins, porphyrin derivatives, methylene blue, toluidine blue, phthalocyanines, indocyanine green, and aminolevulinic acid (ALA) belong to the second-generation PSs [31], [38], [39]. Lastly, third-generation PSs are another category that is specifically targeted for their accumulation at the tumor site reducing the damage to healthy tissues. This type of PSs is conjugated with biomolecules such as carbohydrates and proteins including antibodies or they are integrated into carrier systems such as nanoparticles and quantum dots [31], [37][31], [40]. There are also subgroups that can be considered as natural PSs in the second generation PSs, these are curcumin, riboflavin, and chemicals produced by microorganisms/plants such as anthraquinones, hypericin, hypocrellin, etc [38], [40].

It is thought that an ideal PS should express some features when an issue comes to it to obtain effective PDT. These features are listed below.

- PS should be capable of producing reactive species especially ROS and singlet oxygen.
- PS should absorb long wavelength light or it should have a high absorption coefficient in other words to reach deeper tumors where they present.
- PS should not express any toxicity in the dark environment, it should become cytotoxic when light is applied, and it should accumulate tumor sites selectively.
- PS should be chemically pure, stable, and easily administrable to the body.
- PS should absorb light at a specific wavelength that proteins of the human body such as melanin or hemoglobin do not absorb that wavelength.
- PS should not be expensive, and soluble in tissues including tumors.
- Lastly, PS should be cleared from the body [27], [37].

1.3.3 Light and Light Sources

Many types of light sources such as light-emitting diodes (LEDs), lasers, and even light bulbs that are used in houses were used to reach PDT. Although lasers are expensive, they are the most used light sources for PDT. Although lasers are an expensive choice due to the cost of their self and optical setup to transfer produced light through optical fiber cables, they are chosen because of their specific characteristics such as coherency, collimation, and monochromaticity with narrow spectral width. Produced laser light can be obtained with high output power, with a specific wavelength that matches only the PS absorption peak, with continuous or pulsed, and coherent light is created via stimulated emission. Among the lasers, the most used one is diode lasers for the photodynamic action which enables laser light between 600 and 1200 nm. This range of wavelengths is important for the treatment means reaching the tissues. Shorter wavelengths travel less in the tissue which can be problematic for deeper tumors. But, longer wavelengths such as 850-nm and above do not have enough energy to induce the effect (Figure 1.9). Because of these handicaps, PDT conducted with light between 600 and 850-nm is accepted as a phototherapeutic window [41].

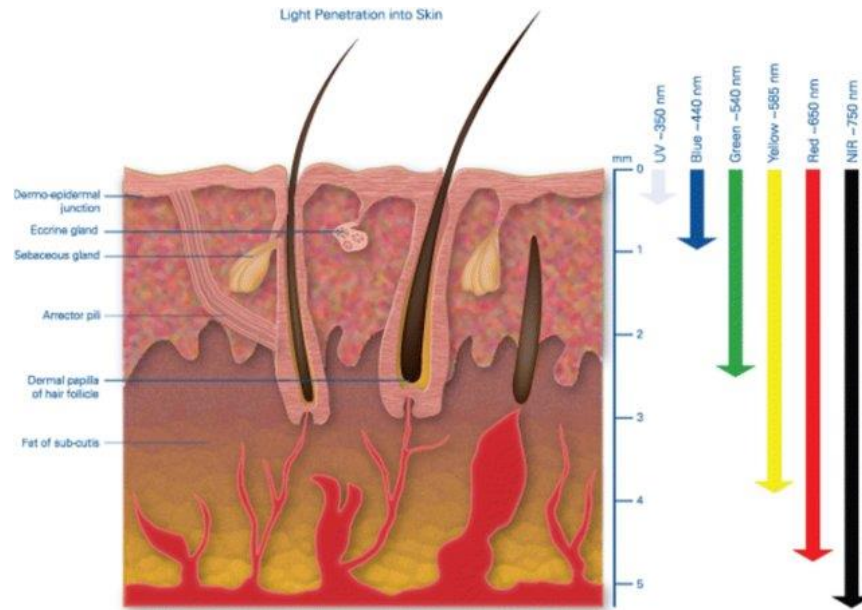


Figure 1.9: Light Penetration Depth in Tissue. Red light travels approximately 4 mm while near-infrared light travels 5 mm and above into tissue [42].

Another widely used light sources are LEDs which are used due to their low cost, easily reachable, and not easily damaged due to high temperature but the light of LEDs is produced via spontaneous emission which makes light incoherent [31]. Because of the incoherent characteristics of LEDs, emitted light diverges and has wide spectral width (main wavelength $\pm 5\%$) which means many wavelengths can be obtained. These properties affect the PS absorption and PDT efficacy of course. In the literature, it was observed that LEDs are used generally for superficial problems endoscopically or interstitially. Less used PDT light source is lamps including fluorescent and incandescent. They create light with a wide spectrum like LEDs can be considered as a disadvantage but they are not expensive, simple to use, and irradiate larger areas. In addition, there is a risk of burns by triggering another mechanism of photothermal therapy if irradiated too long or with high output power [41].

Used light source and PS to induce photodynamic action should be chosen according to two of them because applied light should match the peak of the absorption spectrum of PS and its excited atoms of it. In addition, light energy density should be optimized to obtain PDT and its destructive effects.

1.4 Strategies for Increasing the Efficacy of Anticancer Photodynamic Therapy

As mentioned in previous sections, PDT is an option for cancer treatment besides conventional treatments. This treatment modalities have more advantages than conventional ones such as no side effects, less invasiveness, destroying cancerous tissue together with their microenvironment vascular structure, no scar tissue formation, not being too expensive, selective cancer cell death due to accumulation of PSs at tumor site which explained by enhanced permeability and retention effect phenomenon due to irregular vascularization of tumor and insufficient lymphatic system drainage and selective irradiation at the tumor site [31], [43]. Although these advantages, PDT has some drawbacks and factors that their efficacy is reduced. PDT may not be enough in conditions where cancer metastasizes because of its local applicability [31].

All mechanism of the PDT resistance has not been solved but several conditions were revealed in the literature that takes place during the resistance against this anticancer treatment modality. These are explained step by step in the text. i) Drug resistance: Like chemotherapy drugs and radioresistance, resistance against PS can be formed via removing PS outside from the cell, processing of PS inside the cell, reducing the PS activity, and inactivation of PS showing a similar mechanism of these [35], [44]. It is thought that these characteristics, especially the efflux of PS is due to p-glycoprotein, and ATP-binding cassette (ABC) transporters that facilitate active transport. ii) Repair mechanism: stress formed after the PDT can induce repair mechanisms to heal biomolecule damages via activation of survival genes. iii) Antioxidant defense system: antioxidant defense system is another issue that inactivation of formed reactive species and inactivation diminishes or reduces the efficacy of the process [44]. Antioxidant defense system involves superoxide dismutase (SOD, which takes ROS into redox reaction and results in the formation of oxygen and H_2O_2 , catalase, lipoamide dehydrogenase), and glutathione system that remove ROS. iv) Apoptosis and autophagy: it is thought that apoptosis or autophagy is diminished after the PDT application. As known, PDT induces regulator signaling pathways of both related to increased apoptosis and increases damage repair at the same time. So, the reason

resulting in the elimination of cell death after PDT could be this. PDT may induce anti-apoptotic proteins of Bcl-2 when PS localizes in ER, and diminish apoptosis when PS localizes in the cell membrane. If the applied light energy density is not enough to induce apoptosis, another cell death mechanism dominates which is autophagy and this process can activate the cell survival after PDT. v) Heat shock proteins (HSPs): HSPs are other parameters that are induced due to PDT and reduce its efficacy of it. These are produced in the presence of stressors and PDT can change their expression to be upregulation via creating oxidative stress. vi) NO: NO itself can be toxic to cells or can induce a protective mechanism in the cells via several pathways related to oncogenes and ABC transports and this molecule can reduce the efficacy of PDT. At low NO concentrations, behaving like an antioxidant, can reverse the lipid peroxidations of cell membranes via capturing radicals. If this occurs during the PDT action, the destructive effect of this phototherapy is reduced and cells become resistant to the stress condition. It is shown in the literature that increased inducible nitric oxide synthase (iNOS) expression increases the resistance of cancer cells against PDT and reduces the activation of Cas3 and Cas9 [35], [44]. vii) Hypoxia: Many tumors express the hypoxic condition that is expressed due to increased proliferation, changed cell metabolism, and different vascularization and this low level of oxygen condition make cancer cells more aggressive and resistant to the treatment. It is known that PDT itself changes vascular structure where it is applied and depletes environmental oxygen during the application via expression of vascular endothelial growth factor (VEGF) through hypoxia-inducible factor 1 (HIF) alpha. This results in the additional hypoxic condition that may be cancer cells turn protective mechanisms and resulting in increased cell proliferation and self-survival [35], [45].

It is not surprising that PDT has drawbacks for cancer. To eliminate the drawbacks of this therapy mentioned above and increase its efficacy on cancer death via showing synergy between these two treatment modalities, PDT should be combined with other treatment options. The literature shows that it has been so. There are examples that PDT combined with conventional anticancer modalities such as chemotherapy, radiotherapy, immunotherapy, and novel anticancer treatment techniques such as the application of cold atmospheric plasma and nanotechnology [46]–[52]. Nowadays, combining another phototherapy, photobiomodulation, with PDT is gaining popularity which is normally not used for anticancer purposes.

1.4.1 Photobiomodulation

Photobiomodulation (PBM) or low-level light/laser therapy (LLLT) is a kind of non-invasive phototherapy that is obtained by generally especially red region of visible (VIS) and near-infrared (NIR) electromagnetic spectrum (between 600 and 1100-nm) and used for the reduction of inflammation, increased cell proliferation, and pain relief purposes. Different from the PDT, this therapy does not require any photosensitizing agent to induce photochemical interaction. Its chromophore is mitochondria inside the cells which are not PS. Also, the output of the light that is used for PBM purposes is not above 500 mW and the energy density of light is not high [53]. However, it is crucial to determine the parameters of PBM such as output power, energy density, application time, and wavelength of light which can be changed by cell type due to obtaining PBM because it shows a biphasic dose-dependent characteristic called the Arndt-Schultz curve. According to this rule, you get the therapeutic effects at specific parameters called therapeutic window and you get an enhanced effect by increasing the strength of light parameters [53], [54]. However, above the optimum parameter that you obtain the maximum therapeutic result for the specific disease, no therapeutic effect or even destructive effect is observed. Vice versa, you can not get any therapeutic effect below the therapeutic window [54]. Thus, it is vital to determine the effective parameters to induce the PBM mechanism.

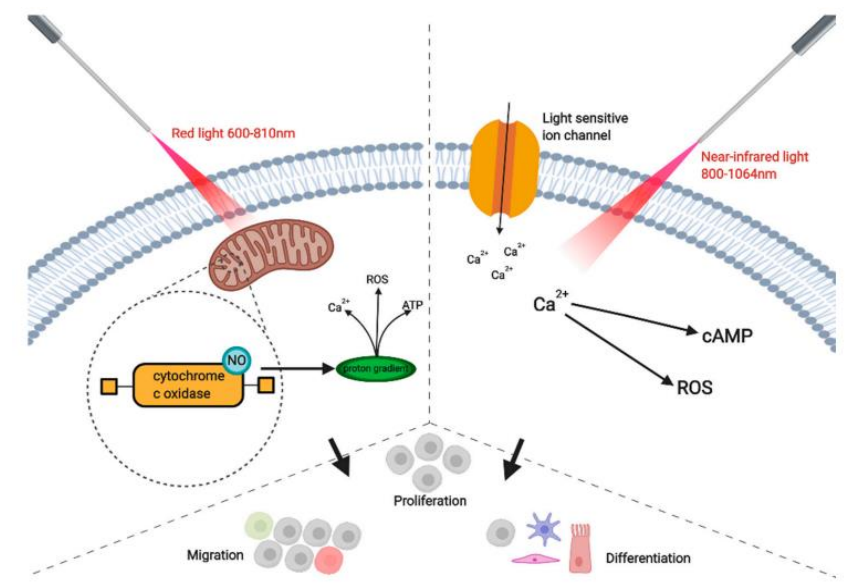


Figure 1.10: Effects of Photobiomodulation on Cells: Light can activate mitochondria and light-sensitive ion channels [53].

The underlying mechanism of PBM is not completely clear yet but there is some evidence that light is absorbed by mitochondrial elements. The wavelengths used for the PBM which vary between 600 and 1100 nm cover the absorption range of cytochrome c oxidase (Cox) transmembrane protein with between red 700 and 780 nm. Cox is the fourth and last element of the respiratory electron transport chain of mitochondria and is responsible for the reception of electrons from cytochrome c and delivery of them to oxygen forming water molecules. Also, this enzyme increases the electrochemical potential for the ATP synthase to produce ATP. Cox has four redox active metal centers such as two copper (Cu_A and Cu_B) and two heme (porphyrin with iron) (heme a and heme a_3) centers [24], [55]. Both centers can be reduced or oxidized, reducing oxygen to water and producing photons for ATP synthase [56]. After the photons of PBM-light are absorbed by Cox, activation of the enzyme results in increased ROS, MMP, ATP production, NO, and Ca^{2+} levels. Activation of pathways leads to increased protein synthesis, cell migration, proliferation, anti-inflammation, anti-apoptotic proteins, and antioxidant enzymes. PBM can do this by increasing the available electrons for the Cox enzyme and gradient results in the increase of MMP, ATP, and ROS levels (Figure 1.10 and Figure 1.11). Besides these, NO is increased in the cells after PBM application [55].

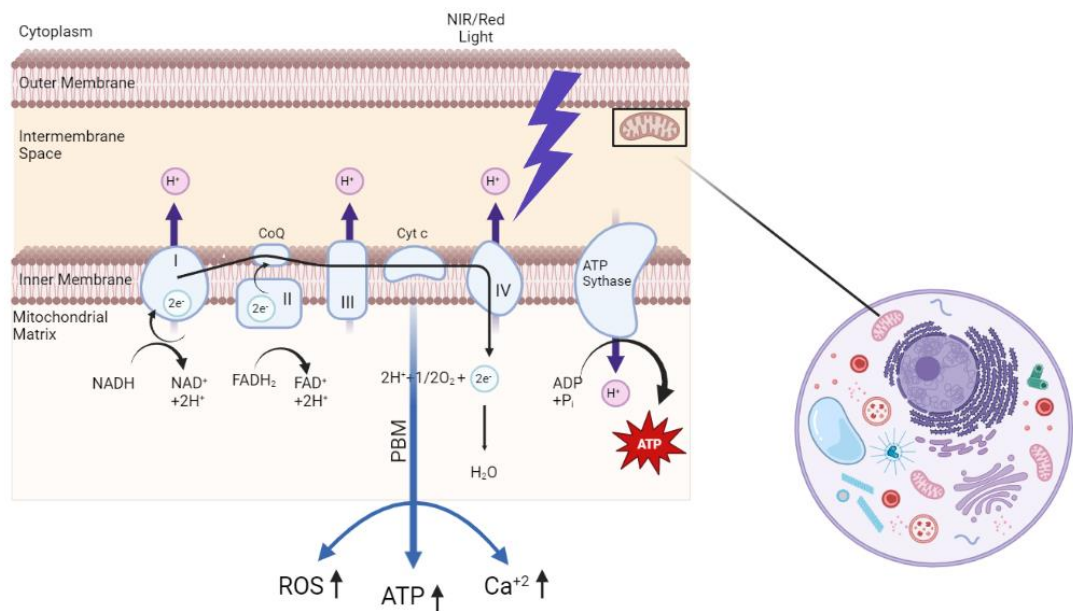


Figure 1.11: Photobiomodulation or Low-Level Light/Laser Therapy (Drawn in BioRender)

NO is related to the oxygen consumption of mitochondria and in some conditions such as activation of HIF for the control of the hypoxic condition and transmission of oxygen to distant cells, mitochondrial cell respiration (use of oxygen) is inhibited by NO binding to the Cox [57]. It is thought that release of excessive NO from the centers of Cox where its non-covalently binding sites via light application reverse the inhibition of cell respiration. Thus, NO release by the PBM starts respiration again via oxygen influx, and ROS are formed as a result. Also, NO can be released from the other binding sites after the light application. According to one theory, light absorption by Cox increases MMP causing increased ATP production due to increased gradient and ROS, Ca^{2+} , and NO increase. This occurs due to changes in mitochondrial structure triggering ATP production and ion passage from the changed mitochondrial pores [55], [56]. In another theory for the explanation of the PBM mechanism, light especially in NIR region application can activate and open light-sensitive ion channels and causing the depolarization of the membrane and increasing the intracellular Ca^{2+} , and ROS [53], [55].

Nowadays, the application of PBM, which its primary application is for proliferation, pain relief, and anti-inflammatory purposes not due to anticancer, on cancer cells to get more effective death is gaining popularity. It is really a debatable issue because the application of PBM into cancer cells can make them more resistant to any anticancer treatment type and result in increased proliferation of cancer cells which is not wanted. In the literature, there are examples of PBM that are combined with other conventional anticancer treatment options of radiotherapy or chemotherapy for the reduction of complications such as oral mucositis/radiodermatitis lesions and pain, or for the prevention of postoperative complications including peripheral neuropathy and oral mucositis via enabling supportive care [58]–[63]. In addition, there is an example that PBM increases the efficacy of radiotherapy inducing cancer death of HeLa cells. Researchers could induce cancer cells to radiotherapy by applying PBM [64].

In addition, there are examples of combined applications of PBM and PDT for anticancer applications. Tsai et al. applied PBM with 810-nm laser light at 1.5 J/cm² energy density before the PDT application with 652-nm lamp light at 1.5 J/cm² energy density on human osteosarcoma cancer cells after 2h incubation with 10 μM mono-L-aspartyl chlorin e6 (NPe6) *in vitro*. They observed higher cancer cell death and higher

ROS formation in combined application due to increased cellular uptake of the PS as a result of increased ATP production after the PBM [65]. Several years later, Negri et al. used the same hypothesis on human melanoma cancer cells. They used two different ruthenium phthalocyanine types as a kind of PS with 4 h incubation with the presence of PBM with 850-nm wavelength LED light at 4.5 J/cm² energy density, and then they experienced PDT application with 660-nm wavelengths LED light at 3 J/cm² energy density *in vitro*. For both PS types, combined PBM and PDT showed increased cancer cell death and they correlated this outcome with increased cellular uptake by increased ATP level after PBM [66]. In much closer years, Joniova et al. conducted a study that enhances PDT efficacy by PBM *in vitro* and *in vivo*. They irradiated human glioma cancer cells with different wavelengths ranging between 635 and 850-nm varying power intensities of laser lights for PBM and ALA PS is administered, then 3 h time is given for the endogenous production of PPIX PS after the PBM. Cells received 405-nm laser light PDT at 2.5 J/cm² energy density *in vitro*. Researchers optimized that most endogenous PPIX-producible PBM light and relative to this conclusion, they observed increased cell death in PBM applied before the PDT group. Also, they correlate the enhanced cell death with the increased amount of ROS production together with singlet oxygen and decreased MMP. Another part involved *in vivo* studies. The selected wavelength, 635, 730, and 808-nm, for PBM, were applied to the tumor site, and then 405-nm laser light at 50 J/cm² energy density was used for PDT. Researchers observed similar effects of optimized *in vitro* parameters *in vivo* also [67]. de Faria et al. investigated the effect of PBM at 780-nm light and 5 J/cm² energy density on two different squamous carcinoma cell lines *in vitro*. They conducted PDT with 630-nm light at 15 J/cm² energy density in the presence of Photogem® PS after 4 h incubation. They observed different outcomes in the meaning of cell viability depending on cell types. In one cancer cell type, prior application of PBM results in higher cell death than that is obtained by PDT due to increased uptake of PS and ROS production but the outcomes of PBM on other cancer cell type is different than the result obtained by PDT [68]. According to the results of de Faria et al., an idea of PBM application before the PDT changes from cells to cells. Also, when the analyses that were checked in those studies are not enough to explain the PBM effect on cancer cells and the PBM effect that increases/decreases the efficacy of photodynamic action.

In this study, it was asked and investigated that human prostate cancer cells, which are the second most common cancer type among men, would show increased cell survival via turning on cellular self-defense or increased cell death via showing elevated PDT process when it is combined with PBM. If pre-treatment of PBM on prostate cancers shows increased or decreased cancer cell death, what are the main contributors to this result? These questions were tried to be answered in this study via various analyses. For that aim, it was hypothesized application of PBM which is not used for anticancer purposes before the PDT enhances the efficacy of photodynamic action and it was investigated whether PBM therapy has an effect on PDT on human prostate cancer cells using 655 and 808-nm laser light. In addition to cellular viability investigations, several mechanistic analyses such as cellular uptake of PSs, and ATP synthesis after PBM; ROS production, MMP change, and NO release after both PBM and PDT were determined. Also, the groups that showed significantly increased cell death over the only PDT experienced live and death analysis via staining.

Chapter 2

Materials and Methods

This study generally includes two main sets. It is aimed to increase the efficacy of photodynamic therapy, and get more effective anticancer treatment via applying photobiomodulation on human prostate cancer cells before the photodynamic therapy applications. In the first main step, 655-nm red diode laser light was applied to human prostate cancer cells for the photobiomodulation process and then cells were irradiated with 808-nm near-infrared diode laser light after specific incubation times with indocyanine green for photodynamic action. This first main set also includes two sub-main steps in which incubation times differ. There are two different incubation times of indocyanine green 1h and 24h with human prostate cancer cells. In the second main step, 808-nm near-infrared diode laser light was applied to human prostate cancer cells to induce photobiomodulation and then cells were radiated with 655-nm red diode laser light after specific incubation times with chlorin e6 for photodynamic therapy. This main step also includes two sub-main steps like the first main step where the incubation times differ. As an incubation time, chlorin e6 was incubated for 2h and 24h with human prostate cancer cells. After the application of photodynamic therapy, cell viability analysis was conducted on human prostate cancer cells. In addition to the cell viability, cellular uptake of photosensitizers after photobiomodulation (with both 655 and 808-nm diode laser lights); the amount of produced ATP after photobiomodulation (with both 655 and 808-nm diode laser lights); live and death analysis via staining after Ce6-mediated photodynamic therapy; the amount of NO released, the amount of produced ROS, change in MMP after photobiomodulation (with both 655 and 808-nm diode laser lights) and Ce6-mediated photodynamic therapy were determined.

2.1 Cell Culture

PC3 human prostate cancer cell line (ATCC CRL-1435) which was supplied by the Bioengineering Department of Ege University was used in this study. The PC3 cells were grown for proliferation in 75 cm² tissue culture flasks in RPMI-1640 cell culture medium (Sigma Aldrich, St. Louis, MO, USA), including 1% L-Glutamine, 1% Penicillin-Streptomycin (Sigma Aldrich, St. Louis, MO, USA), and 10% Fetal bovine serum (FBS) (Capricorn Scientific GmbH, Ebsdorfergrund, DE) at 37 °C and 5% CO₂ humidified atmosphere. The cell culture medium of PC3 cells was changed and replaced every 2 days for a week. PC3 cells were incubated up to their confluency reached 80% and over. After the PC3 cells reached 80% and over confluency, they were detached from the surface where they reside using Trypsin-EDTA 10X (Sigma Aldrich, St. Louis, MO, USA) diluted to 1X with Phosphate Buffered Saline (PBS) (Sigma Aldrich, St. Louis, MO, USA) after washing the cells with PBS. After the detachment of the cells from the surface of the 75 cm² tissue culture flask, 1x10⁵ cells per well were seeded to a 96-well plate to be used in the experiments.

2.2 Photosensitizers

One of the anionic photosensitizers, Indocyanine Green (ICG) (Santa Cruz Biotechnology, Dallas, TX, USA) which its chemical structure shown in Figure 2.1, and one of the cationic photosensitizers, Chlorine e6 (Ce6) (Santa Cruz Biotechnology, Dallas, TX, USA) which its chemical structure shown in Figure 2.2 were used in this study.

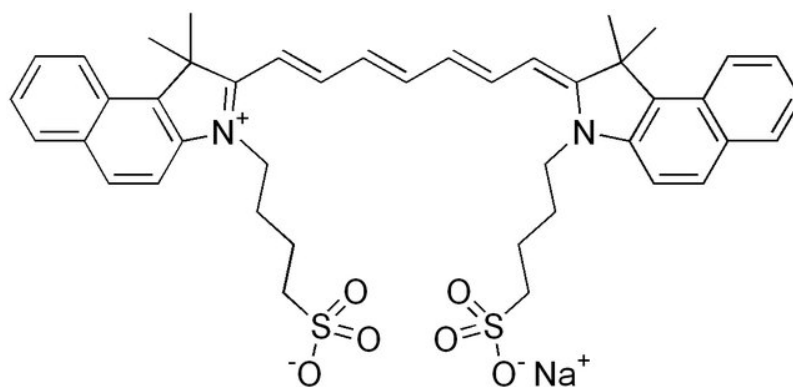


Figure 2.1: Chemical Structure of Indocyanine Green [69]

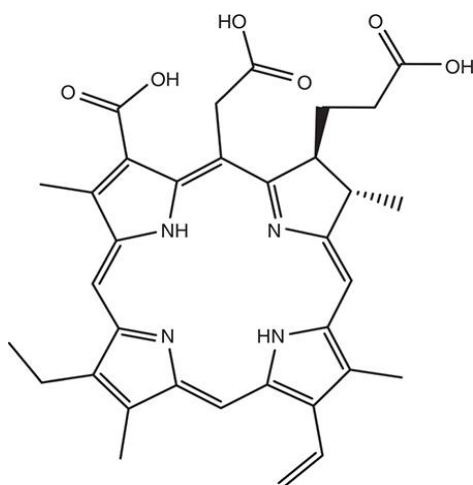


Figure 2.2: Chemical Structure of Chlorin e6 [70]

Stock solutions of ICG and Ce6 were prepared using RPMI-1640 cell culture medium and diluted using the same cell culture medium. ICG stock solution was diluted to obtain 25, 50, and 100 μM concentrations and Ce6 stock solution was diluted to get 2.5, 5, 10, and 25 μM concentrations freshly before performing each experiment.

2.3 Light Sources and Optical Setup

808-nm diode laser (Teknofil, Istanbul, Turkey) and 655-nm diode laser (PS4 III. LED; Changchun New Industries Optoelectronics Tech. Ltd., China) were used as light sources (see Figure 2.3).

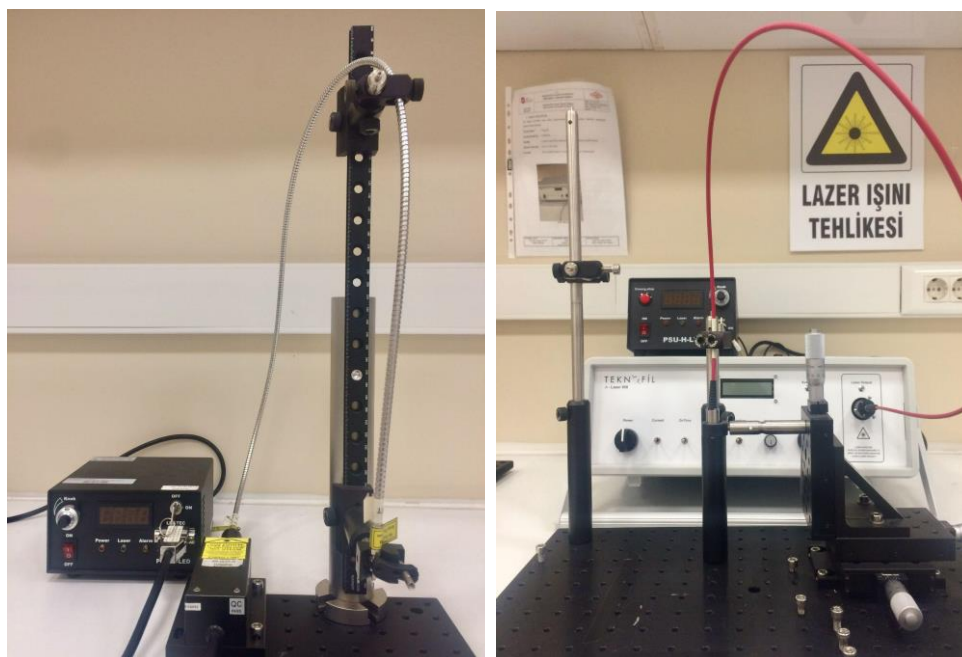


Figure 2.3: 655-nm Diode Laser Device (left) and 808-nm Diode Laser Device (right)

By these laser devices, near-infrared 808-nm, and red 655-nm diode laser light were obtained and used for the experiments. Both 808-nm and 655-nm diode laser devices gave continuous mode of radiation through optical fiber with 2 W and 1 W maximum output power respectively. Laser devices were placed on the optical fiber using various optomechanical equipment to irradiate samples. The tip of the 808-nm diode laser optical fiber and the optical plate was kept constant at 12 cm while the distance between the optical fiber of the 655-nm diode laser and the optical plate was kept constant at 8 cm. From that distance, 808-nm laser light created a circular area of 2.3 cm in diameter and 4.155 cm² in the area, and 655-nm laser light created a circular area of 1.25 cm in diameter and 4.909 cm² in the area that can irradiate the 4 wells of the 96-well plate. The output power of both 808-nm and 655-nm diode lasers was arranged to 0.4 W and applications were performed at that output power. The output of both diode lasers was measured and controlled by a digital power meter (Thorlabs, Newton, NJ, USA) before performing each experiment.

Using Equation (2.1) the application of time needed to get a certain energy density was calculated, and samples were irradiated with these times.

$$\text{Energy Density (J/cm}^2\text{)} = \text{Power (W)}/\text{Area (cm}^2\text{)} \times \text{Time} \quad (2.1)$$

Energy densities of 1, 3, 5, and 100 J/cm² of 808-nm laser light were obtained by application of 18, 54, 90, and 1226 s. Energy densities of 1, 3, 5, and 50 J/cm² of 655-nm laser light were obtained by application of 10, 31, 52, and 900 s.

2.4 PBM-induced Anticancer PDT Applications

Two different sets were created. The first set was irradiated with 655-nm diode laser light for PBM purposes and experienced PDT with the 808-nm diode laser light after different incubation times with ICG. The other set was irradiated with 808-nm diode laser light for PBM purposes and experienced PDT with the 655-nm diode laser light after different incubation times with Ce6 shown in Figure 2.4. Each set includes seven experimental groups with three samples as followed;

-Control Group: Group that experienced neither PS addition nor light application

-PS Group: Group that incubated with PS only

-Laser Group: Group that irradiated with 655-nm light at 50 J/cm² energy density or 808-nm light at 100 J/cm² energy density

-655-nm PBM Group: Groups that irradiated with 655-nm light at 1, 3, or 5 J/cm² energy density

-808-nm PBM Group: Groups that irradiated with 808-nm light at 1, 3, or 5 J/cm² energy density

-Only PDT Group: Group that irradiated with PDT laser light after the specific incubation time of the PS

-PBM+PDT Group: Group that experienced pre-treatment of PBM with laser light and then irradiated with PDT laser light right after the specific incubation times of PS

After the PC3 human cancer cells reached 80% confluency and above, 1x10⁵ cells per well were seeded to a 96-well plate. After their seeding, the cells were incubated

for 24 h at 37°C, and 5% CO₂ humidified atmosphere allowing them time to adhere to the surfaces of the 96-well plate. Then, the RPMI-1640 cell culture medium of prostate cancer cells was removed, different concentrations of PS solutions were added, and cells were incubated with PS for different times in only the PDT group at 37°C, and a 5% CO₂ humidified atmosphere. After incubation of cells, PS solutions were removed and cells were washed once with PBS to get rid of PS present around the cells and get only PS entered inside the cells. And, then fresh cell culture medium was added to the cells, and cells were irradiated with 655 or 808-nm diode laser light that had 0.4 W output powers to the cells for PDT action. In the PBM+PDT group, the cell culture medium of the cancer cells was removed after their seeding and a fresh cell culture medium was added to the cells. nm the cells right after the PBM application. Different concentrations of PS solutions were added immediately and cells were incubated for different times at 37°C, and 5% CO₂ humidified atmosphere. Then, PS solutions were removed and cells were washed once with PBS to get rid of PS present around the cells and get only PS entered inside the cells done in only the PDT group. And, then fresh cell culture medium was added to cells, and cells were irradiated with 655 or 808-nm diode laser light that had 0.4 W output powers to the cells for PDT action done in only the PDT group.

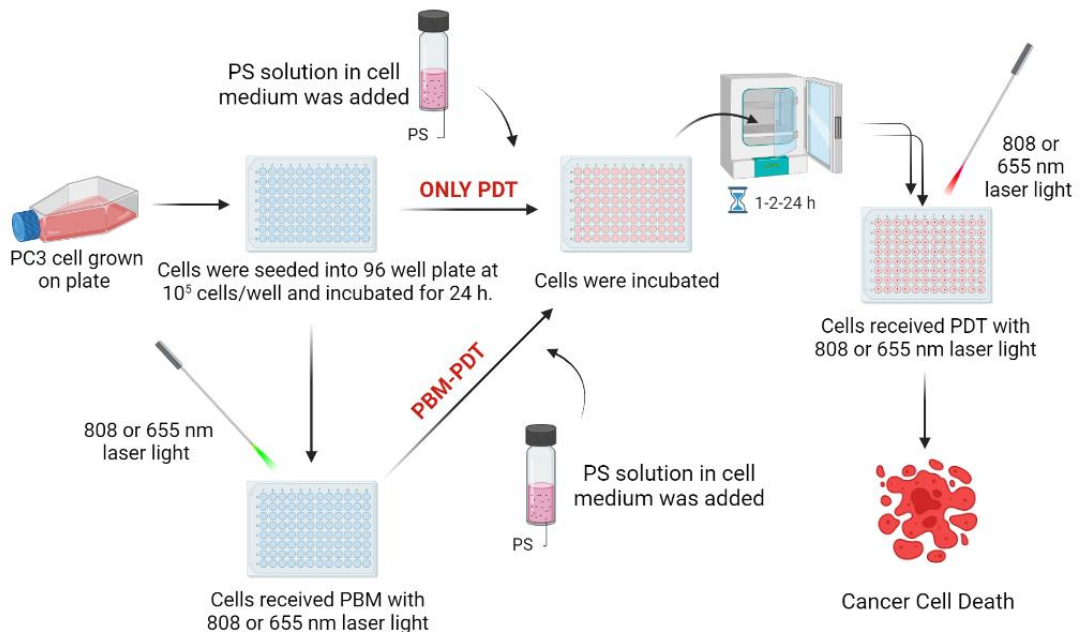


Figure 2.4: Illustration for the Experimental Setup (Drawn in BioRender)

In the PS group, different concentrations of PS solutions were added after the removal of the cell culture medium of PC3 human prostate cancer cells, and the cells were incubated at different times at 37⁰C, and 5% CO₂ humidified atmosphere. Then, PS solutions were removed and cells were washed once with PBS. In the laser, 655-nm PBM, 808-nm PBM groups, fresh cell medium was added to cells and 655 or 808-nm diode laser light that had 0.4 W output was applied to cells. Lastly, cells were incubated with the cell culture medium at 37⁰C, and a 5% CO₂ humidified atmosphere to provide equal conditions in the control group. After the applications were done for each group, necessary analyses were performed.

2.4.1 655-nm PBM-induced ICG-mediated PDT Applications

One set of the study used 655-nm diode laser light for the PBM purposes and 808-nm diode laser for the PDT with the presence of three different ICG concentrations which differ between 25 and 100 μ M. The output power of the 655-nm diode laser was arranged to 0.4 W and applied to PC3 human prostate cancer cells for 10, 31 and 52 s to deliver 1, 3, and 5 J/cm² energy density respectively. The same output power of the 655-nm diode laser was arranged to the 808-nm diode laser as 0.4 W. This set is also subdivided into 2 subsets in which the incubation time of PS with the cells differs. The cells were incubated with ICG for 1 or 24 h. After the incubation of 25, 50, and 100 μ M ICG with the cells, cells were irradiated with 808-nm diode laser light for 1226 s to deliver 100 J/cm² energy density. The cell viability and cellular uptake of ICG were determined after the applications were completed for all control, PS, laser, only PDT, and PBM+PDT groups.

2.4.2 808-nm PBM-induced Ce6-mediated PDT Applications

The second set of the study involves the 808-nm diode laser light PBM and Ce6-mediated PDT conducted with 655-nm diode laser light to PC3 human prostate cancer cells. The concentrations of Ce6 differ between 2.5 and 25 μ M were used in the PDT applications. Both outputs of 808 and 655-nm diode laser devices were kept at 0.4 W. PBM was performed on the prostate cancer cells with irradiating 808-nm diode laser for 18, 54, and 90 s to deliver 1, 3, and 5 J/cm² energy density respectively. PDT was conducted with 2.5, 5, 10, and 25 μ M of Ce6 concentrations and 655-nm diode laser

light at 50 J/cm² energy density (reached by applying 900 s). This set includes two different incubation times of Ce6 with cells at 2 and 24 h. The cell viability, cellular uptake of Ce6, NO release, and MMP change analyses were performed after the applications were completed for all control, laser, only PDT, and PBM+PDT groups

2.5 Cellular Uptake Analysis of Photosensitizers

Triton X-100 analysis (Sigma Aldrich, St. Louis, MO, USA) is a nonionic surfactant causing cells to lyse. By the lysing of cells, intracellular contents are extracted. So, it was used to determine the amount of PS that entered the PC3 human prostate cancer cells. This analysis was performed to determine whether more PS cells entered the PBM-treated cells before the PDT applications. The Triton X-100 application solution was prepared which was 30% Triton X-100 and 70% DMSO and absolute ethanol. Then this solution was added to PC3 human prostate cancer cells after their specific incubation with PS (1 and 24 h for ICG while 2 and 24 h for Ce6). Also, this solution was added to the cells after PBM applications (1, 3, and 5 J/cm² for both wavelengths) and following specific incubation with PS. Then, spectrum analysis was conducted between 300 and 900 nm of wavelengths with a multi-plate microplate reader (SynergyTM HTX Multi-Mode Microplate Reader, BioTek, Winooski, USA). The absorbance values at the wavelength that PS absorbance gives peak were correlated to conclude that PBM effect on cellular uptake of PS.

2.6 Cell Viability Analysis

MTT cell viability assay was used for the determination of cellular viability using 3-(4, 5- dimethylthiazol-2yl)- 2,5 diphenyl tetrazolium bromide (MTT) (Sigma Aldrich, St. Louis, MO, USA). This assay is a colorimetric assay and determines cellular viability according to color change. MTT has a yellowish color itself due to tetrazole but under metabolic activity, MTT is converted to formazan crystals that have a purple color via the succinate dehydrogenase enzyme of the inner mitochondrial membrane which takes part in the electron transport chain shown in Figure 2.5. The absorbance value of purple formazan crystals was measured spectrophotometrically and gives cell viability [71], [72].

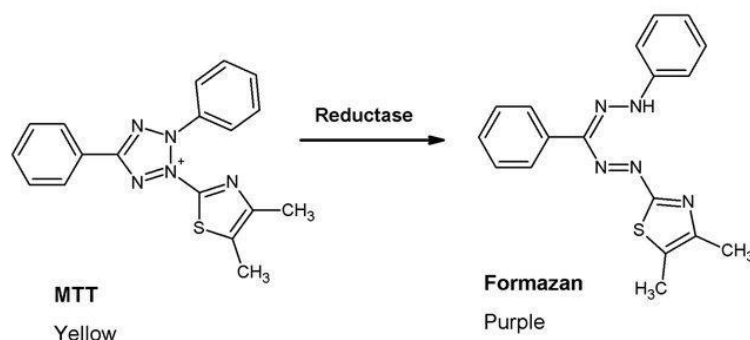


Figure 2.5: Conversion of MTT to Formazan Crystals [73]

MTT assay was performed for cell viability of all experimental groups. MTT stock solution was prepared at 5 mg/mL concentration in distilled water. This 5 mg/mL MTT stock solution was diluted into a 10% MTT solution with a serum-free RPMI-1640 cell culture medium. After all, experiments were performed, the cell culture medium was removed from PC3 human prostate cancer cells and 100 μ L 10% MTT solution was added to each well of the 96-well plate. Cells were incubated for 2 h at 37^oC, and a 5% CO₂ humidified the atmosphere. Then, 10% MTT solution was removed from the cells and 100 μ L dimethyl sulfoxide (DMSO) (Merck KGaA, Darmstadt, DE) was added to wells. After the formazan crystals were dispersed in DMSO, absorbance was measured using the multi-plate microplate reader (Synergy™ HTX Multi-Mode Microplate Reader, BioTek, Winooski, USA) at 570 nm of wavelength. All steps of MTT analysis were performed in the dark to prevent deterioration of MTT.

2.7 Nitric Oxide Release Analysis

The amount of NO released after the light applications were measured. It was determined after both PBM for two wavelengths and Ce6 mediated-PDT applications were completed to obtain the amount of NO caused by PBM itself and PDT. NO is an unstable molecule that is oxidized to nitrite form. For the detection of NO indirectly through nitrite, a Griess Reagent kit (Biotium, Fremont, CA, USA) was used. Griess Reagent kit contains sulfanilic acid and N-(1-naphthyl) ethylenediamine. Sulfanilic acid is converted to diazonium salts by nitrite in an acidic environment. Then formed salts combined with N-(1-naphthyl) ethylenediamine which is an azo dye that gives color shown in Figure 2.6.

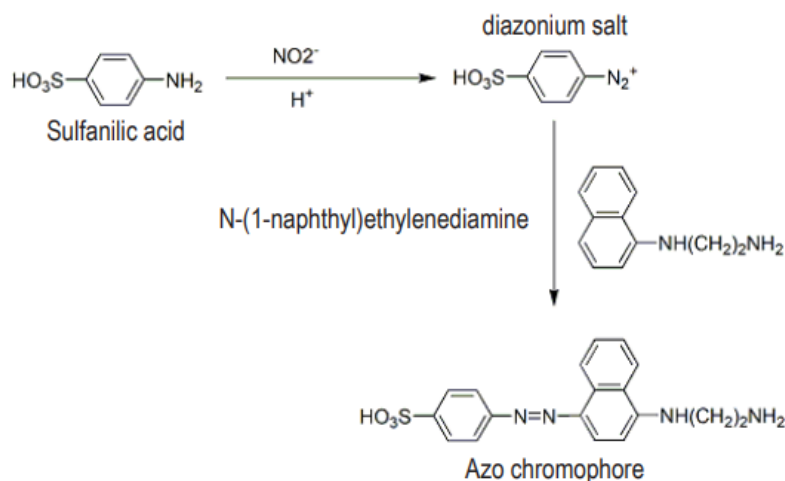


Figure 2.6: Conversion of Sulfanilic Acid to Azo Dye [74]

By measuring the absorbance at 548 nm, the amount of NO can be detected spectrophotometrically. After the applications, a specific volume of supernatant in the cell medium of treated-PC3 human prostate cancer cells was mixed with the same volume of the Griess Reagent solution containing 13.4% Griess Reagent and 86.6% deionized water and incubated for 30 minutes at dark to prevent the breakdown of the dye and losing any signal. After the incubation time, absorbance was measured using the multi-plate microplate reader (Synergy™ HTX Multi-Mode Microplate Reader, BioTek, Winooski, USA) at 548 nm of wavelength. The amount of nitrite in each experimental group was calculated according to the equation gained via the standard curve of nitrite solution curve which was plotted at different concentrations of standard nitrite solution of the Griess Reagent kit.

2.8 ATP Production Analysis

The CellTiter -Glo® 2.0 cell viability assay (Promega Corporation, Madison, WI, USA) was used for the detection of produced ATP after PBM applications for both wavelengths. The assay is generally used for the count of living cells but it determines cell viability through the amount of ATP present in the cells. The oxidative enzyme of luciferase interacts with luciferin which is a light-emitting compound and oxidizes the luciferin to oxyluciferin in the presence of Mg^{2+} and ATP. This produced oxyluciferin is bioluminescent, so its luminescence measurement can be quantified using this assay

shown in Figure 2.7. The amount of ATP present is directly proportional to the produced luminescence. So, the detection of luminescence gives the amount of ATP.

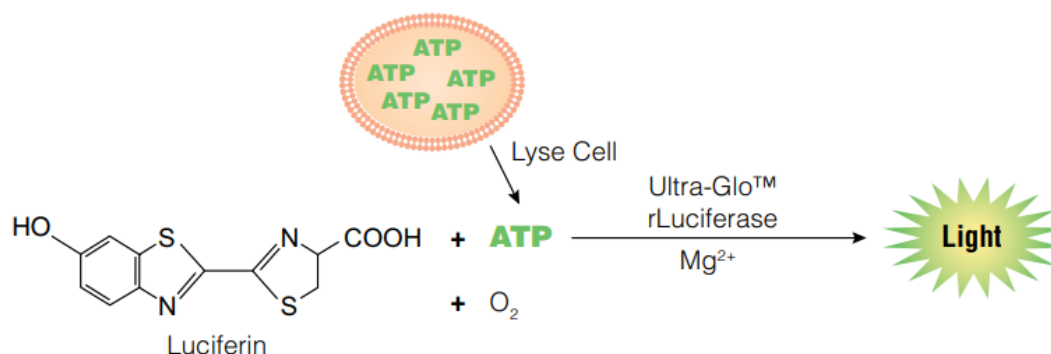


Figure 2.7: Conversion of Luciferin to Oxyluciferin [75]

After applications were completed, a 96-well plate was incubated at room temperature for 30 minutes to equilibrate the content. Then the 100 μ L CellTiter -Glo® 2.0 Assay was added over the 100 μ L PC3 human prostate cancer cells present in the RPMI-1640 cell culture medium (equal volume 1:1). Then, the 96-well plate experienced orbital shake for 2 minutes for cell lysis and got ATP consent into the solution. After the lysis of cells, the 96-well plate was incubated at room temperature for 10 minutes to stabilize the luminescence signal. The luminescence signal was measured at 490 nm wavelength.

2.9 Intracellular Reactive Oxygen Species Production Analysis

The intracellular produced ROS was determined via intracellular ROS production analysis after both PBM applied with two wavelengths and Ce6 mediated-PDT applications were completed. For the ROS assay, 2',7'-Dichlorofluorescein diacetate (DCFH-DA) (Sigma Aldrich, St. Louis, MO, USA) which is a lipophilic and non-fluorescent probe was used. DCFH passes through the cell membrane via passive diffusion and deacetylation. The deacetylated form is 2',7'-Dichlorofluorescein (DCFH) that can be oxidized to DCF which is a highly fluorescent compound in the presence of ROS shown in Figure 2.8. Thus, the measured amount of DCF is directly correlated with the amount of produced ROS.

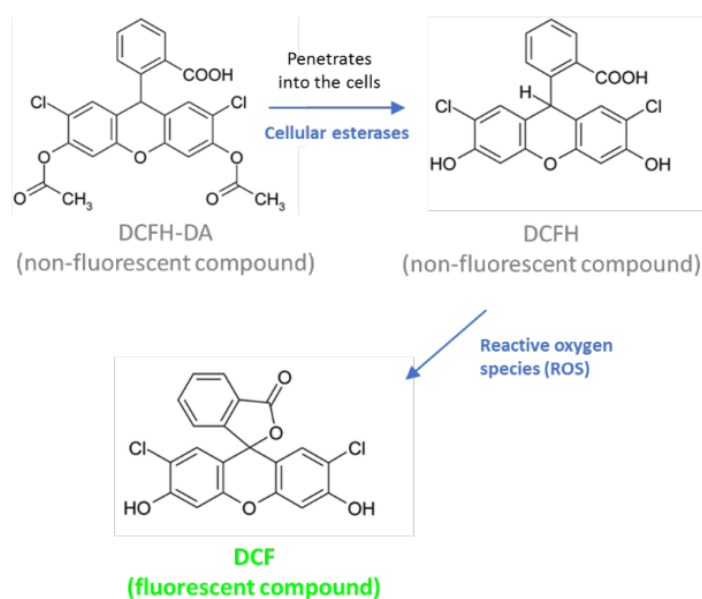


Figure 2.8: Conversion of DCFH-DA to DCF [76]

The stock DCFH-DA solution was prepared at 40 mM in DMSO. Then, this stock solution was diluted to 0.1 mM using RPMI-1640 cell culture medium containing 1% FBS. The supernatant cell medium was removed 24 h after the seeding of the cells, before performing the experimental protocol. 0.1 mM diluted DCFH-DA solution was added to PC3 human prostate cancer cells and cells were incubated for 45 minutes at 37⁰C, and a 5% CO₂ humidified the atmosphere in the dark. After the incubation time, the DCFH-DA solution was removed and the cells were washed twice with PBS to eliminate DCFH-DA that is not entered the cells. Then, the cell culture medium was added to the cells and the experimental protocol was applied. After the completion of all applications, the fluorescence intensity of DCF was measured at a multi-plate reader using 485/20 nm wavelength for excitation and 528/20 nm wavelength for emission.

2.10 Mitochondrial Membrane Potential Change

Analysis

The change in the MMP after both PBM applied with two wavelengths and Ce6 mediated-PDT applications using JC-1 Mitochondrial Membrane Potential assay kit (Abcam, Cambridge, UK). This assay contains tetramethylbenzimidazolcarbocyanine

iodide (JC-1) cationic dye and this dye tends to accumulate in energized mitochondria. Decreased signal of the fluorescent indicates depolarization while an increased signal of it indicates hyperpolarization of the mitochondrial membrane. JC-1 is in the monomer form at low concentrations due to low MMP and gives green fluorescence with 530 ± 15 nm wavelength while it aggregates at high concentrations due to high MMP and gives red fluorescence with 590 ± 17.5 nm wavelength. JC-1 stock solution was prepared with a concentration to be 1 mM with DMSO. To prepare a working JC-1 solution, the stock solution was diluted with PBS to obtain 0.01 mM. The RPMI-1640 cell culture medium was removed from the PC3 human prostate cancer cells and the cells were washed twice with PBS. 100 μ L of 0.01 mM JC-1 solution was added to each well of the 96-well plate and cells were incubated for 30 minutes at 37⁰C, and a 5% CO₂ humidified the atmosphere in the dark. After the incubation ended, the JC-1 solution was removed and the cells were washed once with PBS. Then, the cell medium was added to the cells and experimental protocol was applied. After the completion of all applications, JC-1 fluorescence was obtained from a multi-plate microplate reader (Synergy™ HTX Multi-Mode Microplate Reader, BioTek, Winooski, USA) emission at 528/20 nm wavelength gives green fluorescence when excited at 485/20 nm wavelength and emission at 600/40 nm wavelength gives red fluorescence with excitation at 485/20 nm wavelength.

2.11 Cell Viability Analysis by Acridine Orange/ Propidium Iodide Staining

The acridine orange/propidium iodide (AO/PI) staining (Logos Biosystems, Anyang, Gyeonggi, KR) was used for the imaging of the live and dead cells after the Ce6 mediate-PDT applications in determined groups. Acridine orange penetrates the membranes of living cells and binds to nucleic acids located in the nucleus. After its binding to the double strain DNA, acridine orange fluorescence green color. On the other hand, propidium iodide cannot pass across the cell membrane of living cells. The only way propidium iodide can bind to the nucleic acid is due to penetration through the membrane of dead cells or distributed cell membranes. When propidium iodide binds to nucleic acids of dead or late apoptotic cells, its fluorescence increases, and cells fluoresce red color. Thus, AO/PI makes the visible nucleus of viable cells green

fluorescence and the nucleus of dead cells red fluorescence. The RPMI-1640 cell culture medium was removed from the PC3 human prostate cancer cells after all applications were completed and cells were washed once with PBS. Then, 30 uL of AO/PI stain diluted at 1/10 with PBS was added to the cells. The cells and AO/PI stain were incubated for 30 minutes at 37⁰C, and a 5% CO₂ humidified the atmosphere in the dark. After their incubation, images of the cells were taken with fluorescence microscopy (Carl Zeiss Microscopy GmbH, Axio Vert.A1, Jena, DE) at 20X magnification. Emission at 525 nm wavelength indicates living cells and gives green color when excited at 502 nm wavelength while emission at 617 nm wavelength indicates dead cells and gives red color when excited at 535 nm wavelength.

2.12 Statistical Analysis

Statistical analyses were performed with GraphPad Prism Version 9.4.1 (GraphPad Software Inc., La Jolla, CA, USA) to compare experimental groups. The data obtained from each analysis itself or their normalized version with respect to the control group were analyzed with a one-way analysis of variance (ANOVA). Then, Tukey's post hoc test was used to compare experimental groups with control groups. According to the p-value, statistical difference was determined. If the p-value is less than 0.05, it was considered statistically significant.

Chapter 3

Results

3.1 Effect of Laser Light on PC3 Cells

The metabolic activity of the PC3 human prostate cancer cells was determined with the MTT assay to determine the effect of diode laser lights on them (Figure 3.1). The cell viability of the experimental groups was compared to the control group. The energy densities that were used for the PBM and PDT applications were applied to the cells as 1, 3, 5, and 50 J/cm² for 655-nm diode laser light while 1, 3, 5, and 100 J/cm² for 808-nm diode laser light. Both wavelengths of laser light with these energy densities did not cause any toxicity to the cells. Even, some energy densities increased cell viability. The maximum increase in cellular viability was observed in the 655-nm laser light application at 3 J/cm² energy density causing approximately 21% compared to the control. This was followed by 1 J/cm² for 808-nm laser light application with an approximately 16% increase. Both 655 and 808-nm laser light showed biostimulation effects on the cancer cells at different energy densities but increases are not statistically different except PBM application with 3 J/cm² energy density at 655-nm of wavelength which was significantly different compared to the PBM application with 1 J/cm² energy density at 655-nm of wavelength.

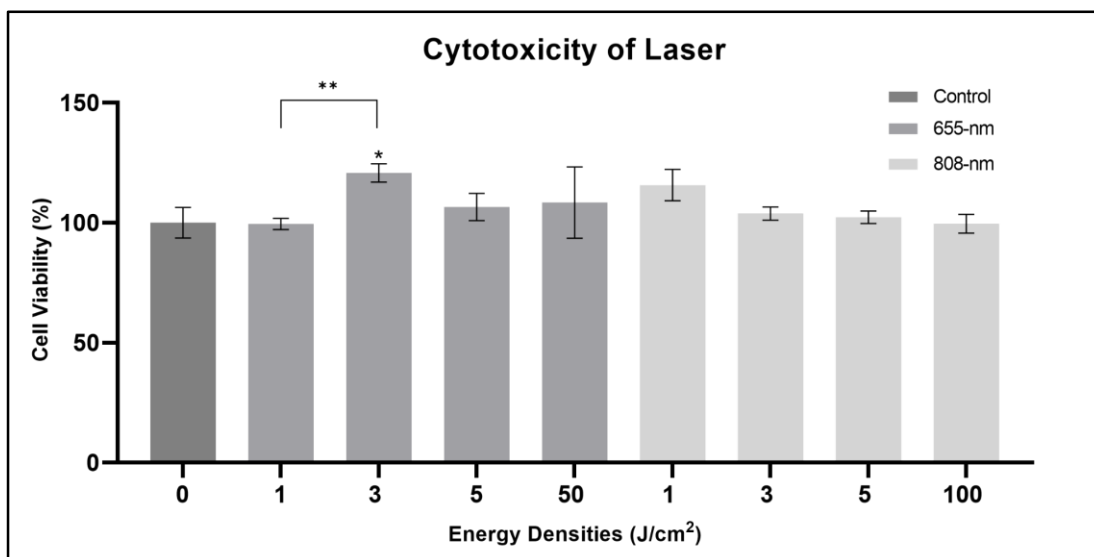


Figure 3.1: Cell viability analysis after laser irradiation. Each bar represented the average of the normalized with respect to the control group. Differences that were statistically significant were represented as * and ** ($p < 0.05$, * indicates significant differences compared to the control and ** indicates significant differences compared to the experimental groups)

3.2 Cytotoxicity of Photosensitizers on PC3 Cells

To determine the cytotoxicity of the ICG and Ce6 at concentrations that were used for the PDT application, the effects of both PSs, ICG, and Ce6, on the PC3 human prostate cancer cells were checked in the dark with an MTT assay. 25, 50, and 100 μM of ICG concentrations did not cause toxic effects on the cells after 1 h incubation which can be seen in Figure 3.2. Even, it can be said that all three concentration incubations within an hour increased the cell viability. But the same concentrations with 24 h incubations caused slight decreases which were not statistically significant. The maximum change in the cell viability which was approximately 19% decrease was reached with 50 μM ICG. However, it is not statistically different.

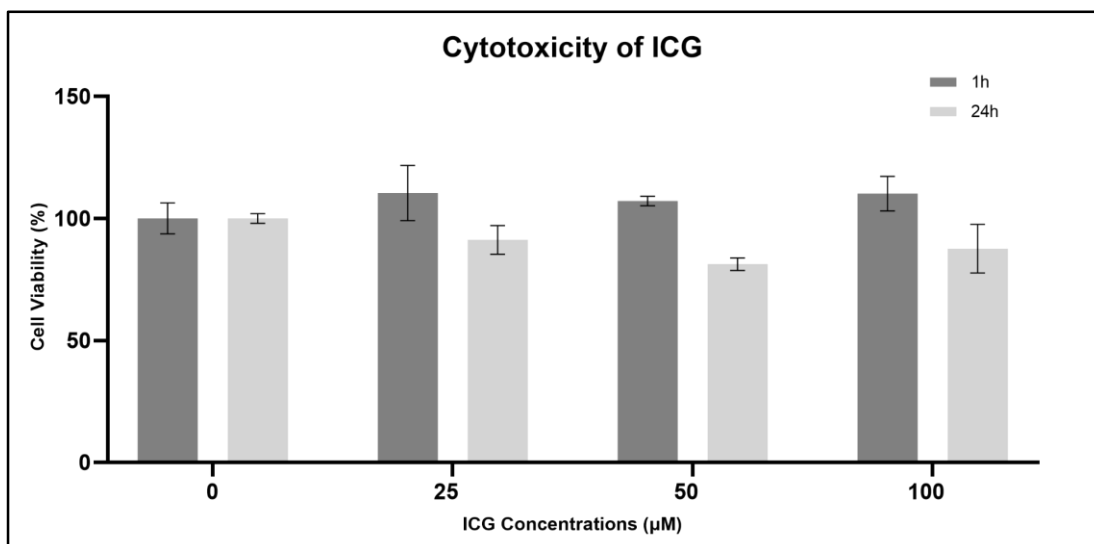


Figure 3.2: Cell viability analysis of 25, 50, and 100 μM of ICG concentrations after 1 and 24 h incubation time. Each bar represented the average of the normalized with respect to the control group.

The cytotoxicity results of Ce6 can be observed in Figure 3.3 for 2 and 24 h incubation times. Four different concentrations of Ce6 (2.5, 5, 10, and 25 μM) also did not show any toxicity to PC3 cells after their 2 and 24 h incubations. A slight decrease which is not statistically significant was observed in incubation with 25 μM which was approximately 17%.

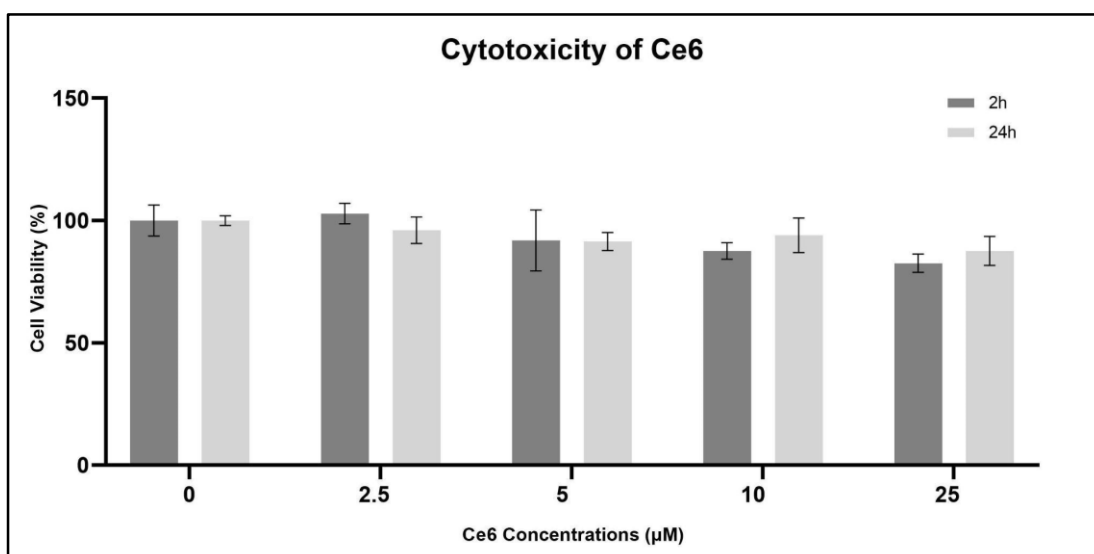


Figure 3.3: Cell viability analysis of 2.5, 5, 10, and 25 μM of Ce6 concentrations after 2 and 24 h incubation time. Each bar represented the average of the normalized with respect to the control group.

3.3 Cellular Uptake of Photosensitizers by PC3 Cells

Cellular uptake of both PSs, ICG, and Ce6, was analyzed using a Triton X-100 assay to observe the PBM effect on cellular uptake by PC3 human prostate cancer cells. The absorbance values at the PSs which gave maximum absorbance were correlated. The cellular uptake of the cells and pre-treated cells with PBM were compared to each other to determine the PBM effect on cellular uptake. All energy densities of 655-nm PBM application before the ICG incubation with 1 h of incubation except one group showed decreased cellular uptake for all concentrations of ICG which are 25, 50, and 100 μM . However, 655-nm PBM application at 3 J/cm^2 increased cellular uptake of 50 μM ICG by 57.7% compared to the non-treated cells which was statistically different (Figure 3.4).

The cellular uptake of 25 μM concentration of ICG after the 655-nm PBM at all energy densities (1, 3, and 5 J/cm^2) was increased after 24 h of incubation. The maximum cellular uptake for this concentration was achieved by 3 J/cm^2 PBM with a 48.48% increase but it was not statistically different. The cellular uptake of 50 μM ICG was only increased by 655-nm PBM application at 5 J/cm^2 energy density. On the other hand, the cellular uptake of 100 μM ICG was decreased by the 655-nm PBM application at all energy densities (Figure 3.4).

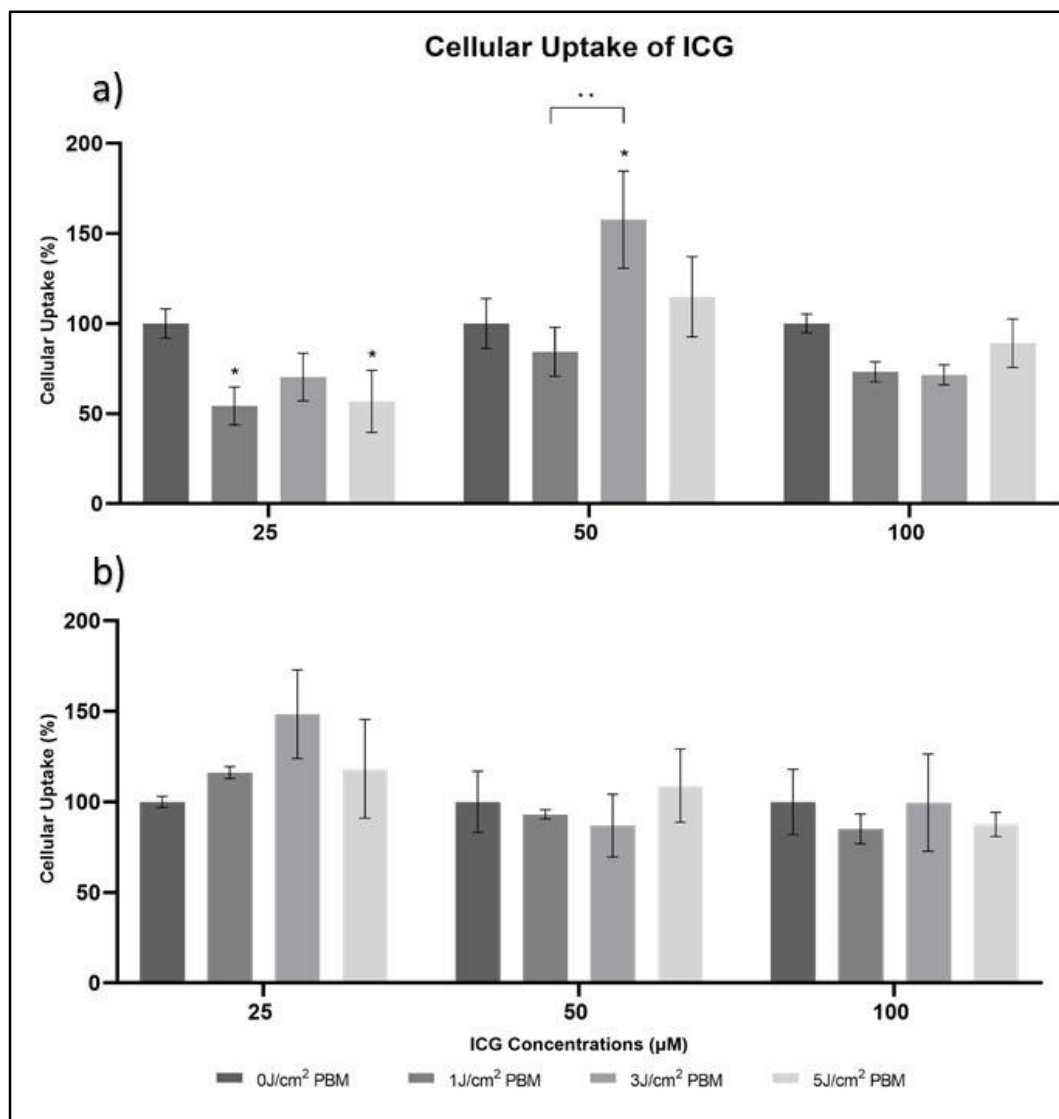


Figure 3.4: Cellular uptake analysis of 25, 50, and 100 μM of ICG concentrations after PBM applications. a) cellular uptake analysis after 1 and b) 24 h of incubation time. Each bar represented the average of the normalized with respect to the control group. Differences that were statistically significant were represented as * and ** ($p < 0.05$, * indicates significant differences compared to the control and ** indicates significant differences compared to the experimental groups)

When the cellular uptake of Ce6 by PC3 cells was investigated, it was obvious that the applications of 808-nm PBM at 1, 3, and 5 J/cm^2 energy densities increased the cellular uptake of all Ce6 concentrations which were 5, 10, and 25 μM after the 2 h incubation. The maximum cellular uptake was achieved with the application of 808-nm PBM at 1 J/cm^2 energy density increasing by 42.89%. The cellular uptakes of 2.5, 5, 10, and 25 μM of Ce6 were also determined after their 24 h incubation with cells. 808-nm PBM

at 1 J/cm² energy density increased cellular uptakes of 2.5, 5, and 10 μM with rates of 5.78, 13.02, and 4.98% respectively. Except in one concentration of 10 μM Ce6, 808-nm PBM at 3 J/cm² energy density resulted in decreased cellular uptakes. In the same manner as the 3 J/cm² energy density, 808-nm PBM applied with 5 J/cm² decreased the cellular uptake of Ce6 except for 5 μM of Ce6 concentration. Overall 808-nm PBM at 1 J/cm² energy density increased the cellular uptake of Ce6 with 2 and 24 h incubation times (Figure 3.5).

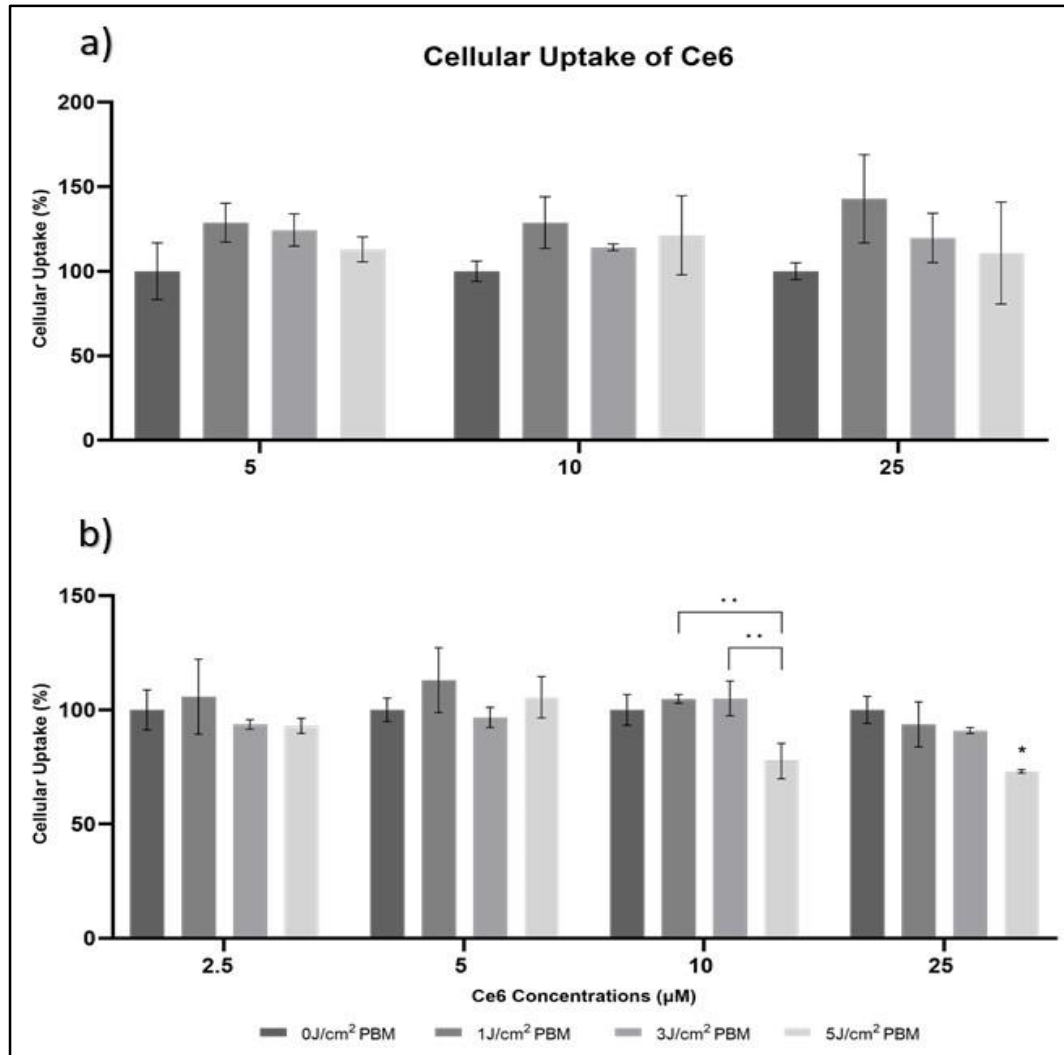


Figure 3.5: Cellular uptake analysis of 2.5, 5, 10, and 25 μM of Ce6 concentrations after PBM applications. a) cellular uptake analysis after 2 and b) 24 h of incubation time. Each bar represented the average of the normalized with respect to the control group. Differences that were statistically significant were represented as * and ** (p < 0.05, * indicates significant differences compared to the control and ** indicates significant differences compared to the experimental groups)

3.4 Phototoxicity of PBM-induced PDT on PC3 Cells

After the completion of the incubations of ICG and Ce6 with PC3 human prostate cancer cells, the cells were irradiated with diode laser lights to induce photodynamic action for cancer cell death in only PDT groups. The ICG-mediated PDT was conducted with an 808-nm diode laser at 100 J/cm^2 energy density while Ce6-mediated PDT was conducted with a 655-nm diode laser at 50 J/cm^2 energy density. In PBM+PDT groups, the ICG mediated-PDT was applied with the same parameters used in only PDT groups after the application of 1, 3, and 5 J/cm^2 655-nm PBM followed by incubation of ICG for 1 or 24 h and while Ce6 mediated-PDT was applied with the same parameters used in only PDT groups after the application of 1, 3 and 5 J/cm^2 808-nm PBM followed by incubation of Ce6 for 2 or 24 h.

ICG-mediated PDT conducted with 25, 50, and $100 \text{ }\mu\text{M}$ ICG decreased PC3 cell viability by 3.87, 12.78, and 49.54% respectively after the 1 h incubation shown in Figure 3.6. The cell deaths obtained by 1 J/cm^2 PBM+PDT groups were 25.65, 26.01, and 39.5% with 25, 50, and $100 \text{ }\mu\text{M}$ ICG respectively. Except for two groups, pre-treatment with PBM diminished the cell death obtained by PDT and resulted in an increase in the cell viability of PC3 cells compared to the only PDT groups. PBM treatment before PDT increased the cell viability up to 60.44% cell viability with $100 \text{ }\mu\text{M}$ ICG at 1 J/cm^2 energy density. 111.24, 93.65, and 60.21% rates in cell viability were observed with 25, 50, and $100 \text{ }\mu\text{M}$ ICG respectively for 3 J/cm^2 energy density. 102.99, 95 and 79.87 % rates in cell viability were observed with 25, 50, and $100 \text{ }\mu\text{M}$ ICG respectively for 5 J/cm^2 energy density. In PBM+PDT groups with 655-nm PBM at 1 J/cm^2 energy density and with 25 and $50 \text{ }\mu\text{M}$ of ICG concentrations additionally increased cell death with rates of 21.78 and 13.23 % respectively obtained from only PDT groups. The maximum cell death of 49.54% was obtained in the only PDT group that was conducted after 1 h incubation of $100 \text{ }\mu\text{M}$ ICG concentration with 808-nm diode laser light at 100 J/cm^2 energy density. In addition, a maximum cell death increase of 21.78% was achieved after 655-nm diode laser PBM at 1 J/cm^2 energy density and 1 h incubation of $25 \text{ }\mu\text{M}$ ICG concentration with 808-nm diode laser PDT at 100 J/cm^2 energy density.

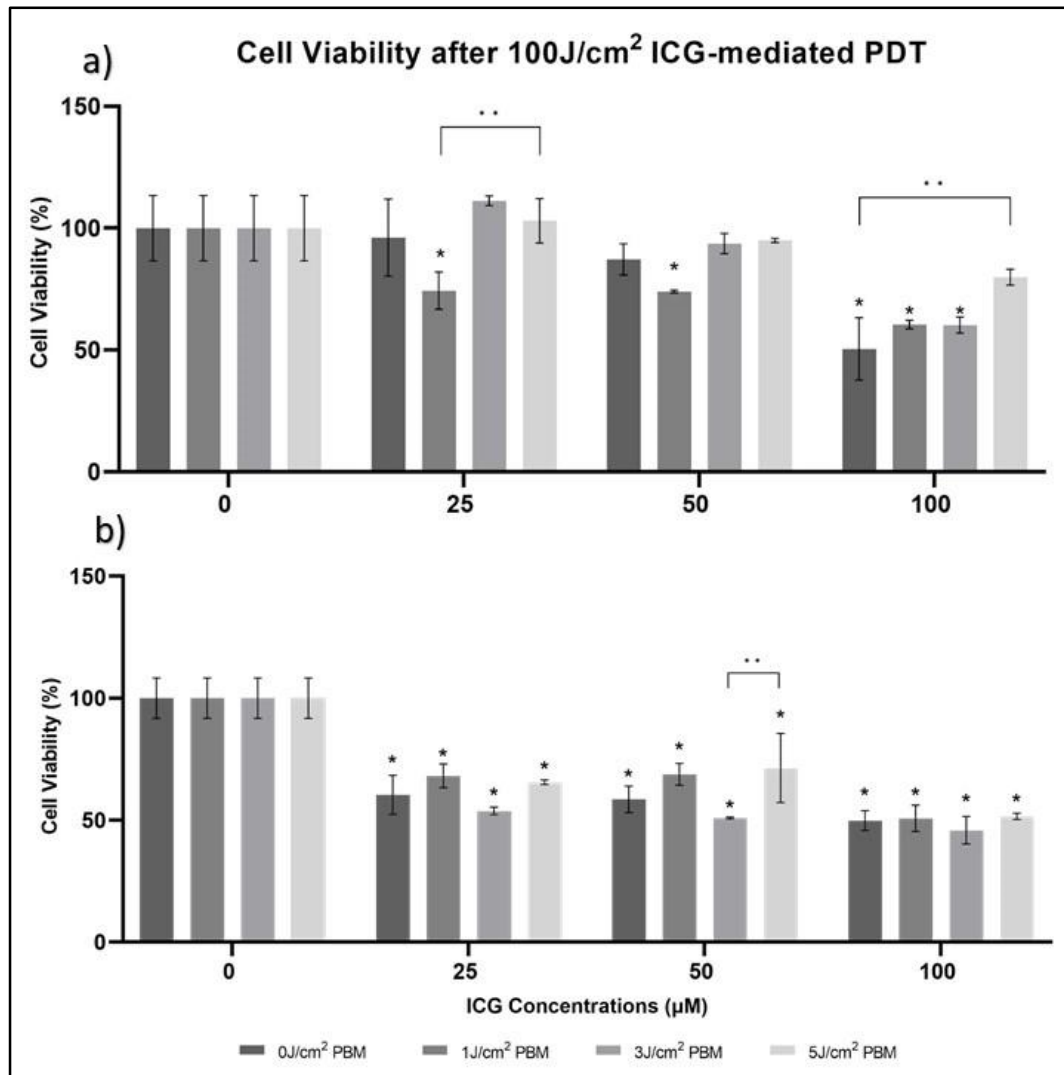


Figure 3.6: Cell Viability analysis after ICG-mediated PDT applications at 100 J/cm² energy density after a) 1 and b) 24 h incubation. Photosensitizer concentrations: 25, 50, and 100 µM of ICG. Each bar represented the average of the normalized with respect to the control group. Differences that were statistically significant were represented as * and ** (p < 0.05, * indicates significant differences compared to the control and ** indicates significant differences compared to the experimental groups)

ICG-mediated PDT that was conducted after 24 h incubation of the same concentrations of ICG (25, 50, and 100 µM ICG) decreased the cell viability to 39.61, 41.48, and 50.15% respectively to the concentrations Figure 3.6. PBM applications at 1 and 5 J/cm² energy density before the PDT clear of the photodynamic action increasing the cell viability to 68.19, 68.82, and 50.78 % with 25, 50, and 100 µM ICG respectively for 1 J/cm² energy density, and 65.58, 71.39 and 51.60% with 25, 50 and 100 µM ICG respectively for 5 J/cm² energy density. More cell deaths were obtained

by 3 J/cm² PBM+PDT groups with rates of 46.24, 49.07, and 54.15% with 25, 50, and 100 μM concentrations of ICG respectively. In PBM+PDT groups with 655-nm PBM at 3 J/cm² energy density with 25, 50, and 100 μM of ICG concentrations additionally increased cell death with rates of 6.63, 7.59, and 4% respectively obtained from only PDT groups. The maximum cell death of 54.15% was obtained in the PBM-PDT group that was conducted after 655-nm diode laser PBM at 3 J/cm² energy density and 24 h incubation of 100 μM ICG concentration with 808-nm diode laser light at 100 J/cm² energy density. In addition, a maximum cell death increase of 7.59% was achieved after 655-nm diode laser PBM at 3 J/cm² energy density and 24 h incubation of 50 μM ICG concentration with 808-nm diode laser PDT at 100 J/cm² energy density.

The other set of this study includes Ce6-mediated PDT. Ce6-mediated PDT decreased cell viability by 16.74, 25.91, and 58.8 % with 5, 10, and 25 μM of Ce6 respectively after the 2 h incubation shown in Figure 3.7. In PBM+PDT groups, more PC3 cell deaths were observed except in one group who has first experienced 808-nm PBM at 1 J/cm² energy density, and then PDT was applied after 5 μM concentration of Ce6 increasing cell viability to 87.44%. The prior application of 808-nm PBM at 1 J/cm² density resulted in an additional 31.45 and 26.15% cell death compared to the PDT groups with 10 and 25 μM concentrations of Ce6 respectively. 3 J/cm² energy density resulted in an additional 1.42, 5.79, and 36.77% cell death while 5 J/cm² energy density resulted in an additional 32.77, 44.88, and 27.25% cell death compared to the PDT groups with 5, 10, and 25 μM concentrations of Ce6 respectively. The maximum cell death of 95.57% was obtained in the PBM-PDT group that was conducted after 808-nm diode laser PBM at 3 J/cm² energy density and 2 h incubation of 25 μM Ce6 concentration with 655-nm diode laser light at 50 J/cm² energy density. Moreover, a maximum cell death increase of 44.88% was achieved after 808-nm diode laser PBM at 5 J/cm² energy density and 2 h incubation of 10 μM Ce6 concentration with 655-nm diode laser PDT at 50 J/cm² energy density.

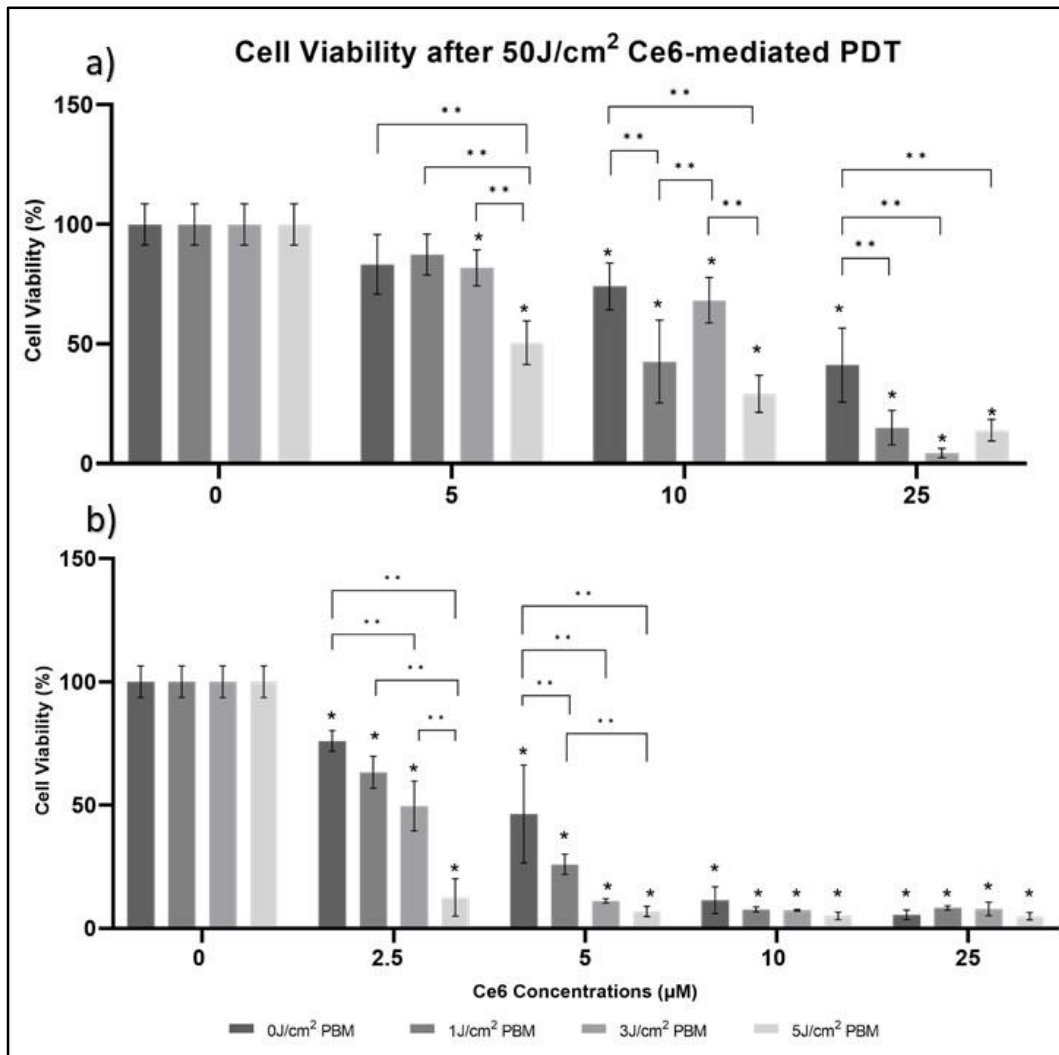


Figure 3.7: Cell Viability analysis after Ce6-mediated PDT applications at 50 J/cm² after a) 2 and b) 24 h incubation. Photosensitizer concentrations: 2.5, 5, 10, and 25 µM of Ce6. Each bar represented the average of the normalized with respect to the control group. Differences that were statistically significant were represented as * and ** (p < 0.05, * indicates significant differences compared to the control and ** indicates significant differences compared to the experimental groups)

Ce6-mediated PDT decreased cell viability by 24, 53.63, 88.62, and 94.55% with 2.5, 5, 10, and 25 µM of Ce6 respectively after the 24 h incubation shown in Figure 3.7. More cell death was obtained in all PBM+PDT groups except at 25 µM concentration of Ce6. 1 and 3 J/cm² energy densities of 808-nm PBM caused a slight increase in the cell viability while 5 J/cm² energy density slightly decreased the cell viability compared to the only PDT group (PDT conducted with 25 µM of Ce6 and 50 J/cm² 655-nm laser light).

Table 3.1: Cell Death (%) in Only PDT and PBM+PDT Groups after 2 h of Ce6 Incubation

Cell Death (%)				
Ce6 Concentrations (μM)	Only PDT	1 J/cm ² PBM+PDT	3 J/cm ² PBM+PDT	5 J/cm ² PBM+PDT
5	16.74 \pm 12.5	12.56 \pm 8.6	18.16 \pm 7.5	49.51 \pm 9.1
10	25.91 \pm 9.8	57.36 \pm 17.3	31.70 \pm 9.6	70.79 \pm 7.8
25	58.79 \pm 15.5	84.95 \pm 7.2	95.57 \pm 1.9	86.05 \pm 4.5

Table 3.2: Cell Death (%) in Only PDT and PBM+PDT Groups after 24 h of Ce6 Incubation

Cell Death (%)				
Ce6 Concentrations (μM)	Only PDT	1 J/cm ² PBM+PDT	3 J/cm ² PBM+PDT	5 J/cm ² PBM+PDT
2.5	24.00 \pm 4.2	36.72 \pm 6.5	50.41 \pm 10.1	87.44 \pm 7.6
5	53.63 \pm 19.9	74.01 \pm 4.1	88.91 \pm 0.9	93.14 \pm 2.1
10	88.62 \pm 5.5	92.37 \pm 0.9	92.68 \pm 0.4	94.94 \pm 1.5
25	94.55 \pm 1.9	91.77 \pm 0.9	92.16 \pm 2.8	95.12 \pm 1.5

808-nm PBM application at 1, 3 and 5 J/cm² energy densities before the PDT conducted with 2.5 μM of Ce6 resulted in 12.72, 26.41, and 63.44% additional cell death respectively compared to only the PDT group. The 1, 3, and 5 J/cm² energy densities of 808-nm of PBM increased the cell death obtained in the only PDT group conducted with 5 μM of Ce6 20.38, 35.28, and 39.51% respectively. The increase in cell death was less in PBM+PDT groups with 10 μM of Ce6 which were 3.75, 4.06, and 6.32% for 808-nm PBM at 1, 3, and 5 J/cm² energy densities respectively. The maximum cell death of 95.12% was obtained in the PBM-PDT group that was conducted after 808-nm diode laser PBM at 5 J/cm² energy density and 24 h incubation of 25 μM Ce6 concentration with 655-nm diode laser light at 50 J/cm² energy density. Moreover, a maximum cell death increase of 63.44% was achieved after 808-nm diode

laser PBM at 5 J/cm² energy density and 24 h incubation of 2.5 μM Ce6 concentration with 655-nm diode laser PDT at 50 J/cm² energy density.

3.5 Nitric Oxide Release in PC3 Cells after PBM and PDT Applications

As shown in Figure 3.8 and Figure 3.9 the amount of NO released after the 655-nm and 808-nm PBM at 1, 3, and 5 J/cm² energy densities were measured using the Griess Reagent kit. After the 655-nm diode laser light application for PBM purposes at 1, 3, and 5 J/cm² energy densities, the amount of NO released increased right after the light applications by 33.7, 3.3, and 2.5 times respectively compared to the control group. However, the released amount of NO was increased compared to the control group after 24 h in 655-nm PBM at 1 and 3 J/cm² energy densities. The amount of released NO by 655-nm PBM applications at 1 and 3 J/cm² increased with a rate of 1.4 and 1.6-fold respectively compared to the control group while 5 J/cm² 655-nm PBM did not change the amount of NO released slightly with a rate of 0.9 fold compared to the control group after 24 h. The maximum increase of 1.6-fold in the amount of released NO was obtained with 655-nm PBM at 3 J/cm² energy density after 24 h application of it.

After the 808-nm diode laser light application for PBM purposes at 3 and 5 J/cm² energy densities, the amount of photodissociated NO increased right after the light applications by 1.1, and 1.6 times respectively compared to the control group. 808-nm PBM at 1 J/cm² energy density did not change the amount of NO dissociated. The amounts of NO released by the 808-nm PBM at 1, 3, and 5 J/cm² energy densities were decreased compared to the control group with a rate of 0.9, 0.8, and 0.8 fold after the 24 h respectively which were not statistically significant.

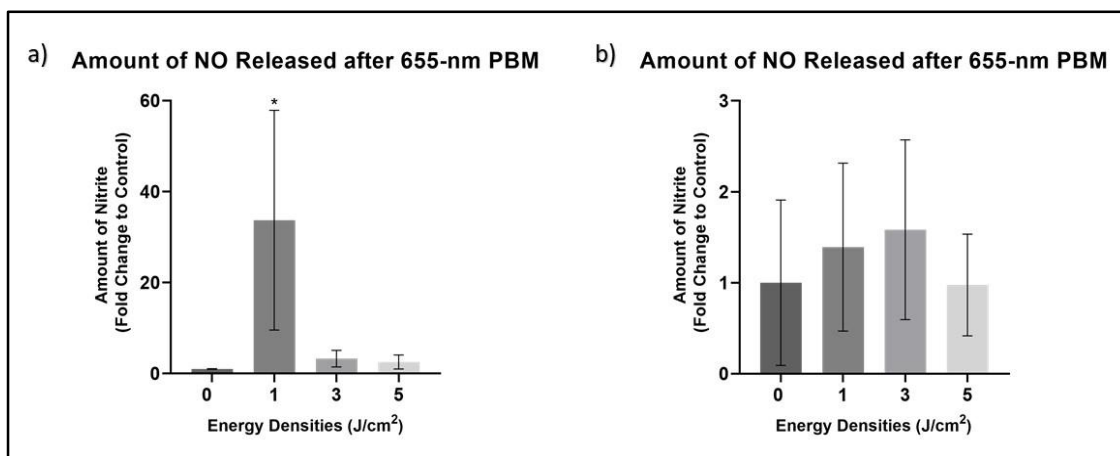


Figure 3.8: Nitrite amounts after 655-nm PBM at 1, 3, and 5 J/cm² energy densities. Measurements were taken a) 0 and b) 24 h after the 655-nm PBM applications. Each bar represented the average of the normalized with respect to the control group. Differences that were statistically significant were represented as * ($p < 0.05$, * indicates significant differences compared to the control group)

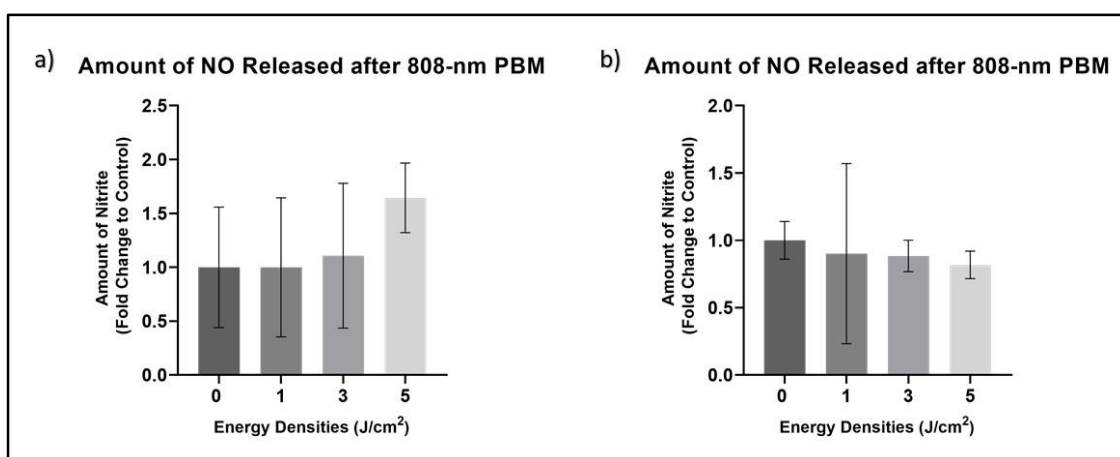


Figure 3.9: Nitrite amounts after 808-nm PBM at 1, 3, and 5 J/cm² energy densities. Measurements were taken a) 0 and b) 24 h after the 808-nm PBM applications. Each bar represented the average of the normalized with respect to the control group.

Also, NO released after the Ce6-mediated PDT for both 2 and 24 h incubation times were checked shown in Figure 3.10. After 2 h incubation of Ce6 with PC3 cells, PDT at 50 J/cm² energy density was applied to the cells, and amounts of NO were 0.3, 1.5, and 1.7 folds for 5, 10, and 25 μ M of Ce6 respectively in only PDT groups. But generally, pre-treatment with 808-nm PBM resulted in increased NO after the Ce6-mediated PDT compared to the obtained amount in only the PDT group. Among the

energy densities of 808-nm PBM, 5 J/cm² energy density resulted in less increase than the other 1 and 3 J/cm² energy densities. The maximum increase of 2.1-fold was obtained 25 μM Ce6-mediated PDT group with cells pre-treated with 808-nm PBM at 1 J/cm² energy density compared to the control. In addition, a maximum increase of 1.2-fold was obtained 5 μM Ce6-mediated PDT group which cells were pre-treated with 808-nm PBM at 3 J/cm² energy density compared to the only PDT group.

After 24 h incubation of Ce6 with PC3 cells PDT at 50 J/cm² energy density was applied to the cells, and amounts of NO were 0.8, 1, 1.3, and 1.2 folds for 2.5, 5, 10, and 25 μM of Ce6 respectively in only PDT groups. In pre-treated cells with 808-PBM at 1 J/cm² energy density increased the 1.3 and 1.5 folds of NO obtained after the Ce6-mediated PDT at 2.5 μM and 10 μM respectively while 3 J/cm² PBM increased the 1.3 fold the amounts of NO obtained after Ce6-mediated PDT at 25 μM of Ce6. The maximum increase of 0.54-fold difference was obtained 2.5 μM Ce6-mediated PDT group which cells pre-treated with 808-nm PBM at 1 J/cm² energy density compared to the only PDT group.

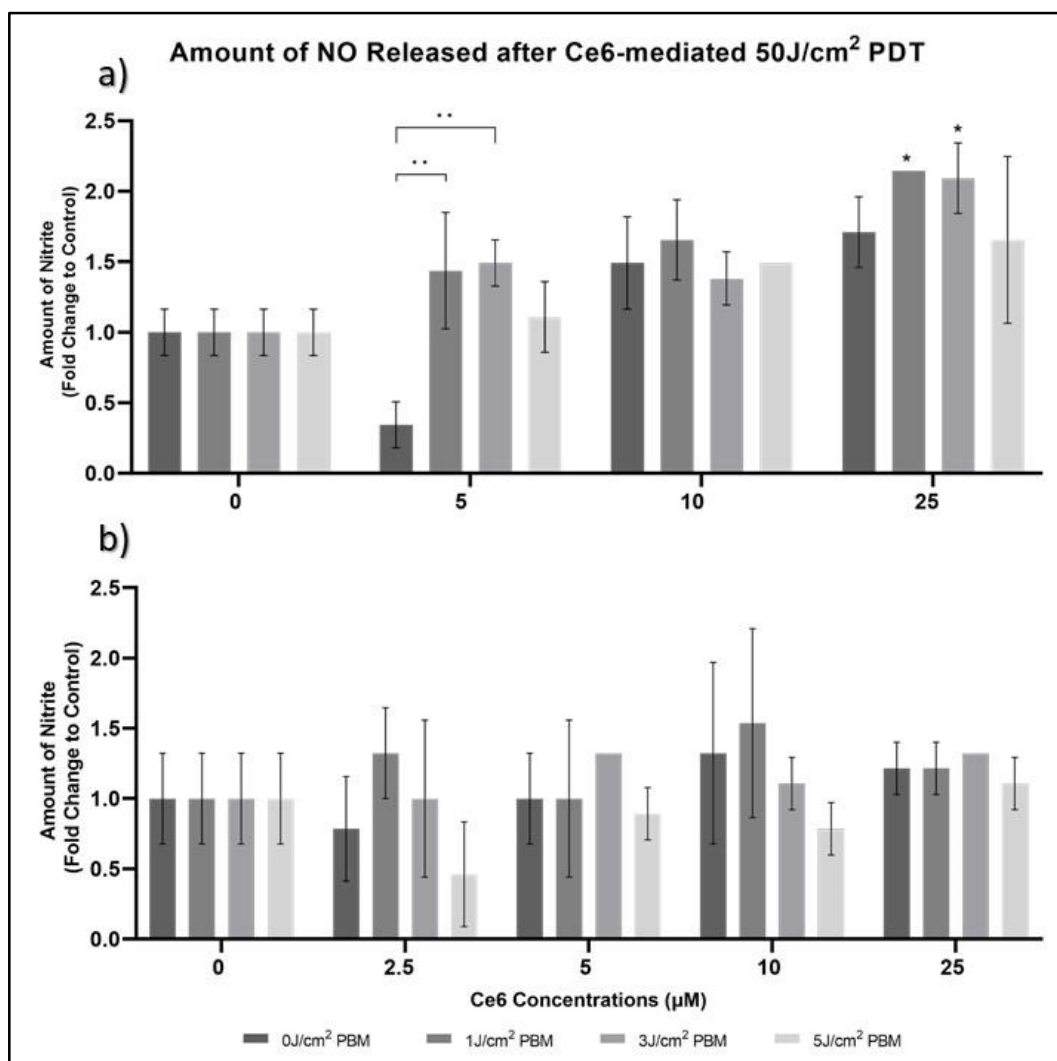


Figure 3.10: Nitrite amounts after Ce6-mediated PDT applications at 50 J/cm² energy density after a) 2 and b) 24 h incubation. Photosensitizer concentrations: 2.5, 5, 10, and 25 µM of Ce6. Each bar represented the average of the normalized with respect to the control group. Differences that were statistically significant were represented as * and ** (p < 0.05, * indicates significant differences compared to the control and ** indicates significant differences compared to the experimental groups)

3.6 ATP Production in PC3 Cells after PBM Applications

After the application of PBM with 655 and 808-nm diode laser light at 1, 3, and 5 J/cm² energy densities on the PC3 human prostate cancer cells, the amount of produced ATP was determined for both wavelengths via the CellTiter -Glo® 2.0 assay. The

amount of ATP after the PBM results can be seen in Figure 3.11. PBM that was applied to the cells with 655-nm diode laser light generally did not change the produced ATP amount compared to the control groups at all energy densities. 1 J/cm² energy density of 655-nm laser light caused a slight decrease in the produced amount of ATP but it was not statistically different. Also, PBM that was conducted with 808-nm diode laser light at all energy densities increased the ATP production in the cells. 1 and 3 J/cm² energy densities increased the production of ATP compared to the control group with the rate of 5.1 and 7.4% respectively. The maximum increase of 27.6 % was reached with the 808-PBM at 5 J/cm² energy density.

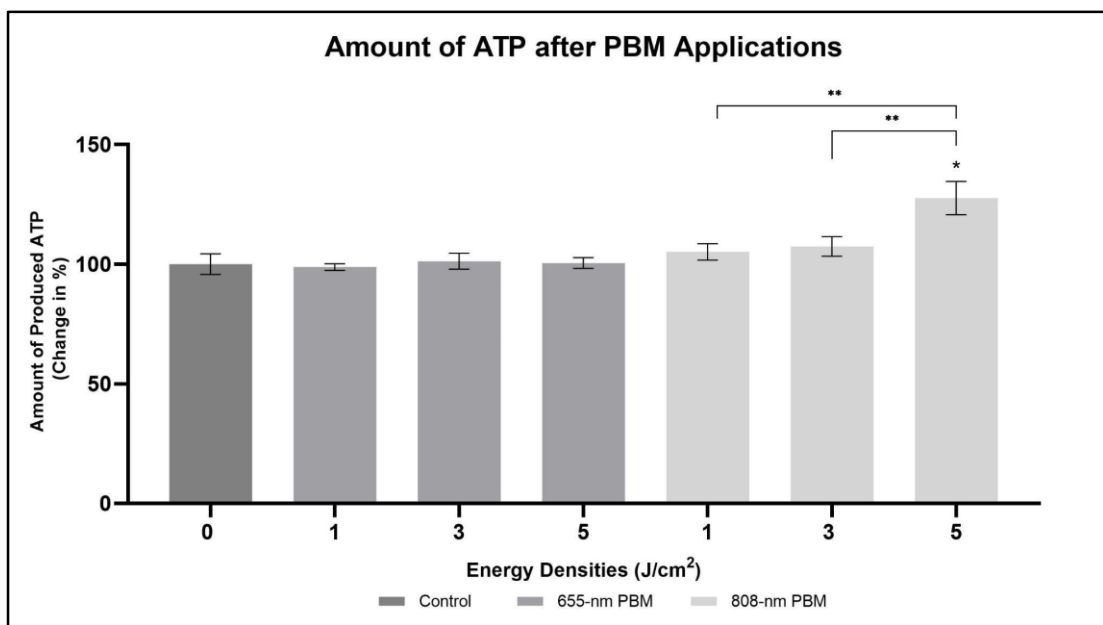


Figure 3.11: ATP amounts after 655 and 808-nm PBM applications at 1, 3, and 5 J/cm² energy densities. Each bar represented the average of the normalized with respect to the control group. Differences that were statistically significant were represented as * and ** (p < 0.05, * indicates significant differences compared to the control and ** indicates significant differences compared to the experimental groups)

3.7 Intracellular Reactive Oxygen Species Production in PC3 Cells after PBM and PDT Applications

DCFH-DA probe was used for the detection of the amount of intracellular ROS that was generated in PC3 human prostate cancer cells after both PBM at 655 and 808-nm

wavelengths and Ce6-mediated PDT applications shown in Figure 3.12 and Figure 3.13. The produced intracellular ROS was determined right after the 655 and 808-nm PBM applications at 1, 3, and 5 J/cm² energy densities, and it was also determined right after the Ce6-mediated PDT applied after the incubation times of 2 and 24 h. ROS production was increased after the PBM applications conducted with both wavelengths at all energy densities compared to the control group. But the maximum intracellular amount of ROS was reached with both PBM conducted with the same wavelengths at 1 J/cm² energy density. The maximum intracellular ROS amount of 112.99% was reached with the 1 J/cm² energy density of 655-nm PBM application while 655-nm PBM at 3 and 5 J/cm² energy densities increased the amount of ROS to the same rate which was approximately 109%. The 808-nm PBM at 1 J/cm², which is the maximum amount of intracellular ROS in all energy densities of 808-nm PBM, increased the ROS level by 8.94% compared to the control. The amounts of intracellular ROS were 100.83 and 103.46% after the 808-nm PBM at 3 and 5 J/cm² energy densities and these results can be observed in Figure 3.12.

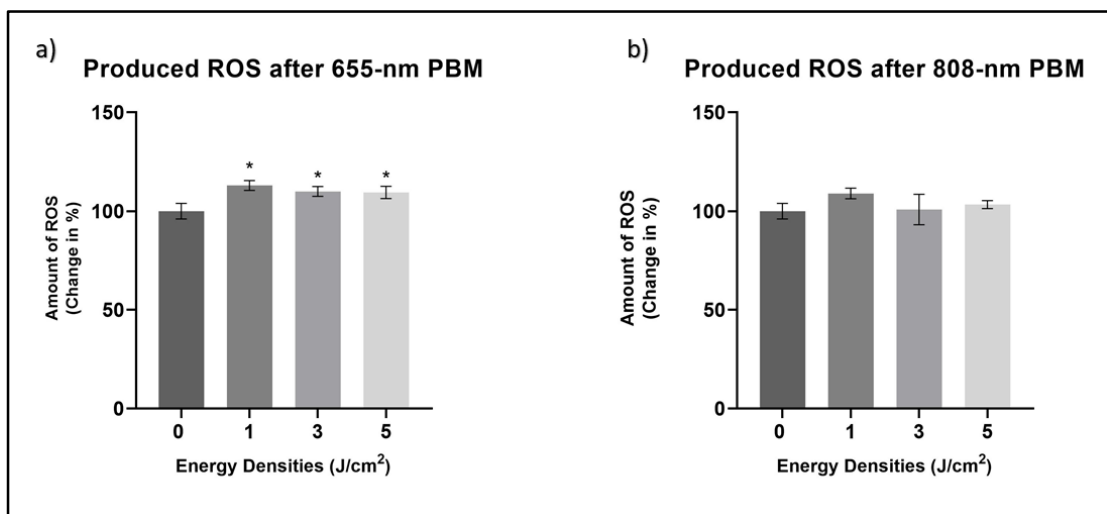


Figure 3.12: Reactive oxygen species formation after a) 655-nm and b) 808-nm PBM at 1, 3, and 5 J/cm² energy densities. Each bar represented the average of the normalized with respect to the control group. Differences that were statistically significant were represented as * ($p < 0.05$, * indicates significant differences compared to the control group)

The amount of intracellular ROS after the Ce6-mediated PDT was also determined after 2 or 24 h of Ce6 incubations. After the Ce6-mediated PDT was conducted after

2 h of incubation, all groups expressed an increased amount of ROS compared to the control group. 50 J/cm² PDT application resulted in increases of 14.21, 13.16, and 20.53% for the 5, 10, and 25 μM of Ce6 in a concentration-dependent manner. But amounts of ROS produced after the 50 J/cm² PDT were higher in PC3 cells pre-treated with different energy densities of 808-nm PBM. 808-nm PBM at 5 J/cm² energy density resulted in an additional 26.11% ROS that was obtained in Ce6-mediated PDT conducted with 5 μM concentration while 1 J/cm² energy density resulted in an additional 16.63 and 20.43% ROS that was obtained in Ce6-mediated PDT conducted with 10 and 25 μM concentrations respectively. The same manner was also obtained in Ce6-mediated PDT after 24h of incubation time. 50 J/cm² PDT increased the ROS amount by 1.37, 9.09, 23.23, and 17.17% at 2.5, 5, 10, and 25 μM respectively compared to the control group. Generally, pre-treatment of cells with 808-nm PBM before the Ce6-mediated PDT increased the produced amount of ROS obtained in only PDT groups. 1 J/cm² 808-nm PBM created 5.69% additional ROS at 10 μM of Ce6 while 5 J/cm² 808-nm PBM created 9.13, 6.58, and 13.71% at 2.5, 5, and 25 μM of Ce6 respectively. Overall, it can be said that pre-treatment of PC3 cells with 808-nm PBM increased the produced amounts of ROS measured after the Ce6-mediated PDT.

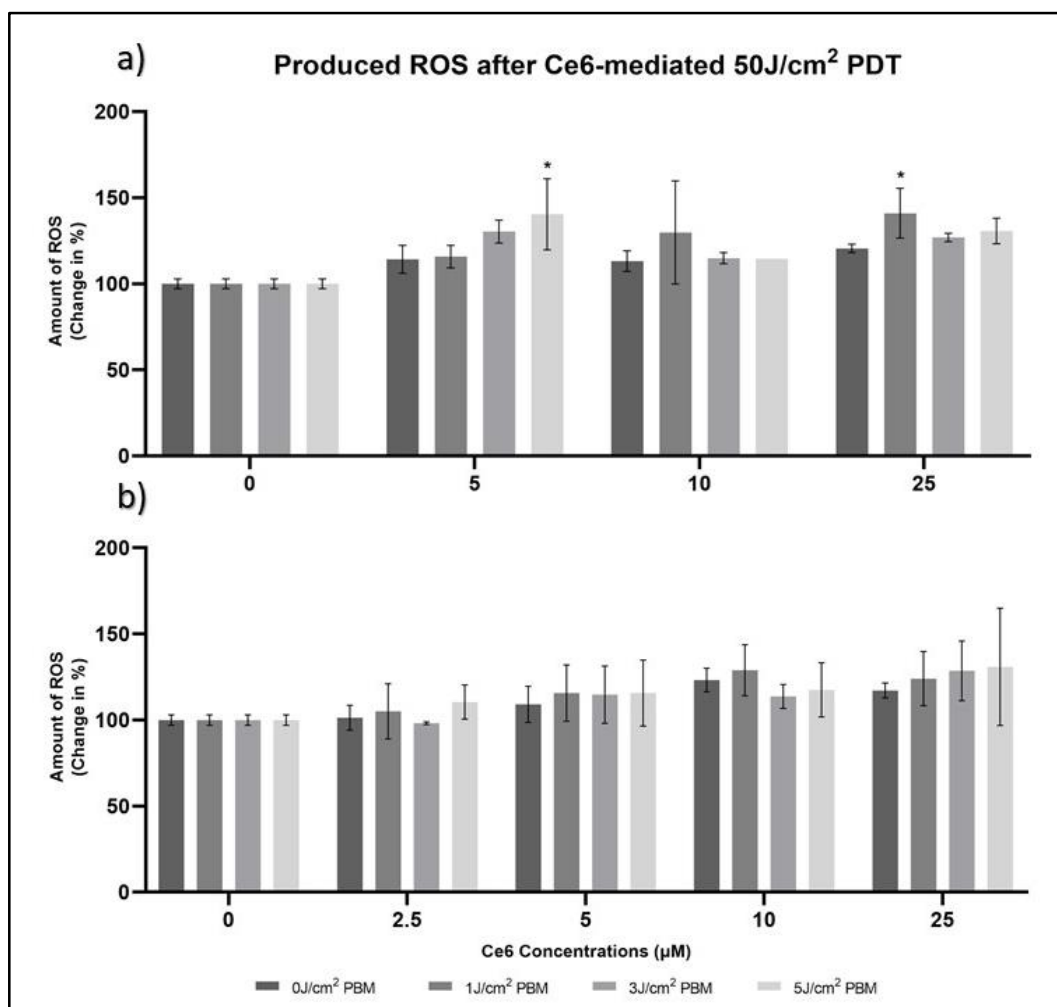


Figure 3.13: Reactive oxygen species formation after Ce6-mediated PDT applications at 50 J/cm² energy density after a) 2 and b) 24 h incubation. Photosensitizer concentrations: 2.5, 5, 10, and 25 µM of Ce6. Each bar represented the average of the normalized with respect to the control group. Differences that were statistically significant were represented as * (p < 0.05, * indicates significant differences compared to the control group)

3.8 Change of Mitochondrial Membrane Potential in PC3 Cells after PBM and PDT Applications

To determine the MMP change in the PC3 human prostate cancer cells after both PBM and Ce6-mediated PDT applications, JC-1 dye was used. The MMP change was determined right after and 24 h after both 655 and 808-nm PBM applications at 1, 3, and 5 J/cm² energy densities while it was also determined right after the Ce6-mediated

PDT after both incubation times which were 2 and 24 h shown in Figure 3.14, Figure 3.15, and Figure 3.16. The MMP increased right after the application of 655-nm PBM at all energy densities. MMP increased with the application of 655-nm PBM at 1, 3, and 5 J/cm² energy densities with 1.82, 6.17, and 3.13% respectively. After 24 h of the application of 655-nm PBM, the MMP increase reached 105.65, 111.15, and 102.39% for 1, 3, and 5 J/cm² energy densities respectively. The maximum increase right after and after the 24 h of PBM application among all energy densities was reached with the application of 655-nm PBM at 3 J/cm² energy density. Surprisingly, MMP decreased compared to the control group right after the 808-nm PBM at 1, 3, and 5 J/cm² energy densities to 70.23, 66.58, and 65.76% respectively. After 24 h of the 808-nm PBM application, MMP increased compared to the control group. Increases of 4.97 and 8.64% in MMP were obtained with 1 and 5 J/cm² energy densities while the maximum increase of 14.56% was obtained with 3 J/cm² energy densities of 808-nm PBM.

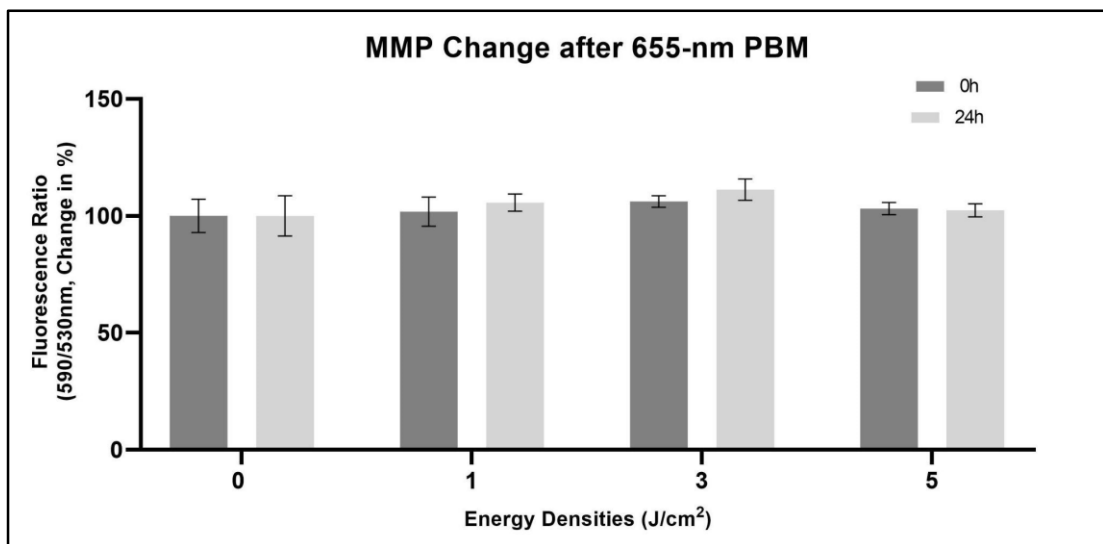


Figure 3.14: Mitochondrial membrane potential change after 655-nm PBM applications at 1, 3, and 5 J/cm² energy densities. Measurements were taken 0 and 24 h after the PBM applications. Each bar represented the average of the normalized with respect to the control group.

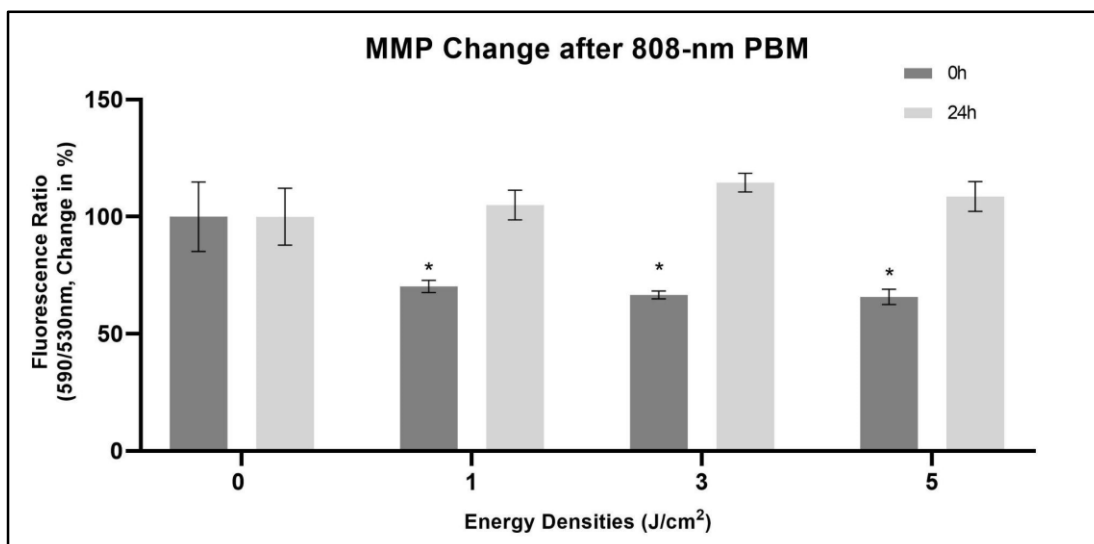


Figure 3.15: Mitochondrial membrane potential change after 808-nm PBM applications at 1, 3, and 5 J/cm² energy densities. Measurements were taken 0 and 24 h after the PBM applications. Each bar represented the average of the normalized with respect to the control group.

The MMP generally decreased after the Ce6-mediated PDT at 50 J/cm² energy density application conducted after 2 h incubation of PS in both only PDT groups and PBM+PDT groups compared to the control group. Only the Ce6-mediated PDT conducted with 5 μM of Ce6 showed elevated MMP compared to the control but it was not statistically different. Also, the MMP of PBM+PDT groups generally decreased more than the only PDT groups. The maximum MMP decreases were achieved by PBM+PDT groups that 808-nm PBM conducted at an energy density of 5 J/cm² compared to other energy densities at the same concentration of Ce6 and they decreased to 76.21, 40.41, and 33.96% for 5, 10 and 25 μM of Ce6 respectively.

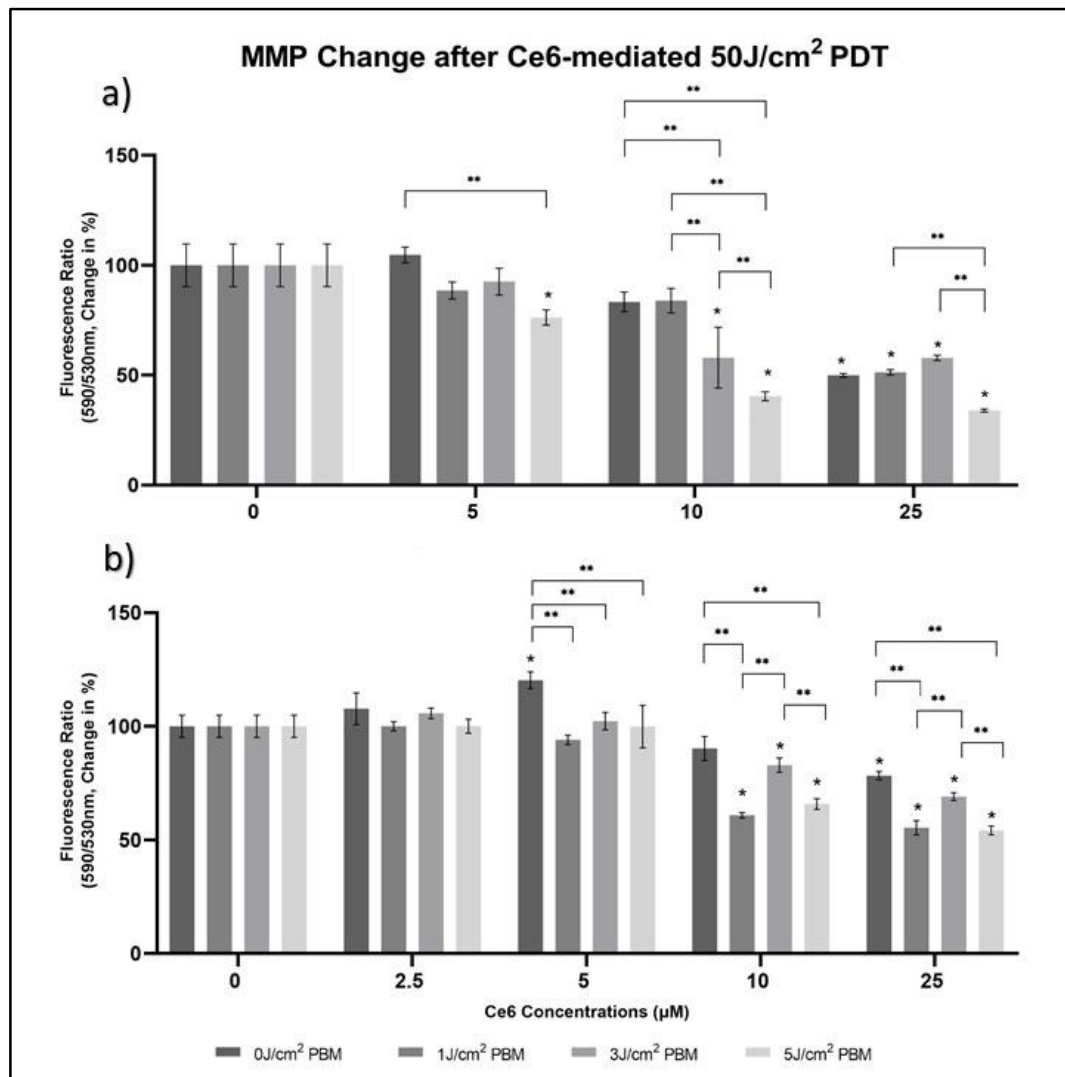


Figure 3.16: Mitochondrial membrane potential change after Ce6-mediated PDT applications at 50 J/cm² energy density after a) 2 and b) 24 h incubation. Photosensitizer concentrations: 2.5, 5, 10, and 25 µM of Ce6. Each bar represented the average of the normalized with respect to the control group. Differences that were statistically significant were represented as * and ** (p < 0.05, * indicates significant differences compared to the control and ** indicates significant differences compared to the experimental groups)

The MMP increased or did not change in both only PDT and PBM+PDT groups after the Ce6-mediated PDT at the same 50 J/cm² energy density application conducted after the 24 h incubation of 2.5 and 5 µM concentrations of Ce6. Especially the application of 1 J/cm² energy density of 808-nm PBM before Ce6-mediated PDT in 2.5 and 5 µM of Ce6 decreased MMP by approximately 10 and 20% respectively. However, MMP decreased compared to the control group in only PDT and PBM+PDT groups in other

concentrations. In addition, obtained MMP decreases were more in PBM+PDT groups of 10, and 25 μM Ce6 concentrations compared to the only PDT groups. Maximum decreases of 34.16 and 45.78% were observed compared to the control group in PBM+PDT groups where 808-nm PBM was conducted at 5 J/cm^2 energy density.

3.9 Acridine Orange/Propidium Iodide Staining after PDT Applications

The results of the AO/PI staining were performed in determined groups according to the maximum cell death change between only PDT and PBM+PDT groups. Green cells represent the living cells that were stained by AO and red cells represent the dead cells that were stained by PI. For the 2 h incubation of Ce6, the 10 μM concentration was determined. So, AO/PI staining was performed on only the PDT group after 50 J/cm^2 655-nm laser light application, and the PBM+PDT group that PC3 cells pre-treated with 808-nm laser light at 5 J/cm^2 energy density and then PDT were applied at the same energy density. For the 24 h incubation of Ce6, the 2.5 μM concentration was determined. Regarding this, AO/PI staining was performed on only the PDT group after 655-nm laser light application at 50 J/cm^2 energy density, and the PBM+PDT group that PC3 cells pre-treated with 808-nm laser light at 5 J/cm^2 energy density and then PDT was applied at the same energy density. The images of the control, only PDT and PBM+PDT groups can be seen in Figure 3.17. In these images, dead/red cells are more intense in PBM+PDT groups at both Ce6 concentrations while more living/green cells are more prominent in control and only PDT groups. Also, the results of AO/PI results were compatible with the cellular viability analysis results. It is clear that pre-treatment PC3 cells with 808-nm PBM at 5 J/cm^2 energy density increased the cellular death obtained by only PDT. According to cellular viability analysis results pre-treatment of the cells with 808-nm PBM at 5 J/cm^2 energy density resulted in additional 44.88 and 63.44% cell deaths were obtained after 2 h incubation of 10 μM of Ce6 and 24 h incubation of 2.5 μM of Ce6 respectively compared to the only PDT. It is obvious that more dead/red cells were visible in the PBM+PDT groups and these results can be seen in the images. Overall, it can be said that AO/PI staining results showing living and dead cells were compatible with the other cellular viability analysis.

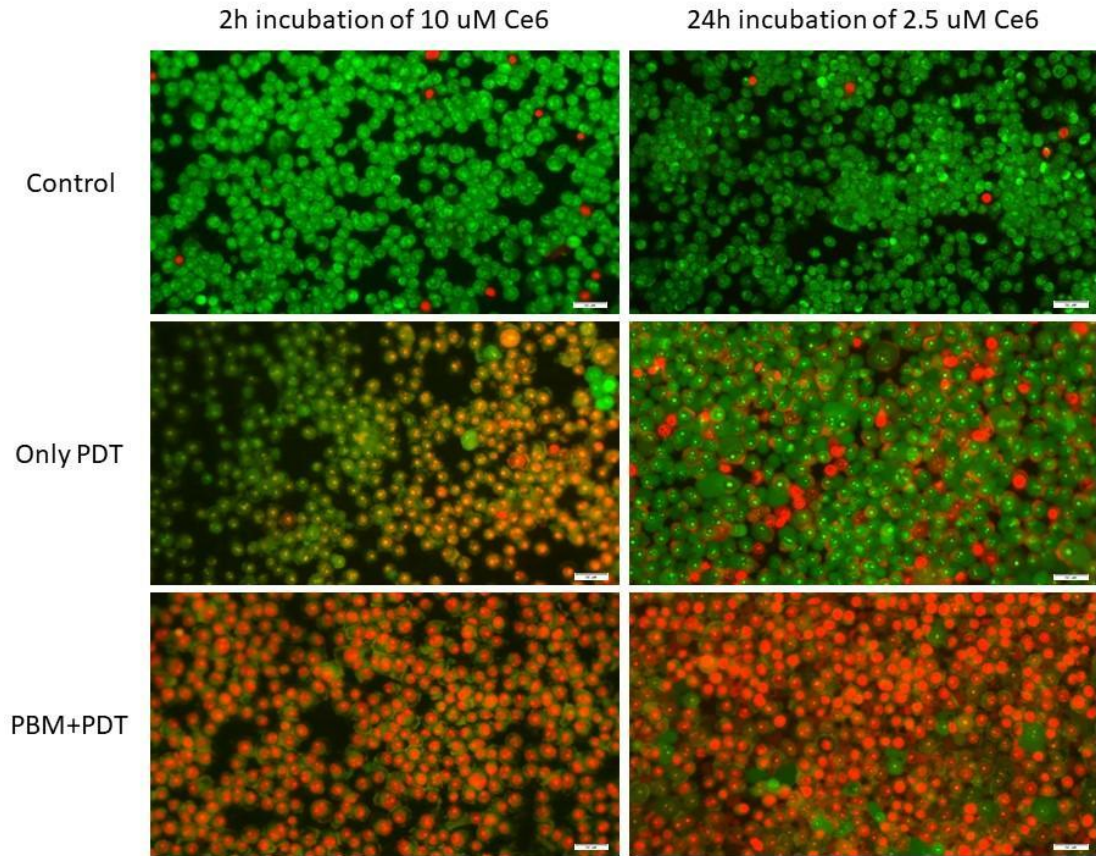


Figure 3.17: Acridine Orange/Propidium Iodide images of PC3 cells with 20X magnification in control, only PDT, and PBM+PDT groups. Ce6-mediated PDT was applied at 50 J/cm² energy density and 808-nm PBM was applied at 5 J/cm² energy density before the PDT. (scale bar: 50 μm, living cells were stained by acridine orange, in green and dead cells were stained by propidium iodide, in red)

Chapter 4

Discussion

It is quite clear that cancer is a global concern affecting many people the world over. Each year new cases are added to the cancer patients list increasing the demand for the therapy. Especially, the cancer types affecting men, prostate cancer has quite big importance having second prevalence coming after lung cancer. It is estimated that about one man in eight will be diagnosed with this cancer type anytime in their lifetime according to the American Cancer Society [13]. Thus, it is pivotal to diagnose cancer with its stages, create new anticancer treatment modalities, enhance the existing anticancer treatment modalities, and get synergistic effects by combining existing anticancer treatment modalities. At that point, the treatment of cancers especially ones that develop resistance against chemotherapy and radiotherapy via novel treatment modalities such as PDT has advantages over the conventional ones enabling selective and effective cancer elimination. Of course, as with other anticancer treatments, some limits and factors inhibit or reduce the efficacy of photodynamic therapy. Researchers tried to solve these limits and drawbacks by combining PDT with different kinds of anticancer treatment modalities [45]–[52].

For that purpose, in this thesis, PDT is combined with PBM. Normally, the use of PBM is not for anticancer purposes, it is for positive outcomes we want to see in healthy cells such as increased proliferation, improved healing, prevented cell death, and promoted repaired mechanisms [77]. In this study, the drawbacks of PDT were tried to be solved and the efficacy of this anticancer treatment was tried to be increased by the application strategy of PBM to the human prostate cancer cells. It is hypothesized with this study that PBM application before the PDT releases the NO from its binding

site in the mitochondria, changing MMP and resulting in increased ATP and ROS production. Due to these changes, it was hypothesized that cellular uptake of therapeutic agents is increased which is a highly energy-dependent mechanism, and then turns into cancer cell death. For that aim, first PC3 cells were pre-treated with 655-nm diode laser light at 1, 3, or 5 J/cm² energy densities before they incubated for 1 or 24 h with different concentrations of ICG (25, 50, and 100 μM), and then they were irradiated with 808-nm diode laser light at 100 J/cm² energy density. After performing 655-nm PBM on PC3 cells, MMP and ATP production were not significantly changed too much from the control group that was measured right after the applications. However, the amount of NO released was increased for all energy densities but the maximum release of NO that was measured right after the light application was observed in 1 J/cm² energy density while changes in the amount of the NO were not different at other energy densities than the control. Also, the amount of ROS that was measured right after the 655-nm PBM applications increased at all energy densities. Although MMP and production of ATP were not increased, increased cell deaths in PC3 cells that were pre-treated with 655-nm at 1 J/cm² energy density that maximum amount of NO was released and then exposed to PDT at 100 J/cm² energy density after 1 h incubation of 25 and 50 μM ICG compared to the cell death obtained from only PDT. In addition, the cellular viability after the ICG-mediated PDT did not show any correlation with the cellular uptake of the PS. Interestingly cellular uptake of ICG was not increased according to the released amount of NO after 655-nm PBM. The cellular uptakes of ICG by PC3 cells were decreased when they were pre-treated with 655-nm PBM at 1 J/cm² energy density which is the parameter that more released amount of NO and more cell death was observed. When the 808-nm PDT was conducted at the same energy density, 100 J/cm², after 24 h of incubation of ICG was examined. The correlate cannot be established with the cellular uptakes of ICG especially 50 and 100 μM concentrations. The only concentration of 25 μM of ICG that its PDT results match. Pre-treatment of PC3 cells with 655-nm PBM at all energy densities increased the cellular uptake of 25 μM of ICG after 24 h incubation but especially PBM at 3 J/cm² energy density showed maximum increased cellular uptake and also showed increased cellular death due to PDT compared to the cells did not pre-treated with PBM. Also, the maximum released NO amounts and maximum changes in the MMP were observed at the 3 J/cm² energy density of 655-nm PBM 24

h after the PBM application. From these results, it can be stated that NO released has an impact on the PC3 cells that can result in increased cell death but this increased cell death is not due to the cellular uptake of the PS itself. Probably, the chemical structure of the ICG resulted in decreased cellular uptake by the PC3 cells. Although the cell membrane permeability increased with the PBM application at 655-nm wavelength, it may have caused serious problems in anionic PS uptake since cells become more negatively charged with the passage of ICG into the cells [78]. Because significant increases in cell deaths were not achieved compared to the only PDT groups with the 655-nm PBM at 1, 3, and 5 J/cm² energy densities followed by ICG-mediated PDT at 100 J/cm² energy density, another experimental set was created and performed using the Ce6 and 808-nm PBM.

Pre-treatment of PC3 cells with 808-nm PBM at 1, 3 and 5 J/cm² energy densities increased the released amount of NO, produced amount of ATP, and produced amount of ROS slightly. However, it decreased the MMP compared to the control group right after the PBM application, but interestingly 24 h after the 808-nm PBM application at all energy densities MMP recovered to values of the control group. The maximum amounts of NO released and ATP were observed after the 808-nm PBM at 5 J/cm² energy density was applied while the amount of ROS was not increased significantly. Also, the cellular uptakes of Ce6 were increased after the 2 h incubation with PC3 cells which were pre-treated with 808-nm laser diode light at all energy densities but 808-nm PBM application decreased the cellular uptakes of Ce6 after the 24 h of incubation with the cells. Especially, 5 J/cm² 808-nm PBM resulted in decreases in the cellular uptakes of Ce6 compared to the control and other energy densities of 808-nm PBM. This enhanced cellular uptake can be correlated due to the viscosity changes after the PBM application [79]–[81]. It is tried to be explained that increased cellular uptake of chemotherapeutic agents when HeLa cells were irradiated with IR pulsed light at 670-nm wavelength and this was correlated with decreased viscosity of the cells after PBM application which enhances cellular uptake [81]. The same phenomenon could take place in this study that resulted in enhanced cellular uptake of Ce6 with the 2 h of incubation by PBM application at 808-nm wavelength. The viscosity change may be stabilized with the PC3 cells in a longer time resulting in no effect on the cellular uptake of Ce6 after 24 h of incubation. When the cellular uptakes and cell viabilities obtained after PDT were tried to be correlated to each other, 2 h incubation of Ce6

with PC3 cells was compatible with the cell deaths in general terms but there is no consistency of cellular uptakes of Ce6 for 24 h incubation and cell deaths observed after PDT. Although the cellular uptakes of Ce6 with the 24 h incubation decreased with the 808-nm PBM, more cell deaths were observed in PBM+PDT groups. The maximum changes of 44.88 and 63.44% in the cell viabilities were observed with the 5 J/cm² 808-nm PBM applications followed by PDT application after 2 h incubation of 10 μM of Ce6 and 24 h incubation of 2.5 μM of Ce6 respectively despite PBM application at this energy density decreases the cellular uptake of Ce6. From these outcomes, an idea comes to mind that increased cell death obtained by PDT which cells pre-treated with PBM is not only related to the increased cellular uptakes. In other words, increased cell death is not only due to the increased cellular uptake of PS because the application of PBM decreased the cellular uptakes, especially in the groups where additional cell deaths were observed that were observed in only PDT. The other mechanisms that resulted from the 808-nm PBM contributed to the enhanced PDT efficacy such as the released amount of NO and produced ATP which is maximum in 5 J/cm² density. The application of PBM at a certain energy density before the PDT at certain concentrations of PS induced the cells and resulted in increased cell death obtained from PDT alone. When the other mechanistic analyses rather than cellular uptakes were examined after the Ce6-mediated PDT at 50 J/cm² energy density and 2 h of incubation time, pre-treatment with 808-nm PBM at 5 J/cm² energy density increased the cellular deaths obtained from the only PDT at 5 and 10 μM concentrations of Ce6 while 3 J/cm² 808-nm PBM increased cell death obtained from the only PDT at 25 μM Ce6. Although the released amount of NO and change in MMP by 5 J/cm² 808-nm PBM energy density was less than other energy densities after the PDT, the highest amount of ATP obtained from the 808-nm PBM at this energy density would an impact on the increased cellular deaths making cells more sensitive to the following anticancer treatment. In addition, the produced amount of ROS after the application of Ce6-mediated PDT at 5 μM of Ce6 after 2 h of incubation which cells were pre-treated with 808-nm PBM at 5 J/cm² was higher than the other energy densities of PBM and only PDT groups. However, other concentrations of Ce6-mediated PDT did not show any correlation in the ROS amounts. Maximum change of 44.88 % in the cell death that was enhanced after the 808-nm PBM at 5 J/cm² energy density at 10 μM Ce6-mediated PDT after 2 h incubation, more decreased MMP was

observed in this group compared to the only PDT and other PBM+PDT groups (1 and 3 J/cm² 808-nm PBM) while the amounts of released NO and produced ROS was the same with the control group.

Generally, produced amounts of ROS after Ce6-mediated PDT at 50 J/cm² energy density after the 24 h incubation of Ce6 was suitable with the cell deaths observed meaning groups that had more cell deaths produced higher amounts of ROS via photodynamic therapy. Also, fewer amounts of NO released and less MMP were observed in groups that more cell deaths especially cells that pre-treated with 808-nm PBM at 5 J/cm² than only PDT and other PBM+PDT groups (1 and 3 J/cm² 808-nm PBM). Maximum change of 63.44% in the cell death that was enhanced after the 808-nm PBM at 5 J/cm² energy density at 2.5 μM Ce6-mediated PDT after 24 h of incubation, a slight decrease in MMP and a decrease in the amount of released NO were observed in this group compared to the only PDT and other PBM+PDT groups (1 and 3 J/cm² 808-nm PBM) while the amount of produced ROS was higher than the control and other PBM+PDT groups (1 and 3 J/cm² 808-nm PBM).

PBM normally increases cell viability by stimulating the mitochondrial membrane receptors which are sensitive to the photons and increasing the production of ATP. Photon absorption (600-810 nm wavelength) by the Cox enzyme releases the NO which has been bound to the iron centers of heme for mitochondrial respiration regulation resulting in decreased ATP production. This release creates a proton gradient increasing MMP which is later used for the production of ATP as well as ROS. Other chromophores rather than Cox can absorb the photons of 810-1064 nm which are light-sensitive ion channels and their activation again increased the ROS level [53]. Many studies were aimed at the positive outcomes of healthy cells gained by PBM but the PBM effects on cancer cells are very limited and not investigated deeply compared to its effect on healthy cells in the literature. Of course, this is due to the concerns about the enhanced cellular viability of cancer cells and making them more aggressive which can have negative outcomes in this situation. Due to this worry, the application of PBM to cancer cells before any anticancer treatment has remained in the background. But it is clear in the literature that some cancer cell types react to the PBM differently in the meaning of cell viability. Some researchers resulted in increased proliferation, some of them observed decreased proliferation and some of them showed that the proliferation of cancer cells was not affected by PBM [82], [83].

Also, these different outcomes are highly affected by wavelength, energy density, and application time of the light. To give some recent examples, Shakibaie et al. observed increased cell viability of breast cancer cells by irradiating them with 629-nm LED light at 17.5 J/cm^2 energy density, Schalch et al. observed decreased cell viability of head and neck cancer cells that were irradiated with 780-nm laser light at 4 J/cm^2 energy density, Chen et al. did not observe a change in the viability of melanoma cells by irradiating them 630-nm LED light at 2.48 mW/cm^2 power density, and Ibarra et al. observed decreased oral squamous carcinoma cell viability when PBM conducted with 660-nm LED light at 3 and 6 J/cm^2 energy densities were applied repeatedly while single PBM with the same wavelength at 3 J/cm^2 increased the cellular viability [84]–[87]. From this study, it is observed that 655-nm red diode laser light caused a slight increase in the cellular viability of PC3 cells at all energy densities. On the other hand, 808-nm PBM did not cause significant increases in which PC3 cells expressed the same cell viability as the control. It is clear from the results of this study, 808-nm wavelength diode laser light did not increase the viability of the PC3 cells that we do not want to see in cancer cells, it can be considered a safe zone, on top of its PBM at 808-nm wavelength induced the PC3 cells before the Ce6-mediated PDT enhancing the cell death obtained from only PDT.

NO is an important molecule that has several roles in physiology [88]. NO competes with oxygen via binding to the affiliation site of oxygen in the Cox reversibly and this binding to the heme a_3 and Cu_B centers of Cox limits the oxygen consumption of the cells. Absorption of the NIR photons by the copper centers of the Cox resulted in increased NO amounts in the cells due to photodissociation [81]. In the literature, many studies showed that NO is released from healthy cells with PBM applications [89]–[92]. In this study, the application of both two wavelengths resulted in an increased amount of NO which cells react differently depending on its concentration. The concentration of NO can control the opening or closing of the large-conductance calcium and voltage-activated potassium channels (BK) via vasodilation. Increased NO level by the PBM opens the BK channels and helps cells to remove intracellular ROS or increases the ATP amount by stabilizing MMP [81]. PC3 cells may increase their ATP amount by stabilizing their MMP with these BK channels. It was observed in this study that PC3 cells tried to stabilize their MMP decrease caused by 808-nm PBM application by increasing it to the back values. Especially, a maximum increase

in the NO and maximum ATP production were observed in 808-nm PBM at 5 J/cm² energy density (compared to control groups and 808-nm PBM at 1 and 3 J/cm² energy densities). In this study, 655-nm PBM at 1,3 and 5 J/cm² energy densities caused a slight increase in the MMP while 808-nm PBM at 1,3 and 5 J/cm² energy densities caused decreased MMP which recovered 24 h after probably with the help of cyclooxygenase enzymes which revolve the MMP to normal level stopping the production of ROS when it decreased [53]. Decreased MMP is not prevalent because healthy cells showed elevated MMP after the PBM application but there are examples in the literature that cancer cells respond to the PBM via decreasing their MMP. Chen et al. observed a decrease of the MMP in the melanoma cells applying PBM using blue LED at 1.12 J/cm² energy density [86]. Doaga et al. observed a decreased MMP level in the human acute T leukemic Jurkat cells after applying PBM at an 830-nm wavelength and 100 mW/cm² power density but they also observed increased MMP after the application of PBM at a 630-nm wavelength [93]. It can be observed that from our results and literature, MMP change is highly influenced by the wavelength of the light. The wavelengths around 600-nm result in increased MMP means hyperpolarization while wavelengths around 800-nm result in decreased MMP means depolarization of the membrane.

Four potential possibilities exist that PBM can have effects on cancer cells. i) PBM cannot have any effect on cancer cells. ii) PBM can directly kill cancer cells at high energy doses due to its biphasic nature. iii) PBM can result in selective cancer cell killing via metabolic differences between healthy and cancer cells. iv) PBM can regulate the immune system against cancer [94], [95]. In this study, we observed enhanced cancer cell death by the Ce6-mediated PDT when PC3 cells were pre-treated with PBM at 808-nm wavelength. These results may be due to the providing the cancer cells a high amount of ATP with the PBM application. It is known that cancer cells have bounding NO in the mitochondria that restrict ATP production and therefore the amount of ATP is less than in healthy cells. ATP produced by the PBM application may enhance the cancer cells' response to the apoptotic stimulus resulting in enhanced apoptosis by the following anticancer treatment [95]. In addition, wavelengths that are used for the PBM are well absorbed by the copper centers of the Cox reducing the redox state of the Cox in the end. However, this reduction may result in changes in the iron states of the heme centers. Changing the states of iron may activate apoptosis and

necrosis because enzymes related the iron metabolism take part in the regulation of apoptosis and necrosis. MMP also can affect cell death [81]. Khokhlova et al. observed mitochondrial damage after the PBM was conducted with 1265-nm laser light at 3.54 J/cm² energy density with colorectal cell death after seven days via enhancing apoptosis [96]. PBM application at 808-nm wavelength resulted in the loss of MMP in this study which may later be resulting in the apoptotic factor release that contributes to cell death. Because the loss of MMP may result in the distribution of the membrane permeability that causes the cytochrome c release into the cytoplasm. In the cytoplasm, cytochrome c couples with apoptotic factors forming apoptosomes that activate the Cas3 and Cas9, and activation of these results in cell death [53], [97]. Also, the amount of produced ROS after PBM at 808-nm wavelength even at low concentration may contribute to the apoptosis later via inactivating the AKT/GSK3beta signaling pathway which is related to cell death [55], [64]. In addition, it is thought that PBM can result in reverse mitochondrial communication which is the reverse situation of normal cell signaling. Normally, cells communicate via signaling from the nucleus to the other cell parts especially cellular organelles but due to the changes in the structure of mitochondria such as changed mitochondrial membrane permeability and ion pumps, the activator protein 1 (AP-1) which regulates apoptosis may be activated [55], [98]. And lastly, another issue that can affect the enhanced cell death by PDT could be the exclusion zone which sites the fourth state of the water where only water molecules exist. It is thought that PBM may separate electrons of photons of water in this zone. This separation of charges makes this zone function like a battery via delivering vibrational energy to the water molecules [99], [100]. The creation of a battery in the water content of cells via PBM may make cells more sensitive to future stimulants which are anticancer in this study.

It is well known that cancer cells show different hallmarks which are specific to them differing from the healthy cells. Researchers hypothesize that cancer and healthy cells react separately to the PBM application and the PBM effect induces the cancer cells greater due to the excessive bounding of NO in the mitochondria [56]. Cancer cells have different glucose mechanisms for energy production called the Warburg effect. The cancer cells produce their energy with aerobic glycolysis which means glycolysis followed by lactate fermentation even in the presence of oxygen probably due to the increased glucose uptake and this takes in the cytosol not in the mitochondria while

the healthy cells produce their energy mostly from the oxidative phosphorylation in the mitochondria [6]. Selective cell death of cancer cells may be accomplished due to metabolic differences such as the Warburg effect and low-level ATP amount in the cancer cells because of this effect [94]. In this point of view, PBM application before the anticancer treatments such as PDT to the tumor site protects the healthy cells and induces the cancer cells for the following cell death obtained from the anticancer treatment. PBM may induce the cancer cells by providing them ATP which has been limited due to restricted cellular respiration and enhancing the cancer cells' response to the apoptotic stimulus and enhanced apoptosis which is energy dependent at the end. Probably, PBM may protect the healthy cells which have had adequate ATP amount via ROS production that can induce the protective mechanisms and reduce the negative effect of the anticancer treatment on healthy tissues via activating the immune system as well [95], [101].

Application of PBM to the cancer cells is a very debatable issue and has negative effects in the end but it was observed in this study that PBM application with 808-nm wavelength at 1, 3 and 5 J/cm² energy density to the human prostate cancer cells is safe and not increased the viability of the PC3 cells dramatically that is expected. And also PBM application at an 808-nm wavelength at these energy densities before the Ce6-mediated PDT increased the PC3 cancer cell death compared to the death obtained from PDT alone which was expressed via cell viability assay and staining. Probably the NO released and increased amount of ATP content after the 808-nm PBM induced the PC3 cells for the following Ce6-mediated PDT application. The ROS produced after the Ce6-mediated PDT were higher in the pre-treated cells with the 808-nm PBM (especially, at 5 J/cm² energy density) and less MMP was observed in these cells. In relation to these results, the cell deaths obtained from the photodynamic action have also increased with the pre-treatment of PBM.

Chapter 5

Conclusion

PDT is a kind of light therapy that is used in the treatment of cancer. Basically, it is based on the conversion of light energy to chemical energy to produce toxic substances such as ROS. The wavelength of the light is important because it should be absorbed with used PS to induce photodynamic action. When the proper light at a certain wavelength and PS are used, ROS is produced which is very toxic to the cells and results in cancer cell death via influencing cell components. Unfortunately, as with other anticancer treatments, there are disadvantages that affect the efficacy of this light therapy. To solve and eliminate these disadvantages, PDT is combined with other anticancer therapies or other therapy modalities such as PBM. PBM application is not preferred in oncology due to the increased cell viability concern. However, this light therapy can result in positive outcomes such as increased cell death and reduced tumor aggressiveness which is obtained from only the anticancer therapy itself by changing its application strategy. In this study, increased prostate cancer cell death was observed when PBM was applied before the PDT compared to the cell death obtained from PDT only and the underlying causes resulting in this increased cell death have been tried to be explained by mechanistic analyses, especially with NO release, and ATP production. And the difference between the cell deaths obtained from only PDT and combined PDT with PBM was greater in low PS concentrations which may reduce the possible side effects of the therapy on surrounding healthy cells. In addition, PBM may have some positive effects on cancer cells by enabling selective cell death and stimulating the immune system via targeting immune system cells against cancer. Of course, increased cell death can be achieved by combining PDT with other conventional anticancer treatments such as radiotherapy and chemotherapy, but side

effects such as the killing of the bone marrow cells and further reducing the immune system are available and must be considered when these therapies are combined. At this point, a more successful, selective, and targeted fight against cancer can be achieved by combining use of PDT with PBM rather than other conventional anticancer therapies by eliminating possible side effects of conventional ones by activating the immune system.

Overall, the application of PBM to the cancer cells before anticancer treatments such as PDT has the potential to increase the outcome of cancer treatment enabling targeted and selective cancer cell death, and it has the potential to reduce the side effects protecting the surrounding healthy cell damage obtained after the cancer treatment via stimulating the immune system and healthy cells. Due to these potentials combination uses of PBM and PDT is very important for dealing with cancer, especially the local ones such as prostate cancer. The effect of PBM on the PDT area cannot be negligible and is worth exploring in future cancer studies whether *in vitro*, *in vivo*, or clinically.

References

- [1] Gabriel J. (Ed.) *The biology of cancer*, 2nd ed. John Wiley & Sons; 2007.
- [2] Cooper GM. *The cancer book : A guide to understanding the causes, prevention, and treatment of cancer*. Jones & Bartlett Learning; 1993.
- [3] Pecorino L. *Molecular biology of cancer: mechanisms, targets, and therapeutics*, 5th ed. Oxford university press; 2021.
- [4] Matthews HK, Bertoli C, de Bruin RAM. Cell cycle control in cancer. *Nature Reviews Molecular Cell Biology* 2021; 23(1):74-88.
- [5] Cramer T, A. Schmitt C. (Ed.) *Metabolism in Cancer*. Springer; 2016.
- [6] Liberti M V, Locasale JW. The Warburg Effect: How Does it Benefit Cancer Cells?. *Trends in biochemical sciences* 2016; 41(3): 211-218.
- [7] Kolenda T, Przybyła W, Kapałczyńska M, Teresiak A, Zajączkowska M, Bliźniak R, et al. Tumor microenvironment - Unknown niche with powerful therapeutic potential. *Reports of Practical Oncology and Radiotherapy* 2018; 23(3):143-153.
- [8] Lorusso G, Rüegg C. The tumor microenvironment and its contribution to tumor evolution toward metastasis. *Histochemistry and cell biology* 2008; 130(6):1091–1103.
- [9] Fares J, Fares MY, Khachfe HH, Salhab HA, Fares Y. Molecular principles of metastasis: a hallmark of cancer revisited. *Signal transduction and targeted therapy* 2020; 5(1): 1-17.
- [10] Barsouk A, Padala SA, Vakiti A, Mohammed A, Saginala K, Thandra KC, et al. Epidemiology, staging and management of prostate cancer. *Medical sciences* 2020; 8(3): 28.
- [11] Bolla M, Van Poppel H. (Ed.) *Management of prostate cancer: a multidisciplinary approach*, 2nd ed. Springer International Pu; 2017.

- [12] Dunn MW, Kazer MW. Prostate cancer overview. *Seminars in oncology nursing* 2011; 27(4): 241-250.
- [13] American Cancer Society. *American Cancer Society Facts & Figures 2022*.
- [14] Siegel RL, Miller KD, Fuchs HE, Jemal A. Cancer statistics. *A Cancer Journal for Clinicians* 2022; 72(1): 7-33.
- [15] Paulsen F, Waschke J. (Ed.) *Sobotta Atlas of Human Anatomy, Internal Organs*, 15th ed. Elsevier, Urban & Fischer; 2013.
- [16] Hayward SW, Cunha GR. The prostate: development and physiology. *Radiologic Clinics of North America* 2000; 38(1): 1-14.
- [17] Mansoori B, Mohammadi A, Davudian S, Shirjang S, Baradaran B. The Different Mechanisms of Cancer Drug Resistance: A Brief Review. *Advanced Pharmaceutical Bulletin* 2017; 7(3): 339.
- [18] Denmeade SR, Isaacs JT. A history of prostate cancer treatment. *Nature Reviews Cancer* 2002; 2(5): 389-396.
- [19] Kirkwood JM, Butterfield LH, Tarhini AA, Zarour H, Kalinski P, Ferrone S. Immunotherapy of cancer in 2012. *CA: a cancer journal for clinicians* 2012; 62(5): 309-335.
- [20] Yan D, Sherman JH, Keidar M. Cold atmospheric plasma, a novel promising anti-cancer treatment modality. *Oncotarget* 2017; 8(9): 15977.
- [21] Misra R, Acharya S, Sahoo SK. Cancer nanotechnology: application of nanotechnology in cancer therapy. *Drug Discovery Today* 2010; 15(19-20): 842-850.
- [22] Bousbaa H. Novel Anticancer Strategies. *Pharmaceutics* 2021; 13(2): 1-4.
- [23] Tucker RD, Platz CE, Huidobro C, Larson T. Interstitial thermal therapy in patients with localized prostate cancer: histologic analysis. *Urology* 2002; 60(1): 166–169.
- [24] Tam SY, Tam VCW, Ramkumar S, Khaw ML, Law HKW, Lee SWY. Review

on the Cellular Mechanisms of Low-Level Laser Therapy Use in Oncology. *Frontiers in Oncology* 2020; 10: 1255.

- [25] Niemz M. *Laser-tissue interactions*, 4th ed. Springer: 2007.
- [26] Abdel-kader M. The journey of PDT throughout history: PDT from Pharos to present. *Photodynamic Medicine: From Bench to Clinic* 2016; 1-21.
- [27] Hamblin MR, Mróz P. (Ed.) *Advances in photodynamic therapy: basic, translational, and clinical*. Artech House; 2008.
- [28] Niculescu AG, Mihai Grumezescu A. Photodynamic therapy—an up-to-date review. *Applied Scienced* 2021; 11(8): 3626.
- [29] Li X, Lovell JF, Yoon J, Chen X. Clinical development and potential of photothermal and photodynamic therapies for cancer. *Nature Reviews Clinical Oncology* 2020; 17(11): 657–674.
- [30] Gunaydin G, Gedik ME, Ayan S. Photodynamic Therapy for the Treatment and Diagnosis of Cancer-A Review of the Current Clinical Status. *Frontiers in chemistry* 2021; 608.
- [31] Correia JH, Rodrigues JA, Pimenta S, Dong T, Yang Z. Photodynamic Therapy Review: Principles, Photosensitizers, Applications, and Future Directions. *Pharmaceutics* 2021; 13(9): 1332.
- [32] Mroz P, Yaroslavsky A, Kharkwal GB, Hamblin MR. Cell Death Pathways in Photodynamic Therapy of Cancer. *Cancers* 2011; 3(2): 2516-2539.
- [33] Ow YLP, Green DR, Hao Z, Mak TW. Cytochrome c: functions beyond respiration. *Nature reviews Molecular cell Biology* 2008; 9(7): 532-542.
- [34] Martins WK, Belotto R, Silva MN, Grasso D, Suriani MD, Lavor TS, et al. Autophagy Regulation and Photodynamic Therapy: Insights to Improve Outcomes of Cancer Treatment. *Frontiers in Oncology* 2021; 10: 610472.
- [35] Rapozzi V, Jori G. (Ed.) *Resistance to Photodynamic Therapy in Cancer*.

Springer; 2015.

- [36] Ghorbani J, Rahban D, Aghamiri S, Teymouri A, Bahador A. Photosensitizers in antibacterial photodynamic therapy: an overview. *Laser Therapy* 2018; 27(4): 293-302.
- [37] Kwiatkowski S, Knap B, Przystupski D, Saczko J, Kędzierska E, Knap-Czop K, et al. Photodynamic therapy—mechanisms, photosensitizers and combinations. *Biomedicine & Pharmacotherapy* 2018; 106: 1098–1107.
- [38] Mfouo-Tynga IS, Dias LD, Inada NM, Kurachi C. Features of third generation photosensitizers used in anticancer photodynamic therapy: Photodiagnosis and Photodynamic Therapy 2021; 34: 102091.
- [39] Kou J, Dou D, Yang L. Porphyrin photosensitizers in photodynamic therapy and its applications. *Oncotarget* 2017; 8(46): 81591.
- [40] Polat E, Kang K. Natural Photosensitizers in Antimicrobial Photodynamic Therapy. *Biomedicines* 2021; 9(6): 584.
- [41] Kim MM, Darafsheh A. Light Sources and Dosimetry Techniques for Photodynamic Therapy. *Photochemistry and Photobiology* 2020; 96(2): 280-294.
- [42] Ash C, Dubec M, Donne K, Bashford T. Effect of wavelength and beam width on penetration in light-tissue interaction using computational methods. *Lasers in medical science* 2017; 32(8): 1909-1918.
- [43] Wu J. The Enhanced Permeability and Retention (EPR) Effect: The Significance of the Concept and Methods to Enhance Its Application. *Journal of Personalized Medicine* 2021; 11(8): 771.
- [44] Casas A, Di Venosa G, Hasan T, Batlle A. Mechanisms of Resistance to Photodynamic Therapy. *Current Medicinal Chemistry* 2011; 18(16): 2486-2515.
- [45] Du Y, Han J, Jin F, Du Y. Recent Strategies to Address Hypoxic Tumor Environments in Photodynamic Therapy. *Pharmaceutics* 2022;14(9): 1763.

- [46] Shi X, Zhang CY, Gao J, Wang Z. Recent Advances in Photodynamic Therapy for Cancer and Infectious Diseases. *Wiley Interdisciplinary Reviews Nanomedicine and Nanobiotechnology* 2019; 11(5): e1560.
- [47] Xu J, Gao J, Wei Q. Combination of Photodynamic Therapy with Radiotherapy for Cancer Treatment. *Journal of Nanomaterials* 2016; 2016.
- [48] Ji B, Wei M, Yang B. Recent advances in nanomedicines for photodynamic therapy (PDT)-driven cancer immunotherapy. *Theranostics* 2022; 12(1): 434-458.
- [49] Karami-Gadallo L, Ghoranneviss M, Ataie-Fashtami L, Pouladian M, Sardari D. Enhancement of cancerous cells treatment by applying cold atmospheric plasma and photo dynamic therapy simultaneously. *Clinical Plasma Medicine* 2017; 7: 46-51.
- [50] Vejdani Noghreiyani A, Imanparast A, Shayesteh Ara E, Soudmand S, Vejdani Noghreiyani V, Sazgarnia A. In-vitro investigation of cold atmospheric plasma induced photodynamic effect by Indocyanine green and Protoporphyrin IX. *Photodiagnosis and Photodynamic Therapy* 2020; 31: 101822.
- [51] Wang M, Geilich B, Keidar M, Webster T. Killing malignant melanoma cells with protoporphyrin IX-loaded polymersome-mediated photodynamic therapy and cold atmospheric plasma. *International Journal of Nanomedicine* 2017; 12: 4117-4127.
- [52] Ha JH, Kim YJ. Photodynamic and Cold Atmospheric Plasma Combination Therapy Using Polymeric Nanoparticles for the Synergistic Treatment of Cervical Cancer. *International journal of molecular sciences* 2021; 22(3): 1172.
- [53] Dompe C, Moncrieff L, Matys J, Grzech-Leśniak K, Kocherova I, Bryja A, et al. Photobiomodulation-Underlying Mechanism and Clinical Applications. *Journal of clinical medicine* 2020; 9(6): 1724.
- [54] Huang YY, Chen ACH, Carroll JD, Hamblin MR. Biphasic dose response in low level light therapy. *Dose-response : a publication of International Hormesis Society* 2009; 7(4): 358-383.

- [55] De Freitas LF, Hamblin MR. Proposed Mechanisms of Photobiomodulation or Low-Level Light Therapy. *IEEE journal of selected topics in quantum electronics* 2016; 22(3): 348-364.
- [56] Hamblin MR. Mechanisms and Mitochondrial Redox Signaling in Photobiomodulation. *Photochemistry and photobiology* 2018; 94(2): 199-212.
- [57] Mason MG, Nicholls P, Wilson MT, Cooper CE. Nitric oxide inhibition of respiration involves both competitive (heme) and noncompetitive (copper) binding to cytochrome c oxidase. *Proceedings of the National Academy of Sciences* 2006; 103(3): 708-713.
- [58] Abraham EH, Woo VH, Harlin-Jones C, Heselich A, Frohns F, Abraham EH, et al. Application and possible mechanisms of combining LLLT (low level laser therapy), infrared hyperthermia and ionizing radiation in the treatment of cancer. *Mechanisms for Low-Light Therapy SPIE* 2014; 8932: 9-25.
- [59] Reyad FA, Elsayed NM, El Chazli Y. Photobiomodulation for chemotherapy-induced oral mucositis in leukemic children: A randomized controlled clinical trial. *Oral diseases* 2022.
- [60] Robijns J, Censabella S, Claes S, Pannekoeke L, Bussé L, Colson D, et al. Prevention of acute radiodermatitis by photobiomodulation: A randomized, placebo-controlled trial in breast cancer patients (TRANSDERMIS trial). *Lasers in Surgery and Medicine* 2018; 50(7): 763-771.
- [61] Santana-Blank L, Elizabeth RS, Santana-Rodríguez JA, Santana-Rodríguez KE. Laser Photobiomodulation as a Potential Multi-Target Anticancer Therapy-Review. *Journal of Solid Tumors* 2013; 3(2): 50-62.
- [62] Robijns J, Lodewijckx J, Mebis J. Photobiomodulation therapy for acute radiodermatitis. *Current opinion in oncology* 2019; 31(4): 291-298.
- [63] Antunes HS, Herchenhorn D, Small IA, Araújo CMM, Viégas CMP, de Assis Ramos G, et al. Long-term survival of a randomized phase III trial of head and neck cancer patients receiving concurrent chemoradiation therapy with or without low-level laser therapy (LLLT) to prevent oral mucositis. *Oral*

oncology 2017; 71: 11-15.

- [64] Djavid GE, Bigdeli B, Goliaei B, Nikoofar A, Hamblin MR. Photobiomodulation leads to enhanced radiosensitivity through induction of apoptosis and autophagy in human cervical cancer cells. *Journal of biophotonics* 2017; 10(12): 1732-1742.
- [65] Tsai SR, Yin R, Huang YY, Sheu BC, Lee SC, Hamblin MR. Low-level light therapy potentiates NPe6-mediated photodynamic therapy in a human osteosarcoma cell line via increased ATP. *Photodiagnosis and Photodynamic Therapy* 2015; 12(1): 123-130.
- [66] Negri LB, Martins TJ, da Silva RS, Hamblin MR. Photobiomodulation combined with photodynamic therapy using ruthenium phthalocyanine complexes in A375 melanoma cells: Effects of nitric oxide generation and ATP production. *Journal of Photochemistry and Photobiology B: Biology* 2019; 198: 111564.
- [67] Joniová J, Kazemiraad C, Gerelli E, Wagnières G. Stimulation and homogenization of the protoporphyrin IX endogenous production by photobiomodulation to increase the potency of photodynamic therapy. *Journal of Photochemistry and Photobiology B: Biology* 2021; 225: 112347.
- [68] de Faria CMG, Costa CS, Bagnato VS. Photobiomodulation effects on photodynamic therapy in HNSCC cell lines. *Journal of photochemistry and photobiology B, Biology* 2021; 217: 112170.
- [69] Diaz Tovar JS, Kassab G, Inada NM, Salvador Bagnato V, Kurachi C. Photodegradation in the infrared region of indocyanine green in aqueous solution. 2019 SBFoton International Optics and Photonics Conference, SBFoton IOPC 2019; 1-5.
- [70] Kruspe S, Meyer C, Hahn U. Chlorin e6 conjugated interleukin-6 receptor aptamers selectively kill target cells upon irradiation. *Molecular Therapy - Nucleic Acids* 2014; 3: e143.
- [71] Abe K, Saito H. Amyloid β protein inhibits cellular MTT reduction not by

suppression of mitochondrial succinate dehydrogenase but by acceleration of MTT formazan exocytosis in cultured rat cortical astrocytes. *Neuroscience research* 1998; 31(4): 295-305.

- [72] Spinner DM. MTT Growth Assays in Ovarian Cancer. In *Ovarian Cancer* 2000; 175-177.
- [73] Chemie VF, Badr M, Trommer WE. The ribosome-inactivating protein gelonin and parts thereof to be employed for a potential treatment of cancer 2012.
- [74] Biotium. Griess Reagent Kit Product Information Sheet. [Internet]. USA; 2020 [access date 23.11.2022], <https://biotium.com/product/griess-reagent-kit/>.
- [75] Promega. CellTiter-Glo® 2.0 Assay Technical Manual. [Internet]. USA; 2018 [access date 23.11.2022], <https://worldwide.promega.com/resources/protocols/technical-manuals/101/celltiterglo-2-0-assay-protocol/>.
- [76] G-Biosciences. DCFHA-DA Redox Probe. [Internet]. USA; 2022 [access date 23.11.2022], https://www.gbiosciences.com/Bioassays/Cell_Health_Assay/REDOX_Probes/DCFH-DA-Redox_Probe.
- [77] Babu Gogineni Shetty SA, Castelino Shetty RA, Faizal Asan M, Subhas Babu G, Lorina Castelino R, Rao K, et al. Applications of Photobiomodulation Therapy in Oral Medicine—A Review. *European Journal of Therapeutics* 2021; 27(2): 177-182.
- [78] Giraudeau C, Moussaron A, Stallivieri A, Mordon S, Frochot C. Indocyanine green: photosensitizer or chromophore? Still a debate. *Current medicinal chemistry* 2014; 21(16):1871-1897.
- [79] Sommer AP, Haddad MK, Fecht HJ. Light effect on water viscosity: implication for ATP biosynthesis. *Scientific reports* 2015; 5(1): 1-6.
- [80] Santana-Blank L, Rodríguez-Santana E, Santana-Rodríguez KE. Cancer, Warburg effect and laser photobiomodulation-progress beyond. *Journal of*

Chinese Clinical Medicine 2011; 6(3).

- [81] Arranz-Paraíso D, Sola Y, Baeza-Moyano D, Benítez-Martínez M, Melero-Tur S, González-Lezcano RA. Mitochondria and light: An overview of the pathways triggered in skin and retina with incident infrared radiation. *Journal of Photochemistry and Photobiology B: Biology* 2022; 238:112614.
- [82] Bensadoun RJ, Epstein JB, Nair RG, Barasch A, Raber-Durlacher JE, Treister N, et al. Safety and efficacy of photobiomodulation therapy in oncology: A systematic review. *Cancer Medicine* 2020; 9(22): 8279-8300.
- [83] Tam SY, Tam VCW, Ramkumar S, Khaw ML, Law HKW, Lee SWY. Review on the Cellular Mechanisms of Low-Level Laser Therapy Use in Oncology. *Frontiers in Oncology* 2020; 10: 1255.
- [84] Shakibaie M, Vaezjalali M, Rafii-Tabar H, Sasanpour P. Phototherapy alters the oncogenic metabolic activity of breast cancer cells. *Photodiagnosis and Photodynamic Therapy* 2020; 30: 101695.
- [85] Schalch TD, Fernandes MH, Destro Rodrigues MFS, Guimarães DM, Nunes FD, Rodrigues JC, et al. Photobiomodulation is associated with a decrease in cell viability and migration in oral squamous cell carcinoma. *Lasers in Medical Science* 2019; 34(3): 629-636.
- [86] Chen Z, Li W, Hu X, Liu M. Irradiance plays a significant role in photobiomodulation of B16F10 melanoma cells by increasing reactive oxygen species and inhibiting mitochondrial function. *Biomedical optics express* 2020; 11(1): 27-39.
- [87] Ibarra AMC, Garcia MP, Ferreira M, de Fátima Teixeira da Silva D, Pavani C, Mesquita-Ferrari RA, et al. Effects of photobiomodulation on cellular viability and cancer stem cell phenotype in oral squamous cell carcinoma. *Lasers in Medical Science* 2021; 36(3): 681-690.
- [88] Quirk BJ, Whelan HT. What lies at the heart of photobiomodulation: Light, cytochrome c oxidase, and nitric oxide-review of the evidence. *Photobiomodulation, Photomedicine, and Laser Surgery* 2020; 38(9): 527-530.

- [89] Monaghan C, McIlvenna LC, Liddle L, Burleigh M, Weller RB, Fernandez BO, et al. The effects of two different doses of ultraviolet-A light exposure on nitric oxide metabolites and cardiorespiratory outcomes. *European journal of applied physiology* 2018; 118(5): 1043-1052.
- [90] Topaloglu N, Bakay E. Mechanistic approaches to the light-induced neural cell differentiation: Photobiomodulation vs Low-Dose Photodynamic Therapy. *Photodiagnosis and Photodynamic Therapy* 2022; 37: 102702.
- [91] Çevik Z, Karaman O, Topaloglu N. Photobiomodulation therapy at red and near-infrared wavelengths for osteogenic differentiation in the scaffold-free microtissues. *Journal of Photochemistry and Photobiology B: Biology* 2022; 112615.
- [92] Pope N, Powell S, Wigle J, Denton M. Wavelength-and irradiance-dependent changes in intracellular nitric oxide level. *Journal of biomedical optics* 2020; 25(8): 085001.
- [93] Doagă IO, Radu E, Katona G, Seremet T, Dumitrescu M, Radesi S, et al. Low level long wavelength laser irradiation effects on human t leukemic lymphoblasts mitochondrial membrane potential. *Rom. J. Biophys* 2008; 18(1): 1-17.
- [94] Hamblin MR. Photobiomodulation and Light Therapy in Oncology. *Orofacial Supportive Care in Cancer* 2022; 255-286.
- [95] Hamblin MR, Nelson ST, Strahan JR. Photobiomodulation and Cancer: What Is the Truth? *Photomedicine and laser surgery* 2018; 36(5): 241-245.
- [96] Khokhlova A, Zolotovskii I, Stoliarov D, Vorsina S, Liamina D, Pogodina E, et al. The photobiomodulation of vital parameters of the cancer cell culture by low dose of Near-IR laser irradiation. *IEEE Journal of Selected Topics in Quantum Electronics* 2018; 25(1): 1-10.
- [97] Kiro NE, Hamblin MR, Abrahamse H. Photobiomodulation of breast and cervical cancer stem cells using low-intensity laser irradiation. *Tumor Biology* 2017; 39(6): 1010428317706913.

- [98] Hennessy M, Hamblin MR. Photobiomodulation and the brain: a new paradigm. *Journal of optics* 2016; 19(1): 013003.
- [99] Santana-Blank L, Rodríguez-Santana E, Reyes H, Santana-Rodríguez JA, Santana-Rodríguez KE. Laser photobiomodulation: A new promising player for the multi-hallmark treatment of advanced cancer. *Int J Cancer Ther Oncol* 2013; 1(1): 01012.
- [100] George S, Hamblin M, Abrahamse H. Effect of red light and near infrared laser on the generation of reactive oxygen species in primary dermal fibroblasts. *Journal of Photochemistry and Photobiology B: Biology* 2018; 188: 60-68.
- [101] Vecchio A Del, Tenore G, Luzi MC, Palaia G, Mohsen A, Pergolini D, et al. Laser photobiomodulation (Pbm)—a possible new frontier for the treatment of oral cancer: A review of in vitro and in vivo studies. In *Healthcare* 2021; 9(2): 134.

Curriculum Vitae

Name Surname : Büşra Sirek

Education:

2015–2016 İzmir Kâtip Çelebi University, The School of Foreign Languages
2016–2020 İzmir Kâtip Çelebi University, Dept. of Biomedical Eng. (BSc)
2020–2023 İzmir Kâtip Çelebi University, Dept. of Biomedical Eng. (MSc)

Work Experience:

2018 Summer Internship Turkish Public Hospitals Authority
2019 Summer Internship Bonegraft Biological Materials Industry and Trade Inc.

Publications (if any):

1. Sirek B, Fidan D, Özdemir GD, Ercan UK, Topaloğlu N. Comparison of the Antibacterial Effects of Photodynamic Therapy and Cold Atmospheric Plasma on Methicillin-Resistant Staphylococcus aureus. In: TIPTEKNO2020: 2020 Medical Technologies Congress; 2020 Nov 19-20; Online. IEEE. 70-73.
2. Sirek B, Topaloğlu N. Improvement of the Chlorin e6-mediated Photodynamic Action with Photobiomodulation Therapy in Human Prostate Cancer Cells. In: TIPTEKNO2022: 2022 Medical Technologies Congress; 2022 Oct-Nov 31-2; Antalya, Turkey. IEEE; 2022. 189-192.
3. Sirek B, Kaya E, Sarı B, Bakay E, Topaloğlu N, Şen Karaman D. Production of a Multifunctional PLGA Wound Dressings Containing Abietic Acid and Chlorin e6. In: TIPTEKNO2022: 2022 Medical Technologies Congress; 2022 Oct-Nov 31-2; Antalya, Turkey. IEEE; 2022. 205-208.